Bio-Inorganic Interface Engineering *via* Solid-Binding Peptides toward Nano-sensing Applications

Dmitriy Khatayevich

A dissertation
submitted in partial fulfillment of the
requirements for the degree of

Doctor of Philosophy

University of Washington
2013

Reading Committee
Mehmet Sarikaya, Chair
William Grady
Tom Horbett
Dan Ratner
Candan Tamerler

Program Authorized to Offer Degree:
Materials Science and Engineering

University of Washington

Abstract

Bio-Inorganic Interface Engineering *via* Solid-Binding Peptides toward Nano-sensing Applications

Dmitriy Khatayevich

Chair of Supervisory Committee:
Professor Mehmet Sarikaya
Materials Science and Engineering Department

Bridging the worlds of molecular biology and inorganic materials is a crucial step in many of today's medical, nano-technology, energy, catalysis and renewable technology fields. By its very nature, this task is highly multidisciplinary, incorporating aspects from surface physics, organic and inorganic chemistry, the tools of nano-technology, and of course, biology from genetic to molecular to structural to organismal levels. Solid-binding peptides are a unique class of biomolecules perfectly suited to build this bridge at the scale consistent with both organic and inorganic systems. These 7-12 amino acid long peptides are biological in origin (consisting of 20 natural amino acids), bind strongly through a number of non-covalent interactions, self-assemble into dense ordered structures, are selected to be highly specific to their target solid materials, and can be fused with other biomolecules through many chemical and biological means to create entities with multiple functionalities. These properties make solid-binding ideal for functionalizing simple and complex inorganic surfaces to impart broad chemical or functional properties to the system in an environmentally friendly and biologically viable fashion, with minimal effect on the properties of the underlying substrate.

This thesis demonstrates the design of surface biofunctionality in proof-of-principle biotechnological and nanotechnological implementations in a variety of applications. As an example of the utility of engineered peptides with state-of-the art nanomaterials systems, the thesis addresses the design and manufacture of a graphene based, peptide enabled nanobio-sensor for molecular detection in a biological medium. The present report, therefore, focuses on a design and application of solid-binding peptides to control the bio-inorganic interface, and simultaneously to impart bio-functionality to an inorganic system. More specifically, in this research group, one of our goals has been is to develop a graphene biosensor for specific, ultra-sensitive detection of cancer markers against a background of serum proteins, through a combination of newly developed molecular biomimetic functionalization and nano-fabrication approaches. In order to build such a sensor three broad steps must be taken: (1) The surface of the sensor must be passivated to prevent non-specific adsorption of undesired proteins. (2) Target-specific bio-functionality must be imparted to the sensor to enable it to capture the targets in the sample. (3) A modular system, the bio-functionality of which can be easily modified, must be developed to simplify detection of a variety of targets. These steps must be taken in such a way as to not negate the sensitivity of the sensor, a graphene field effect transistor (gFET). The work covers experiments aimed at achieving bio-inert and bio-active interfaces (*i.e.* interfaces which do not interact with cells/proteins, and ones that interact with them in a predictable manner, respectively) *via* peptide functionalization, as well as sensor construction, peptide sequence optimization for assembly and property display, and selective detection of proteins from a complex mixture. As an example, using an optimized gFET sensor system, the detection of streptavidin binding against a

background of serum albumin at less than 50ng/ml is demonstrated. Additionally, using a bi-functional graphene binding peptide – antibody binging peptide construct, we demonstrate a modular detection system, which can be modified to detect a given biomolecule, for which an anti-body has been selected, in a single step, by replacing the probing module (the anti-body). Cancer markers are large biomolecules present in the blood or other tissues, which can be used for early diagnosis. Their detection is challenging due to the low concentrations at which they are present, and the difficulty of selecting them against the complex background of other proteins present in the serum. Using our system we demonstrated selective cancer marker detection, specifically immobilizing antibodies as the probe on the sensor surface, using engineered peptide chimeras to detect cancer markers in a serum environment. The system we demonstrate is the first significant step toward creating a fast, sensitive methodology for profiling the low levels of multiple markers simultaneously, a must for accurate, reliable, and rapid diagnosis. Our modular approach, which allows for easy switching of targets, can also be used for other clinical and research applications in general, such as, ligand-receptor interaction studies, screening for drug candidates, and developing vaccines against small viruses.

1. Introduction

The overarching purpose of this work is to produce a graphene field effect transistor-based nanobio-sensor (gFET), functionalized via graphite binding peptides (GrBPs), and capable of selective detection of cancer markers against serum protein background at ng/ml concentrations, thereby, addressing a challenging bio-medical problem, taking advantage of the many unique properties of the self-assembling, solid-binding peptides.

1.1 Motivation

Bridging the worlds of molecular biology and inorganic materials is a crucial step in numerous cutting edge medical, nano-technological, energy, catalysis and renewable technology fields. Nature, through the process of evolution, has designed numerous molecular machines of spectacular efficiency and capabilities unequalled by any artificial approach to date: proteins. They possess enormous chemical and physiochemical diversity, enabling them to perform the myriad of varied tasks needed for life to function. Of particular importance, is the fact that these molecules exist and operate at the nano-scale, lengths comparable to artificial devices produced by the developing field of nanotechnology. Nano-technology can be significantly advanced by reverse engineering the intricate control biological systems exert over self-assembly, selective function, self-repair, hierarchical structuring, and many other aspects of their nano-environment. However, imitation of nature's methods in artificial applications is difficult and often insufficient. We can also borrow tools directly from its tool-box.

1.1.1 Solid-binding peptides

Solid-binding peptides (also known as GEPIs) represent a very promising route to bridging the bio-inorganic divide due to their strong binding capabilities to their target materials in the absence of covalent bonds, biocompatible processing, nature, and ease of conjugation with biological molecules. They are 7-12 amino acid long peptide sequences that have been combinatorially selected through phage or cell-surface display to bind to a specific inorganic material.[1] In brief, a randomized peptide sequence is encoded to be expressed in a flagella (cell) or coat (phage) protein.[2, 3] The library, containing about 10^9 differing peptides, is introduced to the target surface, and then washed with increasing stringency. The organisms that remain bound on the surface are collected and amplified. The process is repeated 4-5 times, and the final clones are sequenced to determine the peptide which gave rise to the affinity **(Figure 1)**. The peptides can then be synthesized ex situ and characterized by SPR or other adsorption measurement techniques.[4] The peptides can be further improved by computational similarity analysis, to isolate the sequences and structures primarily

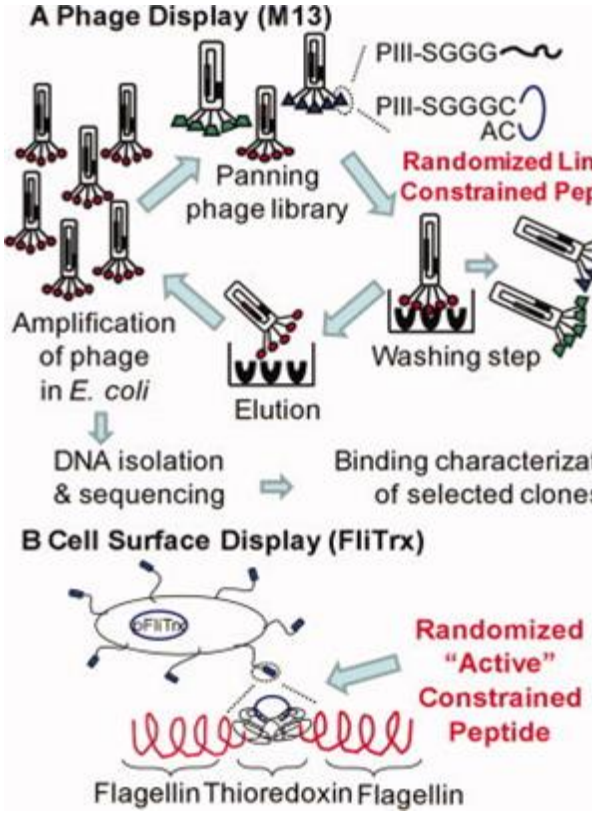

Figure 1. (A) Schematic summarizing the biopanning experiment using phage display system, M13, (B) Insertion site of the random peptide library in cell surface display system, FliTrx.
C. Tamerler, D. Khatayevich, et al. Peptide Science (2010)

responsible for binding.[5] A vast number of solid binding peptides have already been developed for most types of materials including noble metals (Au, Ag, Pt),[6-10] oxides (SiO_2, ZnO, Cu_2O, TiO_2),[5, 11, 12] minerals (hydroxyapatite, calcite, graphite, sapphire),[13, 14] and semiconductors (GaN, ZnS and CdS).[15, 16] The affinities of the peptides for their respective surfaces are measured to be ~ 50 nM to 1 μM.

The resulting peptides are very well suited to addressing the challenges of the bio-inorganic interface and especially in the field of bio-nanotechnology. The high affinity binding, resulting from a sum of weak interactions ensures great stability of the modification, absence of toxic or aggressive chemistry, and minimal perturbation of the properties of the underlying substrate.[17, 18] Moreover, the peptides' biologically derived nature makes fusion with functional biological entities such as enzymes, ligands, receptors and antibodies a relatively simple matter of co-expression, as

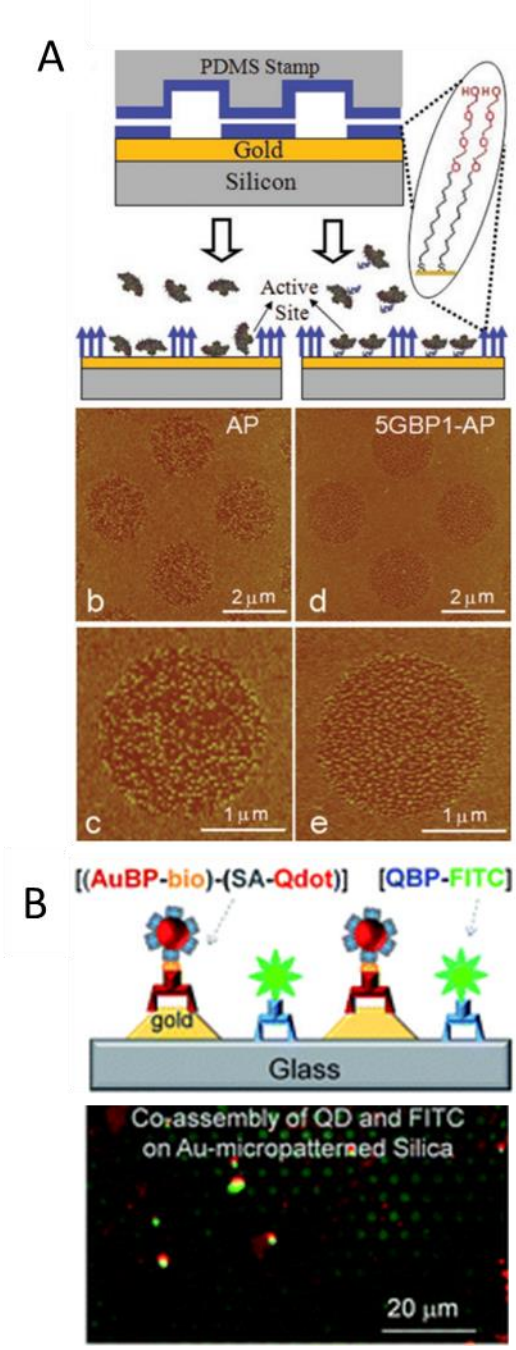

Figure 2. A) Gold-binding peptide functionalized alkaline phosphatase self-assembling on PEG patterned gold substates.
C. Kacar, et al. Advanced Materials (2009)
B) Gold- and silica- binding bi functional peptides co assembled on gold and silica patterned substrates.
M. Hnilova, et al. Soft Matter (2012)

well as reduces the chances that the linker would show toxicity. For example, a gold binding peptide can be fused with an enzyme such as alkaline phosphatase to enable its directed assembly on the micro-patterned gold substrates. The peptide allows the enzyme to retain more of its activity than the non-specifically adsorbed case (**Figure 2 A**).[19] Alternatively, gold- and silica- binding sequences can be labeled with different fluorophores. They can then preferentially assemble on the gold-silica patterned substrates (Figure 2B).[20] Finally, and perhaps most importantly, the peptides are smaller than, but of the same scale as proteins and nano-particles making them, extremely well suited for design and assembly of multi-component nano-systems, without interfering with the performance of the components. A number of such applications have already been demonstrated, including directed self-assembly of nanoparticles, quantum dots, proteins, labeling molecules and enzymes.[21-23] All of the above advantages make solid binding peptides ideal for addressing complex problems involving biological and nanotechnological components. One such problem is the detection of cancer markers.

1.1.2 Cancer and Cancer Markers

Early detection of most types of cancer is one of the primary factors in the outcome of a treatment.[24] To date, however, no established methodology exists for effective, accurate, non-invasive and routine screening for many cancer types, and most cancers are only diagnosed once the symptoms are manifested. Although a number of serum-, urine- and tissue-borne markers have been identified in the literature,[25-27] their practical usefulness remains limited, due to the low concentrations at which they are present in the samples, especially in the early stages, and the difficulty of isolating the markers against the background of a highly concentrated complex mixture of proteins in

serum. The problem is further compounded by the fact that it is generally insufficient to screen for only one type of marker, and elevated levels of a particular marker are an uncertain indicator of the presence of cancer, particularly without an established baseline for a given patient (e.g., PSA level screening yields false positives roughly 65-75% of the time).[28] It is necessary, therefore, to establish a rapid, high throughput, routine, and above all, sensitive technique for cancer marker detection, that is capable of identifying the presence of multiple targets at ng/ml concentrations. For this work we have chosen to focus on pancreatic cancer, one of the most lethal types of malignancies, and the fourth leading cause of cancer related deaths in the US, with the over 45000 cases diagnosed yearly, 85% of which have lethal outcomes.[29] The primary cause of such high mortality rate in the pancreatic carcinoma cases is its high propensity for both local invasion and distant metastasis.[30] The metastasis rate is so high that by the time the disease is diagnosed it is usually in the late, inoperable stages, at which point current therapies have very little impact.[31] Early detection is the single most important determining factor of the outcome of the disease.

There are a number of pancreatic cancer markers identified in the literature, most prominent among them, the carcinoembryonic antigen (CEA),[32] and the cancer antigen 19-9 (CA19-9).[33] The abnormal concentration of CA19-9 has been determined to be above 37u/ml,[34] and that that of CEA above 2.5ng/ml.[35] These markers have been in clinical use for decades, but suffer from low specificity, because they are present in other types of cancer and benign conditions. There are numerous other serum markers for pancreatic cancer (amylin, DUPAN-2, CA242, CAM 17.1, TPS, CA72-4 and other), but none are better than CA19-9 by themselves.[36] Therefore, it is necessary to create a

method for simple detection of a variety of markers, which would give a molecular profile of the disease to allow a more accurate diagnosis.

1.1.3 Graphitic Sensors

Detection of molecular recognition events ex situ has been a well-established approach to drug discovery and molecular biology since the 1960s.[37] More recently, detection of molecular recognition events has been applied in clinical research and practice for diagnosing and monitoring of diseases, including several types of cancer, through the detection of biomarkers in blood, tissues, or urine of the patient.[38] Among the techniques used to detect such markers are the surface plasmon resonance spectroscopy (SPR), [39, 40] quartz crystal microbalance (QCM), [41] various immunoassays, including electrochemical assays, and others. [42-45] The applicability of these techniques to clinical practice remains limited, however, since the markers are present in very low concentrations, against a background of serum or tissue proteins. In the last several years, two-dimensional single layer material field effect transistors (2D-FET) have been employed for ultrasensitive detection of small molecular. [46, 47] Graphene and 1-D carbon nano-tubes (CNT) in particular have been used successfully

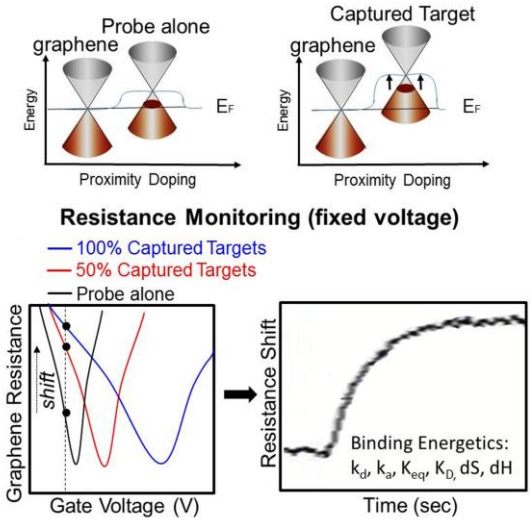

Figure 3. Electronic sensing *via* graphene. A) Sensor state in the absence of analyte. B) Change in sensor state in the presence of captured analyte. C) Signal from the sensor device (real). Resistance is monitored as analyte is added to the sensor. D) Typical sensogram obtained by introducing GrBP5 to bare graphite (SRS device).

T.R. Page et al. Biosensors & Bioelectronics (2012)

and have a very low detection limit, [48-51] with some designs reported to detect femtogram per milliliter concentrations of analyte. [52] Such sensitivity is possible due to graphene's excellent electronic properties, resulting from delocalized π bond structure, and a band gap which is very sensitive to doping **(Figure 3)**. [51, 53-55] Room temperature charge mobilities in graphene have been measured to be around 15000 $cm^2V^{-1}s^{-1}$ or more.[54, 56], graphene is also ambipolar, meaning that negative gate voltages result in large induction of holes, and positive gate voltages result in large induction of electrons.[57] Because of the sensitivity of the graphitic materials' electronic properties, graphene-based sensors can potentially be used to "finger print" and quantify the adsorbing species from the signal, which has already been demonstrated with small molecules, such as dopamine and serotonin.[58-61] In fact, even single gas and bio-molecules have been detected by CNT and graphene based devices.[62] Graphene based sensors offer a unique opportunity for ultra-sensitive detection of cancer markers.

1.2 Research Objectives

Our objective in this research is to draw on the advantages of the two-dimensional material based nano sensors and the solid binding peptides to develop a selective, sensitive nano-sensor for cancer marker detection. To do so, the following scientific and engineering criteria must be addressed:

1) Methodology for optimum peptide enabled functionalization of surfaces;
2) Methodology to prevent non-specific adsorption of proteins to surfaces using peptides;
3) Parameters for peptide mutation and functionalization;
4) Criteria to maintain self-assembly properties of the peptides;

5) Methodology to control surface properties of the resulting peptide/substrate system;
6) System to impart multiple functionalities to the substrate via peptides;
7) Design of the graphene nano-sensor;
8) Design of modular approach to sensor functionalization for versatility;
9) Reliability, sensitivity and selectivity test of the resulting system;
10) Application of the resulting bionano-sensor system to cancer marker detection;

2. Results and Discussion

Sections below describe the results I obtained in experiments on other materials and systems, and the way in which they informed the development and optimization of the graphene bio-sensor for cancer marker detection.

The above design criteria can be grouped into three primary categories, which must be addressed in order produce a selective, sensitive and versatile bionano-sensor: (1) The surface of the sensor must be passivated to prevent non-specific adsorption of undesired proteins; (2) bio-functionality must be imparted to the sensor to enable it to bind specific targets in the sample; (3) a modular system must be developed to allow simple switching between a variety of targets by replacing the probe module. These steps must be taken in such a way as to not negate the sensitivity of the sensor. My work below covers experiments aimed at achieving bio-inert and bio-active interfaces via peptide functionalization, peptide sequence optimization for assembly and property display, and an example of a modular system for selective detection of proteins from a complex mixture.

2.1 Peptide Design for Surface Functionalization

Solid binding peptides have been employed for a wide variety of functionalization applications, ranging from directed enzyme immobilization to surface property modification to mineralization. In all of these cases, the solid binding peptide sequence has been designed to contain three domains, a binding, functional, and linking domain. There are numerous variables to consider when creating such bi-functional constructs. A permissive site must be found in the binding domain, where further modification can take place without interfering with the solid binding capability. Often, such a site must also be a specific chemical group to allow further modification. The functional domain of the bifunctional peptide must be sufficiently short and properly selected so as to not interfere with other properties of the construct. The linker often plays a crucial role in properly displaying the functional domain, as well as preventing the two domains from interfering. Moreover, the optimal order in which the two components are linked must be determined for each system. In the study below, the bi-functional design parameters are determined for a gold-silica bifunctional system.

Objective: To create patterned gold thin films and particle arrays by selective immobilization of gold nano-particles and synthesis of gold from solution by surface-bound bi-functional peptide constructs.

Efficient and controllable fabrication of inorganic nano- or micro-structures on solid substrates is critical for a variety of nano- and micro-technologies (e.g. electronics, photonics, and sensing).[63-65] Arrays of gold nanoparticles, organized on solid supports as a film, are particularly promising for fabrication of high-throughput and cost-effective assay systems with unique photonic properties, as well as for construction of

electrochemical sensor chips and bioelectronic devices.[63, 64] Currently available physical approaches to fabrication of patterned metallic nanostructured surfaces include photo-, e-beam, and nanosphere-lithographies.[66-68] Many of these processes are complex, requiring well-controlled environments, sophisticated equipment, and thus, high operating costs.[67] Chemical approaches involve complex surface functionalization with thiol- or silane-based self-assembled monolayer (SAM) molecules, [69, 70] which can be patterned on solid surfaces using common soft lithography techniques. [71, 72] Patterned SAMs on gold and silica surfaces, in fact, have been used to fabricate various arrays and devices. [72-74] However, there are still considerable processing limitations and drawbacks associated with SAM technology including complexity of surface modifications that are currently undertaken under biologically unfriendly conditions, applicability to only a limited number of materials, high cost, long stacking time, low yield and stability. [68, 74, 75] In addition, since such nanosystems are produced in harsh solvents and conditions, they are often not biocompatible and are of limited practical relevance in biomedical applications. Here, we demonstrate a bio-enabled fabrication route for surface micro-patterning as an alternative to conventional techniques by utilizing hetero-functional solid binding peptides that offer desired versatility as well as multi-material recognition characteristics. Once properly engineered, the combined peptide building blocks can link and hold two different materials within close proximity as well as exhibit catalytic materials synthesis activity. Solid binding peptides have recently, been employed in the form of modular subunits of a hetero-functional fusion constructs, in combination with other proteins and peptides for a variety of directed self-assembly applications. [19, 76, 77] Previously, we reported the selection and identification of gold- [6] and silica-

binding [5] peptides (AuBP and QBP) from combinatorial and de novo peptide libraries and confirmed their high-affinity and selective binding onto respective solid surfaces. [5, 6, 75] In addition to exceptional binding (at sub-micromolar levels) and self-assembly on gold surfaces, the specific AuBP sequences were also reported to catalyze and promote the formation of water dispersible gold nanostructures from aqueous $HAuCl_4$ solutions under ambient conditions without the need for additional reducing or stabilizing agents,[78] such as the case in citrate-enabled gold formation. [79] Here the binding and catalytic activities of these peptides are combined into a single multi-functional unit and demonstrate their effective implementation for an addressable bio-enabled nanofabrication route.

We designed a novel hetero-functional peptide by linking silica- and gold-binding peptide sequences (QBP and AuBP), through a flexible poly-glycine linker. Both peptide sequences were carefully chosen for best binding and synthesis functionalities. [75, 77] Additionally we were careful to avoid sequences dominated by amino acids known to interact with gold, such as cysteine and histidine, [80-84] and which might, in turn, promote the gold reduction and crystal growth **(Table 1).** The patterned QBP-AuBP multi-functional peptide **(Figure 4a-b)** was then utilized as a molecular linker for direct immobilization of gold nanoparticles onto the silica surface (Figure 4c) as well as to control the formation of a gold film by a peptide-mediated reduction process (Figure 4d). The combined approach utilizes the peptide-mediated growth of pre-immobilized gold

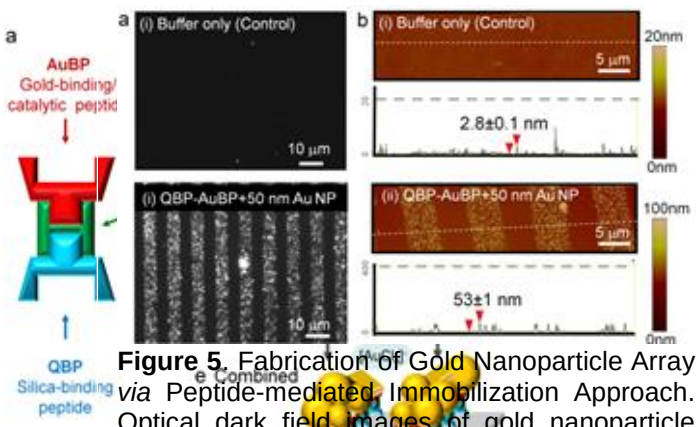

Figure 5. Fabrication of Gold Nanoparticle Array *via* Peptide-mediated Immobilization Approach. Optical dark field images of gold nanoparticle array *via* patterned QBP-AuBP peptide and its control sample (a); Corresponding atomic force microscopy images and the height profiles across the array with and without peptide patterning (b).

Figure 4. Fabrication Routes of Gold Nanoparticle Film Array. Multi-functional peptide design including gold- and silica-binding termini combined by a flexible spacer (GGG) (a); Schematics of the procedure of producing peptide microarray using soft lithography (b); Peptide-mediated immobilization of pre-made gold nanoparticles (c); Peptide-mediated in situ synthesis of gold nanoparticle film (d); Peptide-mediated growth of pre-immobilized gold nanoparticles (e).

Hnilova et al. J. Colloid Interface Sci. 2011

Table 1. Peptide sequences and molecular weights.

Peptide	*Sequence*	*MW (expected)*
AuBP	WAGAKRLVLRRE	1454.7
QBP	PPPWLPYMPPWS	1467.7
QBP-AuBP	PPPWLPYMPPWS-GGG-WAGAKRLVLRRE	3075.6
AuBP-QBP	WAGAKRLVLRRE-GGG-PPPWLPYMPPWS	3075.6

nanoparticles resulting in dense film-like gold nanoarrays (Figure 4e). Finally, we demonstrated the robustness of our approach by combining these two different types of functionality, i.e. assembly and catalytic activity, and produced densely packed and thick gold films by inducing the growth of pre-immobilized “seed” nanoparticles using the engineered multi-functional peptide (Figure 4e).

First, well-defined peptide patterns of controllable size and shape were produced on silica surfaces using micro-contact printing technique. We next incubated the peptide patterned surfaces with pre-made gold nanoparticles of 50 nm size. The resulting gold nanostructure arrays were characterized using dark field (DF) optical microscopy as well as atomic force microscopy (AFM) in tapping mode **(Figure 5**). The micrographs revealed preferential assembly of the pre-made gold nanoparticles on to the patterned peptide templates. The height of the features observed was consistent with the expected height of the construct: 50 nm particle plus a 1-2 nm thick peptide monolayer.

Employing QBP-AuBP peptide that combines both silica- and gold-binding motifs resulted in homogenous and continuous arrays of gold nanoparticle film when compared to randomly organized and discrete low density nanoparticles immobilized by either single QBP or AuBP peptide sequences as evidenced by dark field optical microscopy images **(Figure 6)**.

Additionally, to test the effect of the peptide molecular fusion on the structure and therefore function of the modular components, we reversed the order of single peptide domains to AuBP-QBP. We found that the QBP-AuBP sequence performed significantly better than the reversed permutation (Figure 6e,g). Such a difference implies that in addition to primary sequence, adapted molecular conformation of hetero-functional peptide triggered by the order of gold- and silica-binding domain conjugation is also likely to play an important role in inorganic binding functionality.

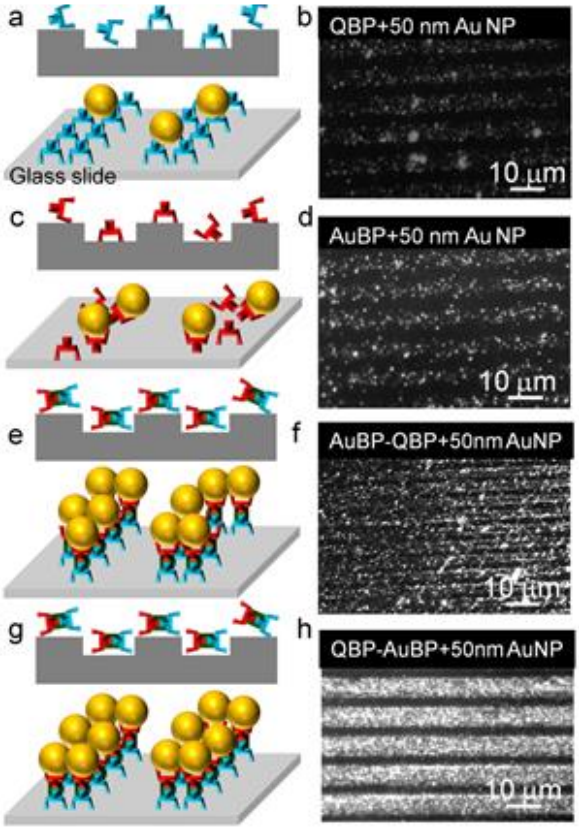

Figure 6. Efficiency of Peptide-mediated Gold Nanoparticle Immobilization. Schematics of peptide-mediated immobilization of gold nanoparticles using single or multi-functional peptides (a, c, e and g); Respective dark field microscopy images of immobilized gold nanoparticles *via* QBP (b), AuBP (d), multi-functional AuBP-QBP (f) and QBP-AuBP permutations (h).

In the next set of experiments, taking advantage of the capability of the gold-binding sequence to reduce gold ions from gold chloride solution, we synthesized the gold nanoparticles in situ on the patterned QBP-AuBP arrays assembled on silica surfaces **(Figure 7)**. Peptide-mediated gold nanoparticle synthesis was achieved using an

aqueous solution of 10 mM gold

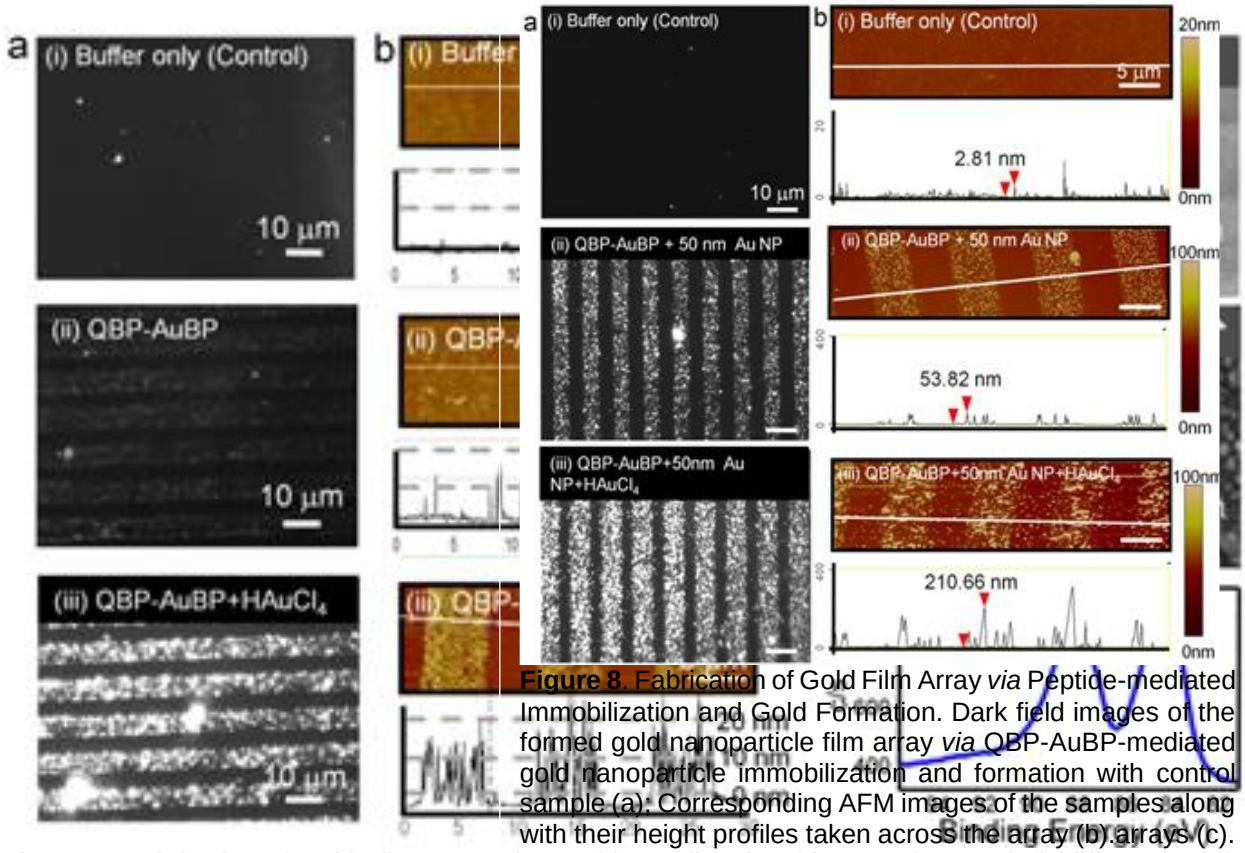

Figure 8. Fabrication of Gold Film Array *via* Peptide-mediated Immobilization and Gold Formation. Dark field images of the formed gold nanoparticle film array *via* QBP-AuBP-mediated gold nanoparticle immobilization and formation with control sample (a); Corresponding AFM images of the samples along with their height profiles taken across the array (b).arrays (c).

Figure 7. Fabrication of Gold Film Array *via* Peptide-mediated Gold Formation. Dark field images of the formed gold nanoparticle film array *via* the patterned QBP-AuBP peptide and its control sample (a); Corresponding AFM images of the samples along with their height profiles taken across the array (b); Scanning electron microscopy images (low and high magnification) and X-ray photoelectron spectroscopy spectrum obtained from gold nanoparticle film arrays (c).

chloride at room temperature without additional reducing agents. Synthesized gold nanostructured arrays were imaged using dark field optical microscopy and AFM in tapping mode (Figure 7). The set of dark field and AFM micrographs in Figure 7 a-b (ii) shows the silica substrate patterned with QBP-AuBP peptide prior to gold reduction. The AFM images confirmed that the peptide formed a homogeneous monolayer with negligible amount of agglomeration. The second set of dark field optical and AFM micrographs on Figure 7 a-b (i and iii) shows a distinctive difference in gold formation on peptide-patterned surface compared to control ones after incubation with HAuCl4, the gold precursor. The results confirmed the formation of 10-20 nm gold particles on top of

the QBP-AuBP patterns. The XPS spectrum from the same sample exhibits a significant presence of gold Au4f peaks, indicative of the formed gold film. The XPS spectra also display nitrogen-bonded carbon at 286.1 eV, as well as the N-C=O bonds at 288.0 eV, indicative of the presence of the intermediate peptide layer. In addition, we observed a decrease in the signals from the underlying elements, such as silicon and oxygen, indicating a partial obstruction of the surface by the newly formed gold. Finally, we demonstrated that these two different types of functionality, i.e. assembly and catalytic activity, can be combined to produce densely packed and thick gold films by inducing the growth of pre-immobilized “seed” nanoparticles using the engineered multi-functional peptide (Figure 3e). As evidenced by dark field and atomic force microscopy results shown in Figure 18a-b after 48 hours of incubation in aqueous gold chloride solution at room temperature, the pre-immobilized 50 nm “seed” particles increased in size to up to 200 nm due to the inherent catalytic activity of the multi-functional peptide **(Figure 8)**.

2.2 Mitigation of Non-specific Interactions

Imparting to a material the ability to resist non-specific biological adsorption has been the cornerstone of biocompatibility research for decades. [85] There are many ways to passivate the surface, including covalent and non-covalent adsorption, changes in surface morphology, changes in surface chemistry and others. In the experiment below I have shown how peptides can be utilized to control cellular adhesion response on a variety of implantable materials.

Objective: To promote or deter cellular interaction with gold, platinum, titanium, and silica glass via immobilization of functional molecules through specific inorganic-binding peptides.

The developments in the area of biomaterials have given rise to numerous compounds, materials systems and devices with a variety of attributes to be used for implantable medical purposes. [86-88] Many of the available materials have already been optimized to have satisfactory physical and mechanical properties. Insufficient or improper interactions between the synthetic materials and the living systems, however, remain a major concern, and often result in failure of the implant. [85, 89-93] The most common strategy to overcome this problem, and enhance the biocompatibility of implants, has been to modify their surfaces with functional molecules. Such molecules are usually selected to perform one of the two functions: to generate cyto-compatible surfaces by carrying specific cell signals or non-fouling surfaces by preventing adhesion of undesired proteins and cells. A number of molecular immobilization systems have been successfully employed to modify the implant surfaces. For example, Rezania *et al* have utilized N-(2-aminoethyl)-3-aminopropyl-trimethoxysilane (EDS) and 4-(Nmaleimidomethyl) cyclohexane-1-carboxylate (sulfo-SMCC) to covalently immobilize cyclic Arginine-Glycine-Aspartic Acid (RGD) peptides on oxide surfaces. [94] The exposure of these modified surfaces to cell cultures has resulted in a marked increase in the cell adhesion. Likewise, Harder *et al* have used self-assembled alkanethiolate monolayers to link oligo(ethylene glycol) (OEG) chains to gold and silver and produce protein resistant surfaces. [95] Messersmith *et al*. have utilized 3,4-dihydroxy-L-phenylalanine (DOPA) to non-covalently attach poly(ethylene glycol) (PEG) to gold and titanium. The DOPA-PEG modified substrates exhibited a marked decrease in the cell adhesion. [96] Other strategies for surface modification with functional molecules include non-specific adsorption [97, 98], photochemical grafting [99], functional self-assembled monolayers

(SAM) [97, 100, 101], covalent attachment [102, 103], and plasma deposition [104], among others.

The conventional immobilization methods listed are often applicable only to a limited range of materials and require the presence of specific functional groups, synthetic pathways, or biologically hostile environments. [101] For this reason, the development of biocompatible and versatile linkers for surface engineering of implants has been a major objective in biomaterials science. [105-107] Inorganic binding peptides offer an attractive alternative to achieve this objective due to their strong binding, inherent non-toxicity, and ease of fusion with other functional proteins and peptides.

Here we have chosen glass, titanium, gold and platinum as model materials to showcase the versatility in the potential use of the peptide-based surface modification platforms. Noble metals have been the material of choice in many biomaterial applications because of their excellent corrosion resistance, mechanical properties and relatively good biocompatibility. They have been widely used in dental implants, stents and tube plating, wiring for electronic implants, and pacemaker electrodes. [85, 108]. Glass- and titanium-based materials have found utility mostly in

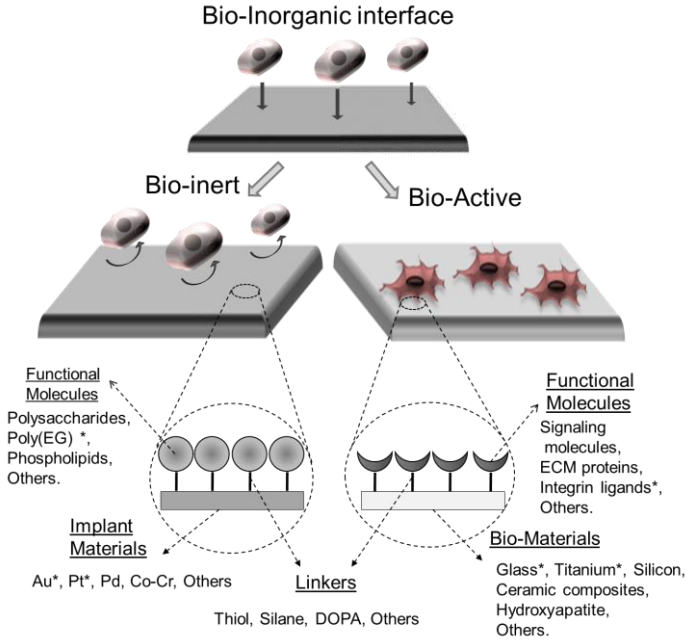

Figure 9. (A) Schematic representation of common approaches for modification of biomaterial surfaces with functional molecules. The functional molecules and materials used in this study are marked with "*"

D. Khatayevich, M. Gungormus et al Acta Biomaterialia (2010)

orthopedic implants. They have been used as bone grafts and coatings for metal implants to improve osteointegration and as bone replacement due to their mechanical properties and excellent stability. [109] Depending on the material, implantation site and intended function, certain devices may call for increased tissue integration rather than a bio-inert behavior, or *vice versa* **(Figure 9)**. For example, applications involving noble metals, such as stents and pacemaker electrodes, often require minimum interaction with the biological environment. By contrast, orthopedic applications of oxides, glasses and glass-based composites favor increased cyto-compatibility to promote hard tissue integration. [88, 110]

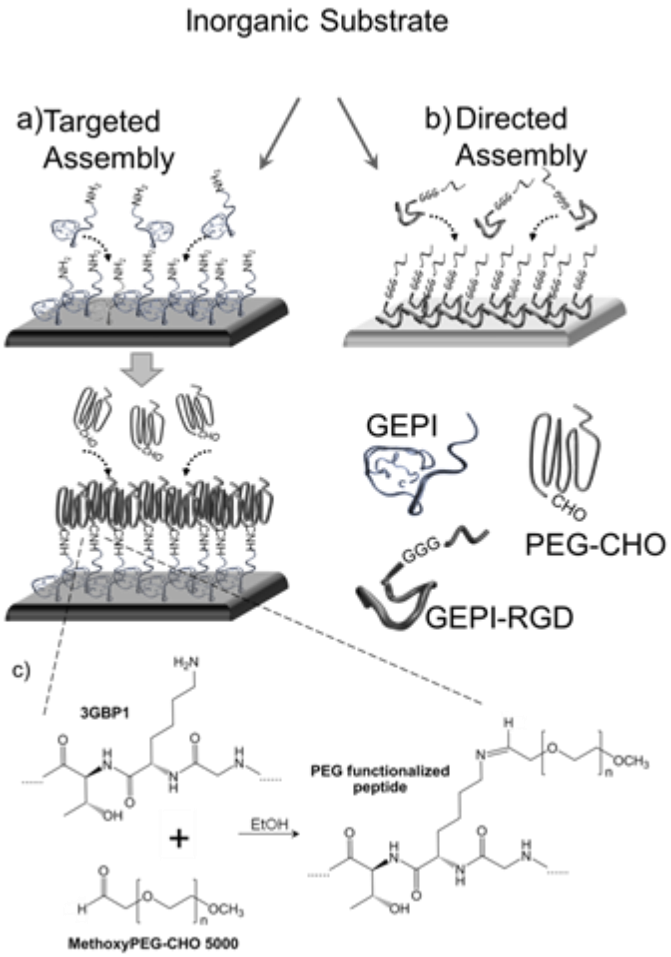

Figure 10.. Schematic representation of surface modification using GEPIs via targeted assembly (a) via functionalization reaction of the free amine groups on the peptides by PEG-CHO, and single step directed assembly (b).

D. Khatayevich, M. Gungormus et al Acta Biomaterialia (2010)

We used an engineered gold binding peptide (3GBP1) [4] and a platinum binding peptide (PtBP1)[10], developed in our laboratories, to generate bio-inert gold and platinum surfaces, respectively. By exploiting the primary amine groups present on the peptides, we covalently bound aldehyde-terminated poly(ethylene glycol) (PEG-CHO) to

the peptides on the surface through targeted assembly **(Figure 10a)**. Water contact angle and cell adhesion assays show that the PEG density and functionality achieved are comparable to surfaces prepared via conventional immobilization methods, such as covalent thiol binding. [95, 111] Similarly, we used a quartz binding peptide (QBP1) and a titanium binding peptide (TiBP1) to generate glass and titanium surfaces with enhanced cyto-compatibility. To this end, we synthesized bi-functional QBP1-RGD and TiBP1-RGD peptides via solid phase peptide synthesis, and immobilized these peptide conjugates on the surface through directed assembly in a single step (Figure 10b). Cell adhesion and spreading assays have shown that the QBP1 and the TiBP1 facilitate the immobilization of RGD on both surfaces while preserving its functionality as a recognition site for the cells. The sequence information and the physicochemical properties of all the inorganic binding peptides and their bi-functional combinations used in the current study are provided in **Table 2**.

Table 2: Amino acid sequences and the physico-chemical properties of the peptides used in the study.

Peptide	Amino Acid Sequence	pI	GRAVY	M.W.	Net Charge
GBP1	NH_2-**M**H**G**KTQ**A**TSGT**I**QS-OH	8.52	-0.743	1446.6	+1
3GBP1	NH_2-(**M**H**G**KTQ**A**TSGT**I**QS x 3)-OH	10.30	-0.743	4303.7	+3
PtBP1	NH_2-CSQS**V**TSTKSC-OH	8.47	-0.867	923.9	+1
AuBP1	NH_2-**WAGA**KR**L**V**L**RRE-OH	11.71	-0.567	1454.7	+3
AuBP2	NH_2-**WAL**RRS**I**RRQSY-OH	12.00	-1.267	1591.8	+4
3AuBP1	NH_2-(**WAGA**KR**L**V**L**RREx3)-OH	12.10	-0.567	4328.1	+9
3AuBP2	NH_2-(**WAL**RRS**I**RRQSYx3)-OH	12.30	-1.267	4739.4	+12
QBP1	NH_2-**PPPWLP**Y**MPPW**S-OH	5.95	-0.650	1467.7	0
QBP1-RGD	NH_2-**PPPWLP**Y**MPPW**S**GGG**R**G**DS-OH	6.26	-0.958	2054.3	0
TiBP1	NH_2-R**P**RENR**G**RER**GL**-OH	11.82	-2.633	1495.6	+3
TiBP1-RGD	NH_2-R**P**RENR**G**RER**GLGGG**R**G**DS-OH	11.70	-2.211	2082.2	+3
RGD	NH_2-**G**R**G**DS-OH	5.84	-1.920	490.4	0
PEG				~5000	

The non-polar residues are displayed with bold characters. The pI indicates the theoretical isoelectric points and the GRAVY indicates the calculated grand average of hydrophaticities of the peptides.

Bio-inert modifications

The surfaces were prepared by sequential incubation of sputtered gold and platinum substrates with 3GBP1 and PtBP1 solutions respectively, followed by incubation with the PEG solution. The surface adsorption and uniformity of PEG on gold were monitored by AFM and contact angle measurements over a range of assembly conditions. The AFM characterization showed a uniform distribution without agglomeration of the polymer on the surface under optimal experimental conditions **(Figure 11 a and b)**. The contact angle measurements confirmed that the gold and the platinum surfaces were successfully functionalized with PEG through GEPIs. No significant changes in contact angle were observed on the surfaces incubated with PEG-CHO alone with respect to the unmodified negative control: about 60 degrees for gold and 48 degrees for platinum (Figure 11c). The adsorption of the peptides alone

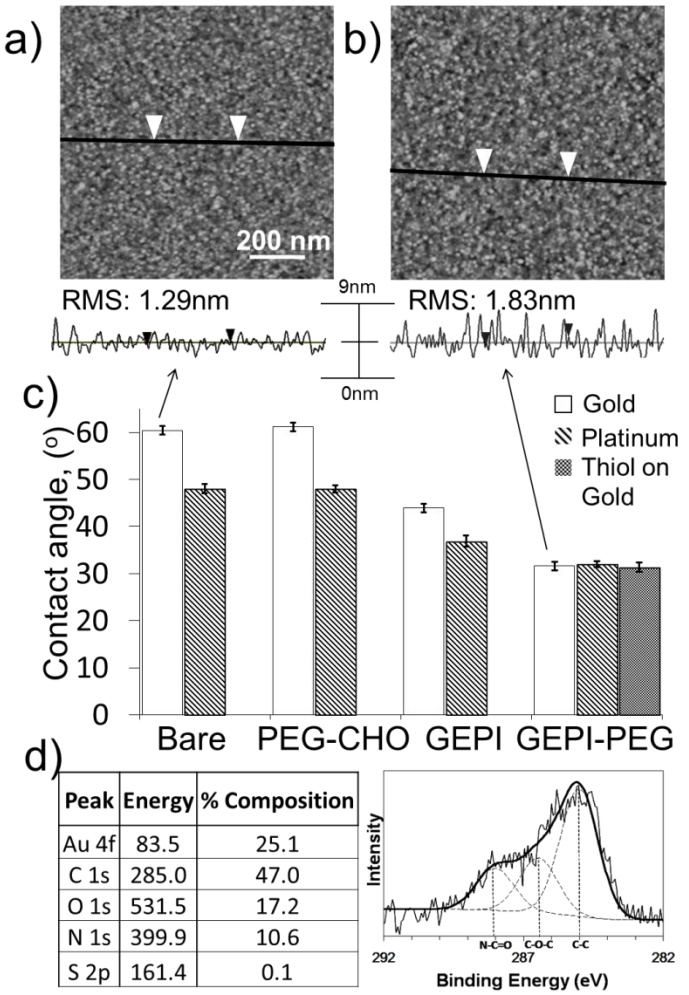

Peak	Energy	% Composition
Au 4f	83.5	25.1
C 1s	285.0	47.0
O 1s	531.5	17.2
N 1s	399.9	10.6
S 2p	161.4	0.1

Figure 11. AFM micrographs and section analysis of a bare (a) and a GEPI–PEG modified (b) gold surface. The size bars correspond to 100 nm. (c) Water contact angles on gold and platinum surfaces after treatment with PEG-CHO alone, GEPIs alone and PEG-CHO conjugated via GEPIs. Thiol-OEG on gold is shown as a positive control. (d)High resolution XPS analysis of the carbon photo-electron emission spectrum ofGEPI–PEG modified substrates.

D. Khatayevich, M. Gungormus et al Acta Biomaterialia (2010)

on the surfaces resulted in about a 25% decrease in the contact angles. This decrease is consistent with the abundance of hydrophilic and polar residues in the peptides (Table 2). The conjugation of PEG with immobilized 3GBP1 and PtBP1 further decreased the contact angles to about 32 degrees for both surfaces. This value is consistent with those reported in the literature and reproduced in this study for OEG immobilized on gold through thiols. Additionally, high resolution XPS analysis of the carbon photo-electron emission spectrum of peptide–PEG modified substrates showed the presence of both amide –CO–NH– groups indicative of the peptide and –C–O–C– groups indicative of PEG (Figure 11d). The gold and platinum surfaces modified with peptide–PEG conjugates exhibited a significant decrease in the non-specific adhesion of NIH 3T3 cells as compared with the unmodified controls. After 2 h incubation with cells in serum-free conditions, and subsequent washing, less than one cell mm–2 was observed on the GEPI–PEG modified surfaces, while 100-fold higher non-specific adhesion was observed on the control surfaces **(Figure 12).** Similar results were obtained with OCCM-30 cells (Not shown). As shown in Figure 12e, the difference between the number of cells per unit area on both the bare and peptide-only surfaces was negligible.

The stability of the 3GBP1–PEG system was also tested in the presence of 1% FBS and 24 h cell incubation. The rich variety of proteins in the FBS provides an environment similar to in vivo conditions by introducing possible peptide–protein, PEG–protein or surface–protein interactions. As expected, the presence of FBS increased the number of cells attached 1.5- to 3-fold in all of the samples compared with the serum-free conditions. This increase was due to the interaction of serum proteins with the material surfaces, which in turn created a more compatible surface for the attachment of cells. The increase in cell attachment on the GBP–PEG modified substrates, however, was still negligible compared with the negative controls. The average number of the cells attached to the 3GBP1–PEG surfaces was 3.1 ± 0.75 cells mm^{-2}, while about 50-fold higher cell attachment was observed on the negative control surfaces. From this observation it can be deduced that the 3GBP1–PEG layer not only resists the adhesion of cells, but also the adsorption of

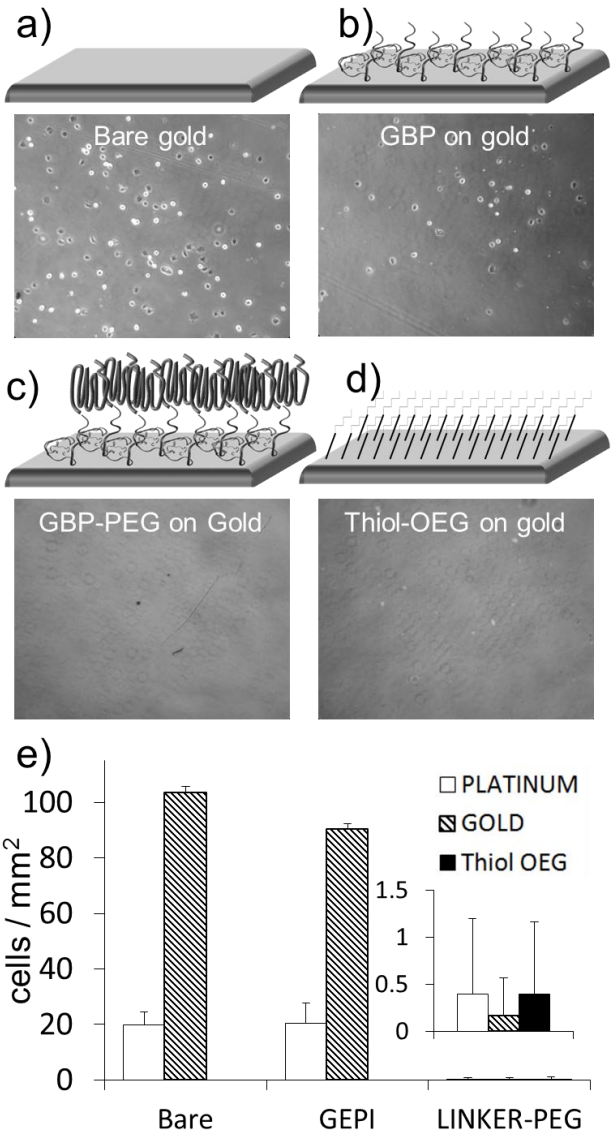

Figure 12. (a–d) Optical microscopy images of NIH 3T3 cells remaining after washing on modified and unmodified gold substrates. (e) The number of NIH 3T3 cells per area remaining after washing on modified and unmodified gold and platinum surfaces.

D. Khatayevich, M. Gungormus et al Acta Biomaterialia (2010)

serum proteins. SEM analysis showed that the 3GBP1–PEG layer was still stable after 24 h cell incubation in 1% FBS. After 24 h the cells on the bare gold surface displayed the typical fibroblast morphology, with some of the cells displaying clustering rather than a homogeneous distribution (Figure 12a). On the 3GBP1–PEG modified surfaces no additional cell adhesion was observed at 24 h. Energy-dispersive X-ray spectroscopy (EDXS) analysis confirmed that the PEG layer was still present on the surface with a prominent carbon peak (Figure 11d). Additionally, we have attempted to achieve PEG conjugation on gold with two other gold-binding peptides (AuBP1 and AuBP2) selected via bacterial cell surface display. Although all of these peptides have demonstrated selective affinity for gold, conjugation of PEG with AuBP1 and AuBP2 did not result in a sufficient decrease in the water contact angles **(Figure 13)**. This may be due to the fact that AuBP1 and AuBP2 are much smaller in size (12 a.a.) compared with 3GBP1 (42 a.a.), facilitating conjugation with PEG. To test this possibility, we prepared a single repeat of GBP1 and triple tandem repeats of AuBP1 and AuBP2 (3AuBP1 and 3AuBP2) and attempted PEG functionalization as described above. As expected, the triple repeat 3AuBP2 resulted in better coverage compared with the original peptide, but not 3AuBP1. The failure to achieve complete coverage with both the original and the triple repeat of AuBP1 implies that the conjugation

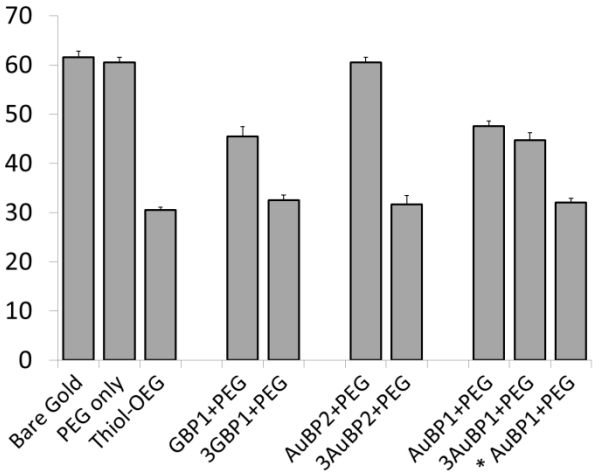

Figure 13. Water contact angles of the gold surfaces modified with single and triple tandem repeats of the three different gold-binding peptides, GBP1, AuBP1 and AuBP2.

D. Khatayevich, M. Gungormus et al Acta Biomaterialia (2010)

of PEG with lysine residues impairs the stability of the peptide on the surface. The lysine residues may be essential for binding, either by directly interacting with the surface or by contributing to the structural stability of the peptide on the surface. To investigate this hypothesis, we selectively conjugated PEG-CHO with AuBP1 while the primary amine on the lysine residue was protected and only the N-terminal primary amine was available. In this way, conjugation can only occur through the primary amine at the N-terminus. As expected, selectively conjugated AuBP1 resulted in a contact angle comparable with the positive controls (Figure 13).

The differences in the degree of functionalization with different peptides indicate that both the relative size of the peptide and the number of available groups suitable for conjugation are important factors governing the extent of surface functionalization. Since combinatorial selection against a surface usually produces not only one but a set of multiple peptides for the target surface, one can select the most suitable peptide for the desired application among the set of peptides, as demonstrated here.

It is interesting that PtBP1 does not obey this generalization. Despite the relatively small size of the peptide compared with the PEG molecule, sufficient conjugation and coverage was achieved without the need for a tandem repeat of the peptide. This may be due to the constrained nature of the peptide. The disulfide bridge between the cysteine residues introduces a structural constraint and, therefore, increases the stability of the peptide. Constrained peptide architecture, in turn may render the peptide less susceptible to steric effects.

Bio-active surface modification

Cellular adhesion and spreading was evaluated on titanium and glass surfaces using NIH 3T3 mouse fibroblasts in the absence and presence of serum proteins to assess the cyto-compatibility of the surfaces. The glass and titanium surfaces were prepared in a single incubation step by placing them into the QBP1-RGD and TiBP1-RGD solutions respectively. Adhesion of the NIH 3T3 cells to glass and titanium surfaces modified with RGD chimeric peptides were increased by 3.5- to 5-fold in serum-free and 2-fold in 1% FBS conditions, compared with negative controls **(Figure 14 a and b)**. A decrease in adhesion was observed especially on glass surfaces incubated with RGD alone in serum-

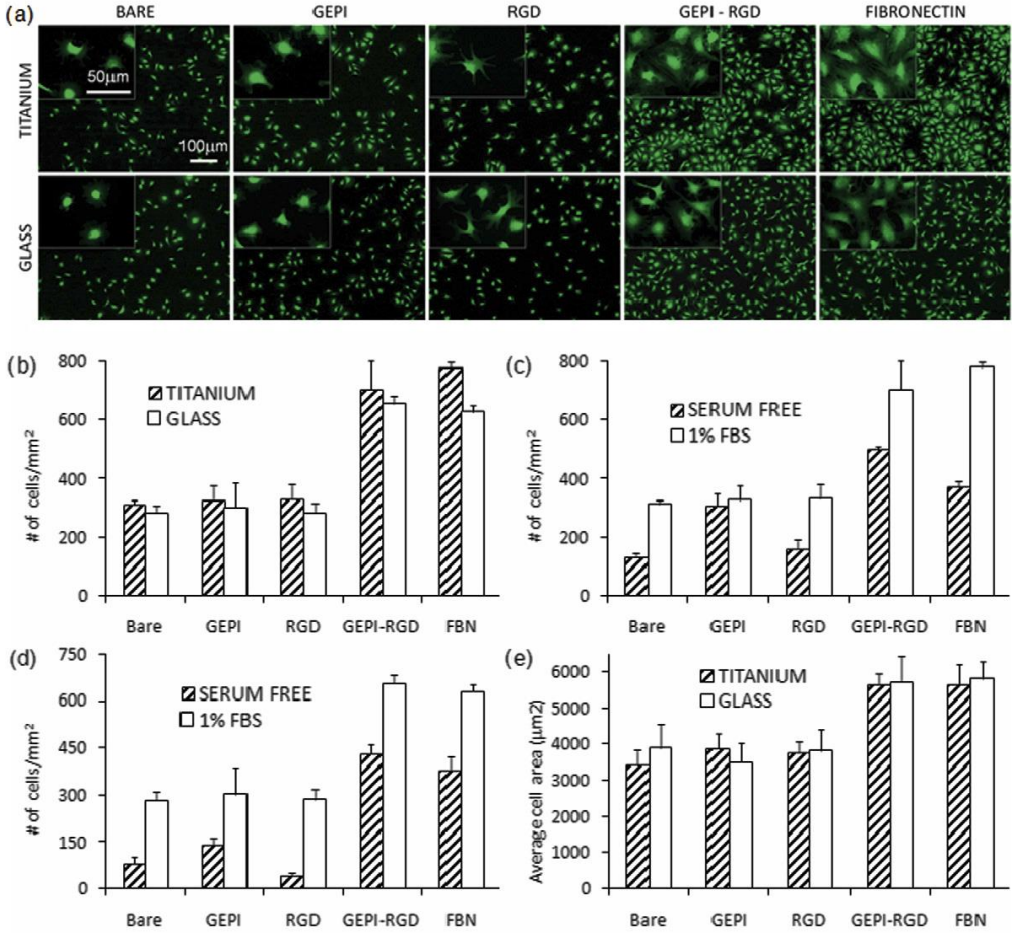

Figure 14. (a) FM micrographs of phalloidin stained NIH 3T3 cells on glass and titanium surfaces. (b) The number of adhered NIH 3T3 cells per mm2 in the presence of 1% FBS. The comparison of cell adhesion in serum-free and 1% FBS conditions on the titanium (c) and glass (d) surfaces. (e) Average cell spreading on titanium and glass surfaces in the presence of 1% FBS.

D. Khatayevich, M. Gungormus et al Acta Biomaterialia (2010)

free conditions. Such a decrease may originate from the dissociation of non-specifically adsorbed RGD peptides from the surface into the medium. The unbound RGD in the medium may then interact with the RGD-binding sites on the integrin receptors and act as an integrin antagonist to prevent further cellular interactions with the surface. Conversely, a slight increase in adhesion was observed on the surfaces modified with QBP1 and TiBP1 alone. Although within the margin of error, this effect may be due to the inherent chemical properties of the peptides. The abundance of non-polar residues in the peptides (Table 2) is likely to result in an increase in the hydrophobicity of the glass surface. Contact angle measurements showed that QBP1 indeed resulted in a 19% increase to a value of 46 degrees compared with bare glass. Consequently, when amphiphilic molecules on the cell membrane, such as proteins, interact with the non-polar residues an increase in non-specific adsorption on the surface may be observed. As opposed to serum-free conditions, no significant differences in adhesion were observed between the three negative control surfaces (Bare, GEPI alone and RGD alone) in 1% FBS conditions. Cell coverage on all of the control surfaces was about 300 cells mm–2. Adsorption of serum proteins on the surfaces rendered the control surfaces cytocompatible. On the peptide–RGD modified surfaces, however, a combined effect of the serum proteins and the bifunctional peptides was observed. The number of cells increased by 30– 35% in the presence of serum proteins on GEPI–RGD modified surfaces relative to the serum-free conditions (Fig. 14c and d).

In tissue engineering applications the integrin ligands were not only used to modify surfaces for increased cell adhesion but also for enhanced cell viability and function. To test whether the RGD chimeric peptides resulted in any enhancement in cell viability, cell

spreading was evaluated in addition to cell adhesion. ImageJ image processing software (NIH) was used to analyze cell spreading. An increase of about 1.6-fold in cell spreading was observed on both materials modified with chimeric RGD peptides compared with bare surfaces (Fig. 14e). A similar increase was observed on fibronectin modified surfaces. The results indicate that the presence of both material binding and RGD domains in the designed bifunctionalmolecular construct is necessary to promote cell adhesion and proliferation.

2.3 Modular Bio-sensor Design

In designing a biosensor, it is desirable to be able to easily adapt the system to detect a variety of targets. For example, functional tissue patterning in multicellular organisms relies on cell-cell interactions specifying cell fate. Proper stomatal patterning is critical for plant productivity and survival. Genetic studies in Arabidopsis have suggested that secreted peptides, EPFs, are recognized by cell-surface receptors with extracellular leucine-rich repeat (LRR) domains, ERECTA-family LRR-receptor kinases (LRR-RKs) and TMM LRR-receptor-like protein (LRR-RLP), to enforce stomatal patterning. One of the methods by which we quantified the ligand receptor interactions *ex situ* was through detection of ligand binding to immobilized receptors on SPR and QCM biosensor platforms. The specifics of the implications of our measurements are not relevant, but the sensor design can give insight into the proper approach to designing the cancer probing device.

Objective: To create a sensor functionalization procedure to detect a variety of ligand-receptor interactions from a complex solution of peptides.

The preparation of sensors was as follows: Gold-coated QCM and SPR slides were incubated with anti-GFP in phosphate (non-specific adsorption). The surfaces were then blocked in a 2 % bovine serum albumin (BSA) solution to minimize nonspecific interactions. The resulting samples were incubated with a membrane fraction of either control (GFP only) or receptor-GFP construct solution and additional BSA blocking to yield receptor-immobilized biosensor chips **(Figure 15)**.

Purified, bioactive MEPF1 and MEPF2 peptides were used to perform ligand-receptor binding assays using biosensor platforms of QCM (quartz crystal microbalance) and SPR (surface plasmon resonance). For both techniques, we first immobilized purified ERECTAΔK-GFP, ERL1ΔK-GFP TMM-GFP, or control GFP from *N. benthamiana* on gold surfaces via anti-GFP antibody linkages and then introduced the purified MEPF-His peptide solutions.

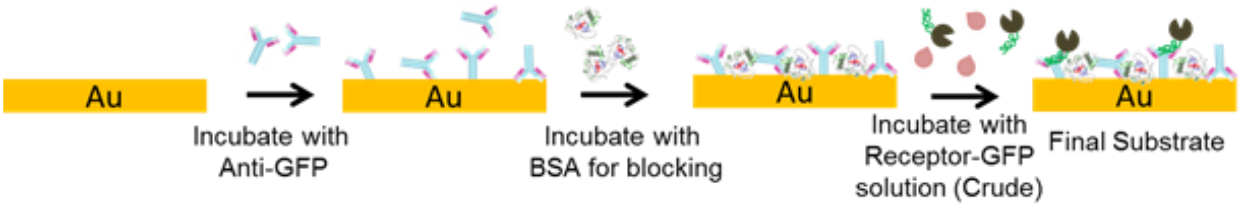

Figure 15. Fabrication of biosensors for ligand-receptor interaction detection
J. S. Lee, et al, Genes and Development (2012)

Robust binding of MEPF1 and MEPF2 to the ectodomain of ERECTA and ERL1 was detected as a function of frequency change (for QCM) or the shift in surface plasmon resonance wavelength (for SPR). Based on the SPR sensorgrams, the binding of MEPF1 to both ERECTA and ERL1 was rapid, saturable and in similar kinetics. The QCM data supports this observation. By contrast, no obvious binding of MEPF1 to TMM-GFP or control GFP was detected by either SPR or QCM. MEPF2, unlike MEPF1, exhibited binding to TMM in addition to ERECTA and ERL1. The apparent affinity difference for TMM by MEPF1 and MEPF2 was consistently detected in three different methods.

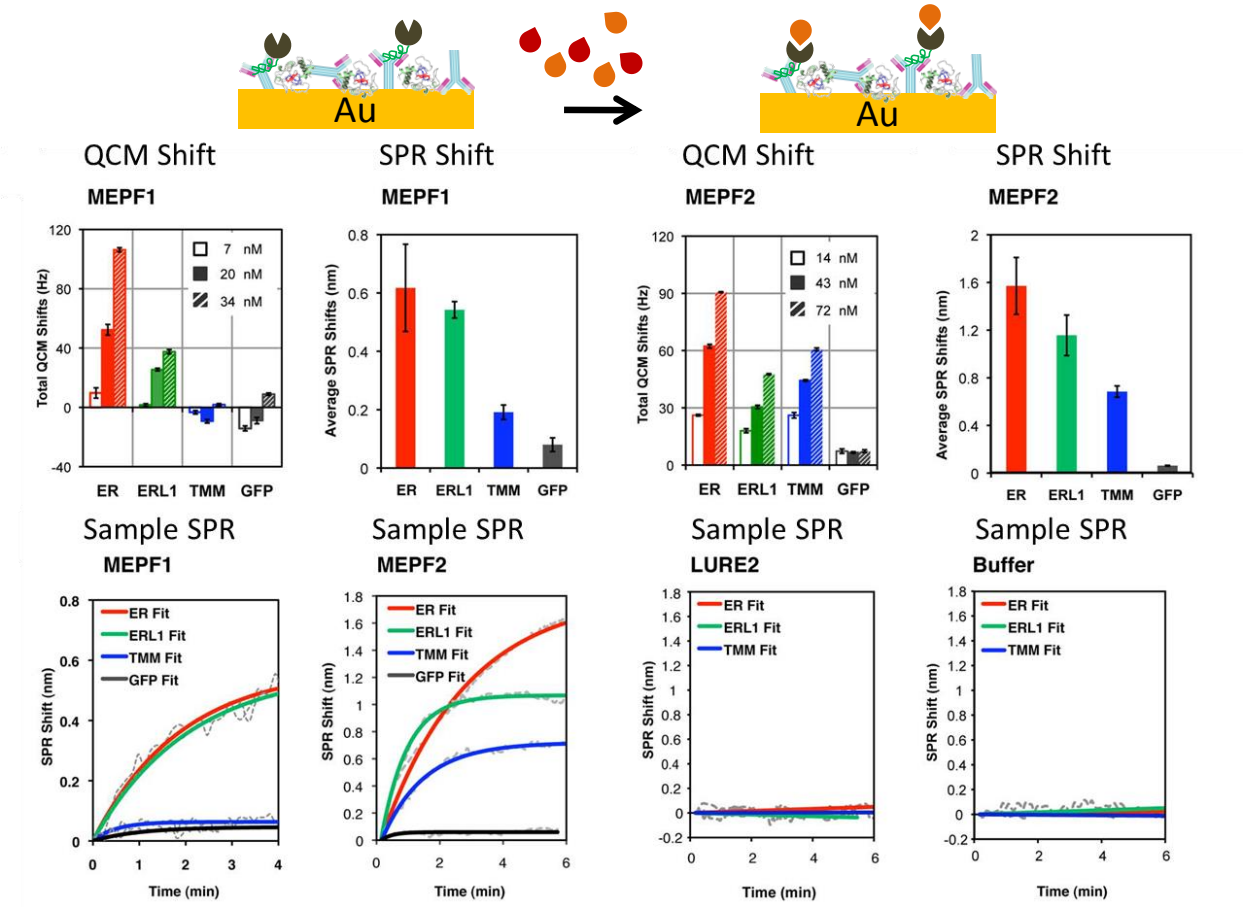

Figure 16. SPR sensograms and overall shifts, with corresponding to the QCM results of MEPF-1 and -2 ligands interacting with ER, ERL1, and TMM receptors. Lure and Buffer given as controls.

Additionally, we detected a difference in the binding kinetics of MEPF2 to ERECTA and ERL1, with ERECTA having higher saturation **(Figure 16)**.

To address the specificity of ligand binding, we further performed SPR analysis using a similar, but unrelated peptide LURE2. LURE2 showed no binding to ERECTA, ERL1, or TMM with the same tested condition (300 nM of total refolded peptide solution), and its sensorgram was identical to buffer-only control. Furthermore, heat denaturation of MEPF1 and MEPF2 severely compromised their binding to receptors. Together, the results demonstrate specific, direct binding of bioactive MEPF peptides to the ERECTA-family RKs as well as their differential binding to TMM (Figure 16).

2.4 Controlling the Surface Chemistry of Graphite by Engineered Self-Assembled Peptides

In the above experiments we have demonstrated that solid-binding peptides can be employed for functionalization and passivation of surfaces, and that a modular bio-sensor system can be created by substitution of antibody-bound probes. In the subsequent experiments we apply these principles to graphitic materials and the graphene nanobio-sensor.

Controlling interfacial properties of materials through surface functionalization of solid substrates has been a major challenge in medicine and nanotechnology for the last two decades.[112, 113] The precise display of function and chemistry is particularly critical for engineering bio-inorganic interfaces, where the orientation and density of the immobilized molecules may have direct bearing on the performance of the resulting assembly, such as, for example, the specific activity of immobilized enzymes.[114] As described above,

solid binding peptides are extremely well suited for surface functionalization and display due to their strong binding, chemical diversity, modular capacity and biologically friendly processing. Rather than covalent bonding, prevalent in synthetic linkers, such as silanes, thiols, and phosphanates, short peptides bind through weak forces at multiple positions along the peptide/solid interface with the advantage of assembling and functioning in aqueous solutions.[6, 115] As biocompatible coatings, therefore, solid-binding peptides are particularly well suited for applications in medical and biological fields because they are produced and function under biological conditions, and have not shown any toxicity in cell culture studies.[17, 18]

Graphite, graphene and carbon nano-tubes (CNT) have been employed for both biomedical and nanotechnological applications due to their anti-microbial activity, high conductivity, optical transparency, and surface sensitive properties.[53-55, 116, 117] These graphitic materials have been employed for biosensing applications in particular due to their excellent electronic properties, resulting from delocalized π bonds on the surface.[118-120] A number of functionalization routes through covalent bonding, i.e. the introduction of carboxylic groups, have been employed to control the interface with graphitic materials.[121, 122] In parallel, however, to preserve the intrinsic properties of these materials, methods of non-covalent functionalization via π–π stacking using aromatic chemistry have been used to assemble functional molecules.[123, 124] In addition to these successful chemical functionalization techniques, a non-invasive approach using peptides could present a biocompatible alternative to controlling the surface properties of graphite. Here, we demonstrate precise control over the hydropathy of graphite through single-step self-assembly of peptides and their engineered mutants.

The graphite binding peptides are modular and can be designed to self-assemble into stable monomolecular films on graphite, exposing predictable surface chemistry through the display of specific amino acids. The highly oriented pyrolytic graphite (HOPG) has an atomically flat surface which is ideally suited to demonstrate, using atomic force microscopy and contact angle measurements, the display of tailored chemistries on graphite through controlling the binding and assembly of the designed peptides, in the absence of roughness effects.[125]

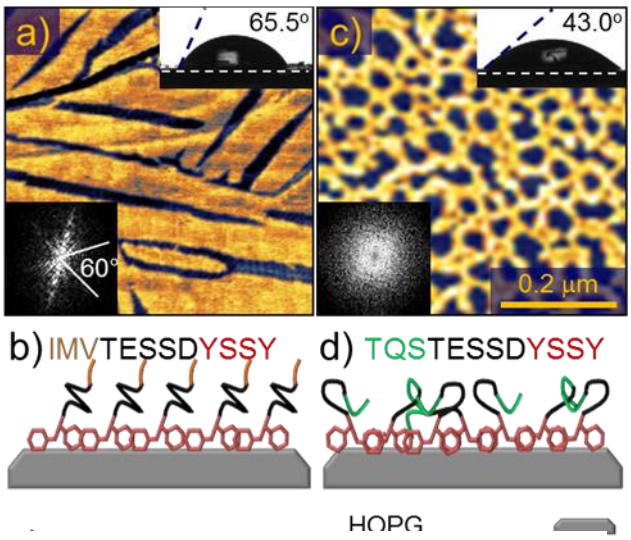

Figure 17. (a) Atomic force microscopy (AFM) image of the peptide GrBP5-WT on graphite with (b) Corresponding sequence (N- to C-terminus) and schematic. (c) AFM image of GrBP5-Phil mutant on graphite with (d) Corresponding sequence and schematic. Insets show the contact angles and the Fast Fourier Transforms of the images to highlight presence or lack of ordering. Schematics (b), (d) and (e) Illustrate the hypothetical conformation of the peptides within the film which produce the observed contact angles, binding through the aromatic region and displaying either the ordered hydrophobic or disordered hydrophilic residues.

D. Khatayevich, et al. Langmuir (2012)

Various graphite-,[126] graphene-,[127-129] and CNT-binding [130, 131] peptide sequences and poly amino acids have been identified in literature. They have been employed for applications such as bioinorganic nano-structure formation,[132] as well as non-specific control of surface chemistry.[127]

The dodecapeptide used in this work, GrBP5-WT (Sequence: IMVTESSDYSSY, affinity constant: Ka=3.78µM-1) [133] is unique among graphite- and CNT-binding peptide sequences identified so far, as it forms long-range ordered, uniform, and crystallographic

molecular nanostructures on HOPG **(Figure 17a)**, which can be controlled through sequence mutation. The abbreviation WT denotes the original, unmodified, sequence of the peptide, which we call “wild type”. In previous work,[133] it was found that the self-assembly of GrBP5-WT arises from a combination of binding through the aromatic rings of tyrosine residues at the C-terminus, and ordering through intermolecular interactions among hydrophobic tail domains (Figure 17b). The formation of ordered morphology, apparent from Figure 17a, and evidenced by the FFT, seems to be a result of both lattice matching with the underlying HOPG, which results in six-fold symmetry and assembly conditions, such as concentration, which, along with intermolecular interactions, determines the size of features.[133] Replacing the hydrophobic residues at the N-terminus with hydrophilic ones, therefore, inhibits formation of the ordered phase (OP) and causes the peptide film to remain in the amorphous phase (AP) because of the lack of intermolecular interactions (Figure 17c and d). Furthermore, it was found that an ordered film of GrBP5-WT displays hydrophobic property on the graphite surface (Figure 17a). These findings motivated us to hypothesize that ordered structures of GrBP5-WT leave the N-terminus amino-acids free for rational control of intermolecular interactions as well as further functionalization, and predictable display of specific chemistry. Based on this hypothesis, we aim here to demonstrate that the wettability of graphite can be controlled by varying the N-terminal sequence of the GrBP5-WT peptide. Specifically, we design two mutants (i.e., variants of the WT peptide) which exhibit hydrophobic or hydrophilic properties while retaining their ordered structure and predictable display capability. The hydrophobic mutant GrBP5-Phob is produced by substitution of the three N-terminal amino-acids of the wild type with a more hydrophobic LIA sequence **(Table 3)**.

The hydrophilic hybrid mutant SS-GrBP5 (Figure 17e, Table 3), on the other hand, is designed by the addition of two hydrophilic serine residues to the N-terminus of the wild type peptide.

To characterize the wettability of the peptide-functionalized graphite surfaces, freshly cleaved HOPG substrates were incubated in 1μM aqueous peptide solutions (Table 3) for several time intervals, resulting in samples of peptide films on the graphite surface that range from sparse to near-confluent monolayers. The wettability of these films was quantified by contact angle goniometry, and the coverage was determined by atomic force microscopy (AFM) The plot of contact angle vs. coverage values exhibits a coinciding linear correlation below 70% coverage for all peptides **(Figure 18a, red)**, meaning that the contact angle contribution of the peptides in the amorphous phase does not depend on sequence. Above 70%, they also display linear relationships but with slopes that vary greatly with sequence (Figure 18a, blue). To quantitatively compare the wettability of different peptides, we applied Cassie's Law,[137] which describes the contact angle, cos θ, of a macroscopic droplet on a chemically heterogeneous surface via the relation: cos θ = ϕg cos θg + ϕp cos θp (ϕg,p : coverage and θg,p : contact angle for graphite and peptides, respectively). By fitting this equation to the experimental data, effective contact

Table 3. Peptide sequences, weights, and hydropathy indices

Peptide	Sequence	Mol. Mass	G.R.A.V.Y.[a]
GrBP5-WT	IMV-TESSDYSSY	1381.4	-0.242
GrBP5-Phob	LIA-TESSDYSSY	1335.3	-0.283
GrBP5-Phil	TQS-TESSDYSSY	1354.3	-1.542
SS-GrBP5	SSIMV-TESSDYSSY	1555.6	-0.321

[a] Grand average hydropathy index

angles are extrapolated for fully covered surfaces of each peptide, θp, (**Table 4**). Between 0 and 70% coverage, all peptides display little difference in θp (about 28°±4°). The θp

values above 70% coverage of GrBP5-WT and GrBP5-Phob, however, are drastically different.

These results are also reflected in the corresponding AFM experiments (Figure 18b) where peptides are observed to form one of the two phases on the surface: either a long-range ordered phase (OP) at high coverage, exhibiting six-fold symmetry, or a sparse amorphous phase (AP) at low coverage without recognizable crystallographic symmetry in the formed film. There is an transition threshold from AP to OP at about 70% coverage. Ordered peptide films also exhibit more uniform and narrow distributions of thickness as measured by AFM , which is apparent from the average roughness values in Table 4 Only GrBP5-Phil, with no hydrophobic tail, remained disordered under all incubation conditions.

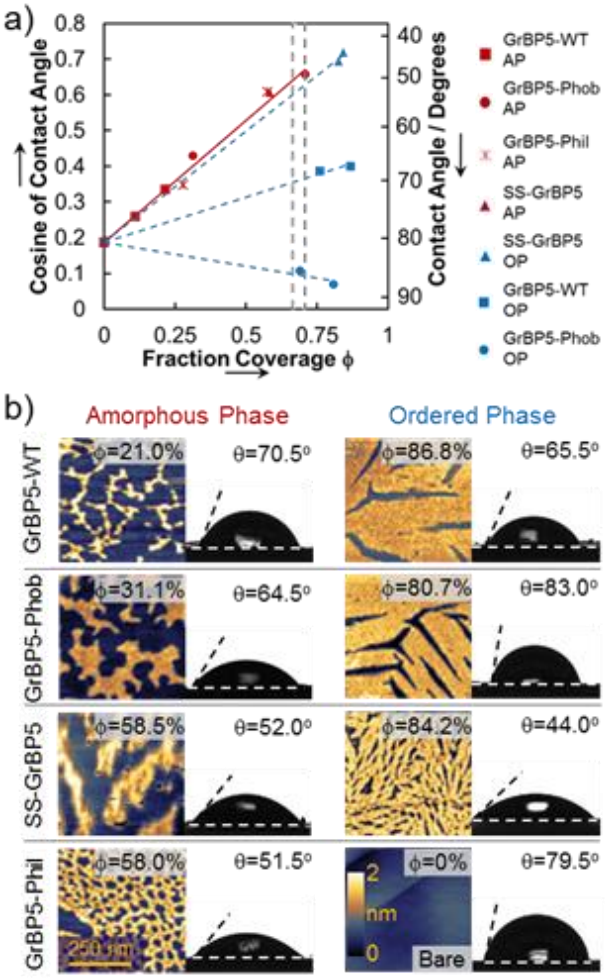

Figure 18. (a) Plot of contact angle θ versus fraction coverage ϕ of peptides on graphite. The blue lines indicate linear trends above 70% coverage; the red line represents the linear trend for all peptides below 70% coverage. The change in slope between ordered (OP) and amorphous (AP) trend lines indicates the change in the displayed chemistry. The grey lines indicate the AP to OP transition region (b) AFM images showing typical examples of AP and OP structures, as well as the corresponding coverage and

Table 4. Projected contact angles of a theoretical 100% peptide-covered sample for each peptide and phase, and corresponding measured roughness values.

Peptide	θ_p AP (0-70% coverage)	AP Roug. nm	θ_p OP (>70% coverage)	OP Rough. nm
GrBP5-WT	30.0°±2.5°	0.92	64.0°±1.0°	0.39
GrBP5-Phob	23.0°±11.5°	0.53	87.0±0.5°	0.36
GrBP5-Phil	32.0°±12.0°	0.72	No Order	No Order
SS-GrBP5	25.5°±5.5°	1.20	36.0°±1.0°	0.34

The similarity in the θp contact angles of all peptides in the AP below 70% coverage may indicate that the exposed amino acid domain is conserved among mutants and is predominantly hydrophilic. This is most likely due to the random alignment of peptides displaying polar residue- and a serine-rich domain in the central portion of the peptide (Table 3). Conversely, the contrast between the contact angle contribution of GrBP5-WT (64.0°) and GrBP5-Phob (87.0°) in the OP implies that the three amino-acids at the N-terminus are uniformly exposed towards the solution, since they are the only ones that differ between the two peptide sequences.

Both the binding and ordering capabilities of the peptides were retained in the SS-GrBP5 mutant (Figure 18). Even in the ordered state, the SS-GrBP5 mutant has a contact angle contribution close to that of the AP (Table 4), indicating that hydrophilic residues are displayed in both of its phases of the peptide films. The difference in the contribution of the two phases, about 9°, confirms a transition from AP to OP, seen clearly in Figure 18, on surfaces functionalized by SS-GrBP5.

The uniform display of N-terminal residues by self-assembling peptides forming confluent ordered films on graphite that appears to be occurring, results in a wide range of wettability values. It is, therefore, plausible to further tune the contact angle through a simultaneous high coverage, single-step, co-assembly of peptides with varying wettability. We chose the two mutants that retained their assembly capabilities and exhibited the widest range of θp, i.e., 36.0° and 87.0°, to achieve precise control over the wettability of graphite surfaces at a constant coverage. For this, 1μM aqueous solutions of GrBP5-Phob and the SS-GrBP5 were mixed in appropriate proportions and incubated on HOPG for 3 hours, assuming the complete solubility of the two peptides solutions. The AFM images and contact angle versus fraction coverage dependencies are shown in **Figure 19**. While the peptide coverage of these films remained at around 80%, the contact angles of functionalized surfaces varied from 44.0° to 83.0°. The linear nature of the plot and the uniformity of the AFM images indicate that GrBP5-Phob is homogeneously dispersed within the film formed by SS-GrBP5. Moreover, by adding a third term to Cassie's equation ($\cos\theta = \phi g \cos\theta g + \phi p_1 \cos\theta p_1 + + \phi p_2 \cos\theta p_2$), we were able to

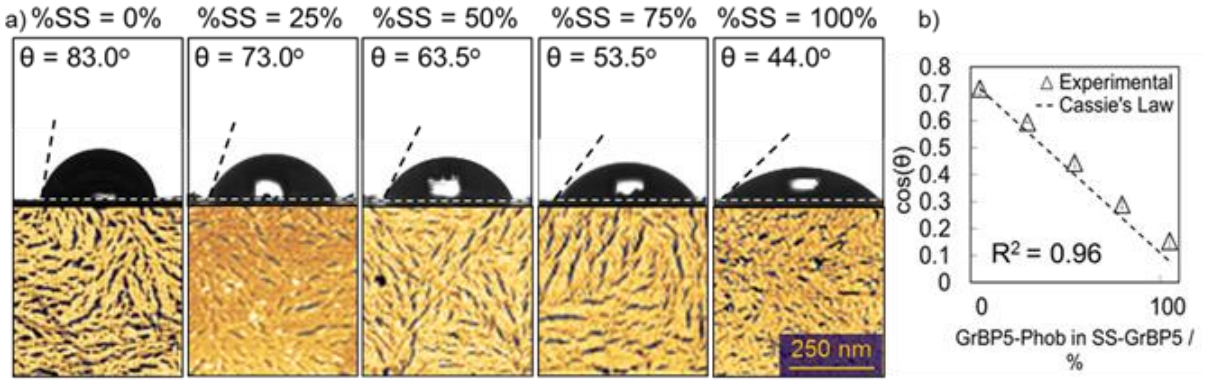

Figure 19. (a) Contact angles and AFM images of ordered co-assembled peptide monolayer containing SS-GrBP5 and GrBP5-Phob. Coverage for all surfaces is greater than 80%. (b) Plot of cosine of the contact angle versus % of GrBP5-Phob mixed in SS-GrBP5 shows agreement with the trend predicted by Cassie's Law.

Khatayevich, et al. Langmuir (2012)

predict the cosine of the contact angle resulting from a given mixed monolayer based on

the θp values from Table 4 (Figure 19). The agreement between the prediction and the data is quite close (Coefficient of determination, based on sum of squares of error is R^2 = 0.96). The small discrepancy in the predicted and measured values could result from a slight variation in the binding affinities of the two peptides, whereby SS-GrBP5 is present on the surface in slightly higher proportion than the GrBP5-Phob under the same incubation conditions.

2.5 Selective Detection of Proteins in Solution via Graphene Sensors Enabled by Self-Assembled Mixed Peptide Monolayer

To turn a 2D-FET into a biosensor, target-specific bioprobes must be immobilized on the sensor‘s surface in a controlled and simple process while, at the same time, preserving the functionality of the 2D sensor substrate. Instead of covalent bonding, prevalent in synthetic linkers, short peptides bind through weak forces at multiple positions at the peptide/solid interface enabling them to assemble and function in aqueous solutions. [6, 115] Solid-binding peptides are particularly well suited for applications in medical and biological fields because they are produced and function under biological conditions, and have not shown any toxicity in cell culture studies.[17, 134] The dodecapeptide GrBP5-WT (Sequence: IMVTESSDYSSY, affinity constant: Ka=3.78μM-1) is unique among graphite- and CNT-binding peptide sequences identified so far, as it forms long-range ordered, uniform, and crystallographic molecular nanostructures on graphitic materials, which can be controlled through sequence mutation **(Figure 20)**.[133] GrBP5-WT is modular and can be designed to expose predictable surface chemistry through the display of specific amino acids, making it ideal

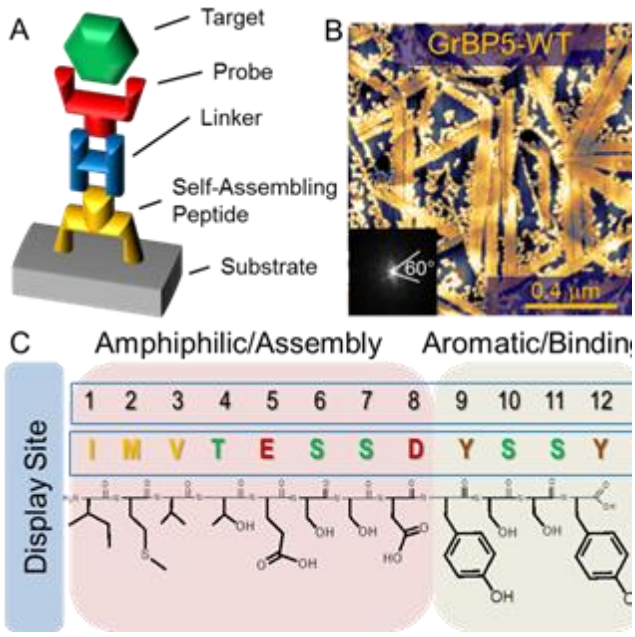

Figure 20. A) Conceptual schematic of the peptide based approach to biosensor functionalization; B) GrBP5-WT image showing the formation of ordered phase; C) sequence and property/function map.

for presenting molecular probes, antibodies, and other sensing molecules in a controllable fashion (Figure 20A). Moreover, it has been shown that two mutants of GrBP5-WT can be simultaneously assembled to display a combination of properties.[135] Multifunctionality is critical to the application of a biomarker sensor in clinical practice, since in addition to possessing sensitivity, it must be capable of discriminating for the target against a background of proteins present in the sample. It is necessary to simultaneously impart the targeting and the anti-fouling capabilities to the sensor.

In the present study, we demonstrate selective detection of a model protein against a background of serum protein using a graphene sensor functionalized *via* co-assembled, multifunctional, self-assembling peptides, which simultaneously display the probe and prevent non-specific adsorption. In particular we employ a 4-probe graphene field effect transistor (gFET) sensor **(Figure 21)**, functionalized using simultaneously co-assembled mutants of GrBP5-WT, displaying biotin, or hydrophilic residues at the N-terminus **(Table 5)**, to detect streptavidin (SA) against a background of bovine serum albumin (BSA). We also develop a regeneration protocol, which allows us to utilize a single sensor for over 12 experiments. Through this study we establish a methodology for single-step bio-

functionalization of graphitic sensors toward sensitive detection of biomolecules, which can be applied to a variety of analytes in complex solutions.

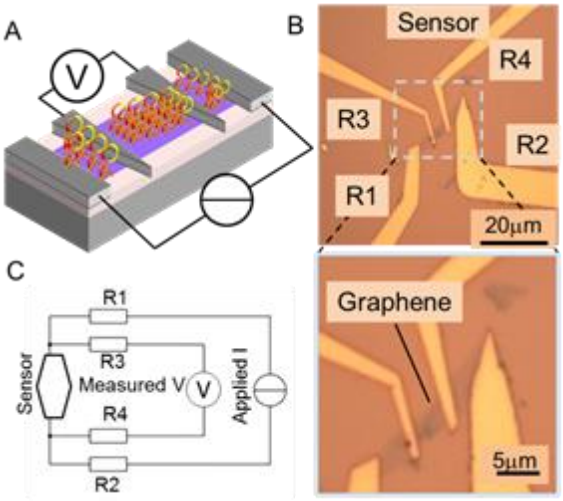

Figure 21. A) Schematic illustration of the four-probe bio-functionalized graphene sensor; B) Optical microscopy image of the sensor device; C) Equivalent circuit of the device.

Additionally, we created a modular probe approach to make the bio-sensor more versatile. By fusing the SS-GrBP5 with an anti-body binding motif, we were able to immobilize anti-maltose binding protein (anti-MBP) on the sensor surface and selectively detect maltose binding protein (MBP) against a background of BSA. The results of this study are discussed in section 4.1

Table 5. Peptide sequences weights and hydropathy indices

Molecule	Sequence	Mol. Mass [g/mol]	G.R.A.V.Y. [a]
GrBP5-WT	IMVTESSDYSSY	1381.4	-0.242
Bio-GrBP5	bio-IMVTESSDYSSY	1624.3	0.185
SS-GrBP5	SS-IMVTESSDYSSY	1555.6	-0.321
Bio-SS-GrBP5	bio-SS-IMVTESSDYSSY	1798.5	0.264

[a] Grand average hydropathy index.

Graphene Biosensor

We fabricated the graphene biosenor, using electron beam lithography, in a four probe configuration (Figure 21). Such configuration is advantageous, because it minimizes the effect of contact resistance on the measurement, increasing the signal to noise ratio. This is accomplished by supplying a constant current via contacts R1 and R2, and monitoring the voltage between the contacts R3 and R4 at negligible currents (Figure 18c).

In order to test the capabilities of the graphene field effect transistor sensor, as well as to ensure that our peptide-based functionalization scheme appropriately displays the probe, we created a biotin-graphite binding peptide (bio-GrBP5) fusion molecule (Table 3). By sequential introduction of increasing concentrations of the peptide to the sensor, we were able to determine the ultimate sensitivity of our system, and to create, what appears from AFM images to be, a dense, uniform monolayer of self-assembled biotinilated peptide **(Figure 22a, c)**. We then introduced streptavidin to the system in sequentially increasing concentrations to determine the sensitivity limit for binding of secondary analyte. The AFM images (Figure 22b), along with the sensogram (Figure 22c) demonstrate binding of streptavidin to the biotinilated sensor. The height difference of about 2nm is observed between the peptide only and the SA added surfaces. Moreover, we found that the sensitivity of our device is between 20 and 50ng/ml, both in the bare and functionalized state. The differences in morphology in the two AFM images

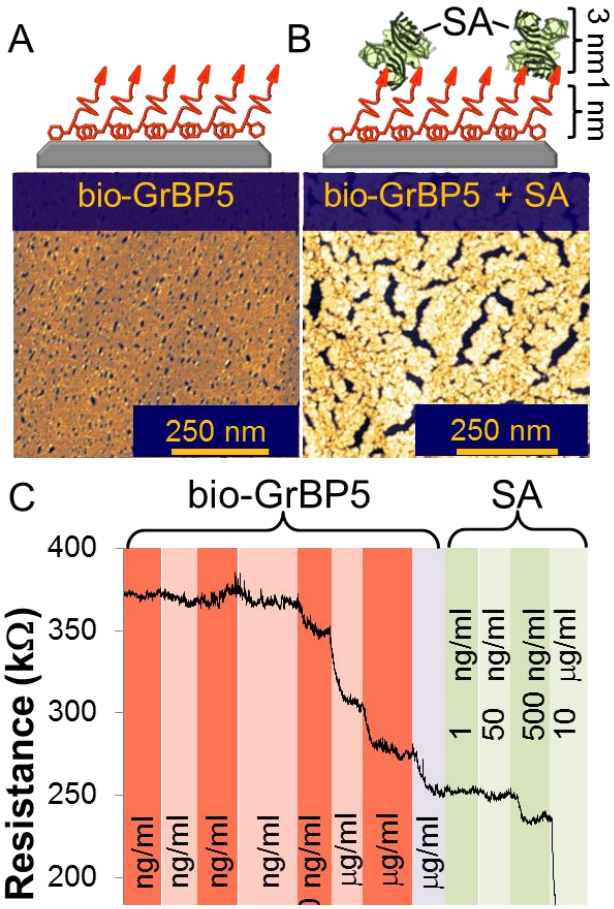

Figure 22. A) AFM image and schematic of 10mg/ml bio-GrBP5 self-assembled on graphite; B) AFM image and schematic of 10mg/ml streptavidin captured by the bio-GrBP5 monolayer; C) Corresponding sensogram of sequential addition of increased concentrations of bio-GrBP5 followed by the sequential addition of increased concentrations of streptavidin.

indicate that there is a certain amount of instability introduced into the peptide by the analyte, however, the coverage remains above 85% after two hours of testing, which is well beyond the time required to achieve apparent binding equilibrium. Additional stability experiments are discussed in section 2.6. As a control, we also tested the binding of SA to the un-functionalized sensor, finding that no detectable binding occurs in the range of concentrations used. The response of our sensor is consistent with that reported previously for graphene-based biosensors.[51, 138] The decrease in resistance in the presence of the biomolecule is explainable through increased doping of the graphene layer by ionic and partial charges of the peptidic molecules. The sign of the resistance change is dependent on the gating conditions of the graphene field effect transistor, which are not controlled in the present device. The change in resistance can, therefore, be treated as arbitrary intensity units for the purposes of binding quantification.

Mitigation of Non-specific Adsorption

Non-specific adsorption of undesirable proteins present in solution is a major concern when testing for biomarkers in clinically relevant samples. Serum albumin constitutes about 50% of the blood serum proteins, and is, therefore, a good model protein to serve as the background against which SA may be detected. **Figure 23A** shows the effect of adsorption of bovine serum albumin (BSA) on graphite after washing (corresponding sensogram Figure 23D). The protein is present on the entire surface and agglomerates into fibers probably as the result of drying in sample preparation. The sensogram shows robust detection of binding at 50ng/ml, followed by increased binding with overall resistance shift of almost 200kΩ at 10μg/ml. In order to prevent non-specific adsorption of BSA, we employed the SS-GrBP5 mutant (Table 3), identified in an earlier study as

one capable of assembling into ordered monolayers and presenting hydrophilic chemistry (36^{o} contact angle at 100% coverage).[135] Such a contact angle value is similar to those achieved in literature by self-assembled monolayer polyethylene glycol anti-fouling systems (about 32^{o}).[17, 95, 111] The contact angle value has been strongly linked to anti-fouling properties in a variety of systems.[139] We, therefore, hypothesized that our self-assembled peptide monolayers, which are dense and exhibit similar contact angles, would also be anti-fouling. To test this hypothesis, we assembled SS-GrBP5 peptide (Figure 23B) on the sensor surface, and introduced BSA to the system (Figures 23C and

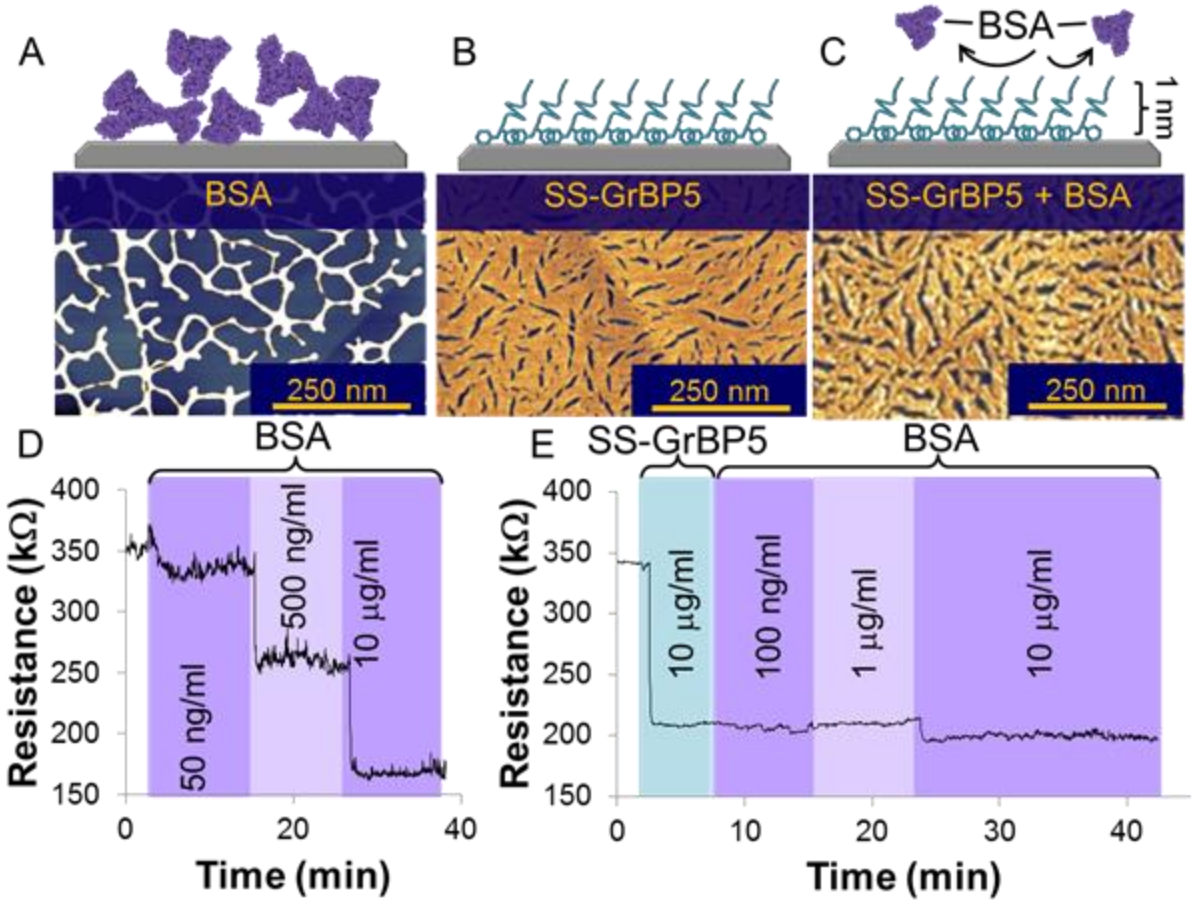

Figure 23. A) AFM image and schematic of 10mg/ml BSA Adsorption to bare graphite; B) AFM image and schematic of 10mg/ml SS-GrBP5 on graphite; C) AFM image and schematic of 10mg/ml BSA adsorption blocked by SS-GrBP5 – functionalized graphite; D) Sensogram of sequentially increasing concentrations of BSA added to bare sensor; E) Sensogram of sequentially increasing concentrations of BSA added to SS-GrBP5 functionalized sensor

E). The binding of BSA was seemingly inhibited by the SS-GrBP5 mutant, resulting in no detectable binding at less than 10μg/ml concentrations of BSA. The AFM image of the surface after incubation with 10μg/ml BSA for 90 minutes (Figure 23C) shows a small amount of protein present sparsely on the surface and very low degradation of the underlying peptide monolayer. The apparent added stability, as compared to the bio-GrBP5 mutant, is possibly the result of the more amphiphilic nature of the SS-GrBP5 monolayer, which is more likely to remain robustly oriented between the hydrophobic graphite and water. As a control experiment, we introduced BSA to a monolayer of bio-GrBP5 and detected significant binding of BSA, indicating that it is specifically the addition of SS to the peptide, which results in anti-fouling properties. See section 2.6 for additional discussion of stability.

Multi-Functional Surfaces through Peptide Co-Assembly

By combining the passivating SS-GrBP5 with the biotinylated probe peptide bio-GrBP5, we created a sensor we believe should be capable of selective detection of streptavidin in a bovine serum albumin solution. A mixed peptide monolayer consisting of 25% bio-GrBP5 and 75% SS-GrBP5 was formed in a single step from a solution with an overall concentration of 10μg/ml. The AFM of the resulting monolayer **(Figure 24A)** is interpreted to mean that the peptides self-assembled into the dense, ordered structure with no discernible segregation, leading to the likely conclusion that the peptides are miscible. Guided by the results in Figure 23, we introduced 5μg/ml BSA to the sensor and

detected no shift in the resistance of the sensor (Figure 24C). We then introduced sequentially increasing concentrations of SA to the sensor, while maintaining the levels of BSA, and were able to reliably detect streptavidin at 100ng/ml, although some signal was present at even lower concentrations (Figure 24C). The AFM image of the graphite surface at the final conditions (Figure 24B) showed less coverage by SA than the biotin-only surface (Figure 22B). The overall stability of the bio-GrBP5 appears to have been improved by co-assembly with SS-GrBP5, displaying very high coverage and density. SS-GrBP5 also seems to retain its anti-fouling function despite a 25% reduction in coverage, owing to the fact that the overall order of the monolayer is maintained by the self-assembling sequence of bio-GrBP5 inclusion.

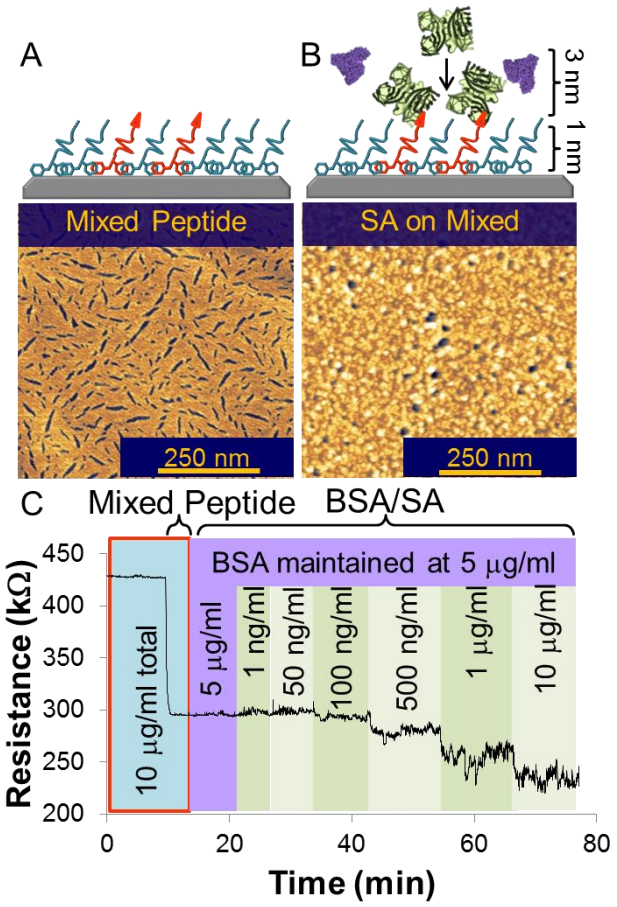

Figure 24. A) AFM image and schematic of mixed peptide monolayer on graphite B) AFM image and schematic of selective detection of streptavidin against a BSA background; C) corresponding sensogram, where 25% bio-GrBP5, 75% ss-GrBP5 peptide mixture is introduced first, followed by BSA, which shows no binding, and finally, streptavidin, which is captured selectively.

Determination of Critical SS-GrBP5 Coverage

To quantify the minimum percent of SS-GrBP5 in the mixed monolayer necessary to maintain the anti-fouling properties of the surface overall, and to characterize the co-assembled monolayers, we measured the Kd of BSA adhering to the sensor as the function of fraction of probe peptide in the SS-GrBP5 mixed monolayer. In addition, we created a second biotin-functionalized peptide Bio-SS-GrBP5 (Table 5), in order to test the effect of the extra linker on the display of the probe within the mixed monolayer, and its availability. We first performed contact angle measurements on maximum coverage mixed monolayers at various ratios of the probe peptides with SS-GrBP5 **(Figure 25A)**. The cosines of the resulting contact angles exhibit a linear correlation with the fraction coverage, which is consistent with the Cassie's Law, indicating that the peptides are fully miscible, and are distributed evenly on the surface. The apparent Kd values, shown in figure 25c, exhibit a transition between no binding and 9.5×10^{-9}M. The Kd values were calculated by fitting the signal change versus concentration plots with the Langmuir equation ($R = R_{max} (K_{eq}C/(1+K_{eq}C))$, where R is the resistance change from the no analyte present level, to maximum apparent binding at a given concentration, R_{max} is the change in resistance at the apparent equilibrium, and

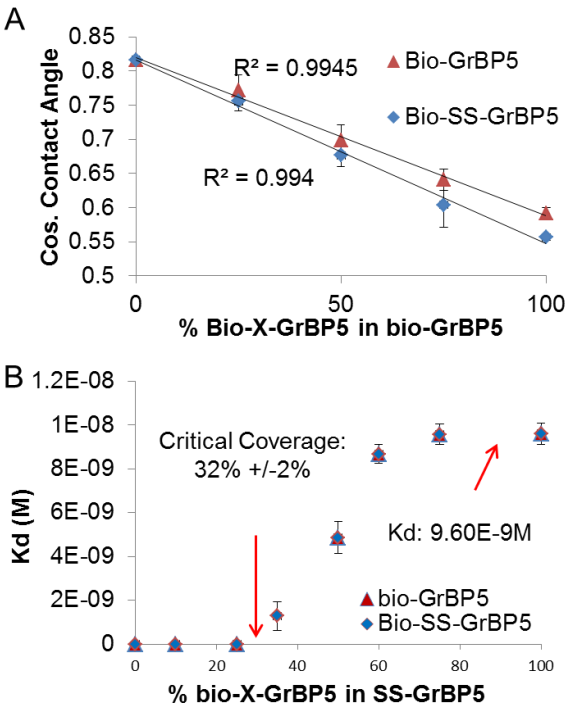

Figure 25. A) Plot of the cosine of the contact angles, showing linear correlation; B) Plot of apparent Kd values of BSA-sensor interaction as a function of Bio-GrBP5 and Bio-SS-GrBP5 in SS-GrBP%, indicating the critical coverage of about 34%

C is the experimentally introduced concentration of the analyte. In taking this approach we make the following assumptions, which may be inaccurate: the change in resistance is proportional to the amount of analyte on the surface, concentration remains constant in solution during the experiment and an equilibrium is achieved at higher concentrations, The transition in apparent Kd values occurs because R_{max} corresponds to a smaller number of binding events than the true Kd. The linear extrapolation of the transition region indicates that the critical coverage is 32% +/-2% of bio- or bio-SS-GrBP5 in the mixed monolayer, meaning ratios of 2:1 probe to passivating peptide are possible. No difference in critical coverage were observed for between bio-GrBP5 and bio-SS-GrBP5 mixed monolayers, indicating that the resistance to non-specific adsorption is imparted by the SS-GrBP5 component, independent of the probe peptide sequence.

Biotin Probe Display Optimization and Biotin-Streptavidin Kd Measurements

The availability of the probe can be a critical factor in biosensor functionalization, affecting the number of active binding sites, and therefore, the ultimate sensitivity limit of the sensor. To test the availability of biotin probe in our system, and to optimize its accessibility for binding, we conducted a series of measurements to determine the apparent Kd values of streptavidin-biotin interactions using both bio-GrBP5 and bio-SS-GrBP5 mixed monolayers. We hypothesized that inserting the SS linker into the peptide would increase the accessibility of biotin, and decrease the Kd of the interaction. The summary of these experiments is given in **Figure 26**. By optimizing the concentration range for our SA-binding experiments, we again observed a transition of apparent Kd values from no binding to a stable value, apparently due to the low availability of binding sites at low probe coverages. By linearly extrapolating the transition region of the Kd plots

(Figure 26c and d) we arrive at a value of approximately 7%, which represents the quantity of inactive/unavailable probes on the surface.

The equilibrium Kd values obtained via bio-GrBP5 ($1.82x10^{-9}$M) vary significantly from those obtained via bio-SS-GrBP5 ($1.10x10^{-13}$M). This is consistent with our hypothesis that the display of the probe above the dense self-assembled peptide monolayer is necessary for accurate quantification. The value we obtained from the bio-SS-GrBP5 based system correlates well with the established literature values ($5x10^{-14}$M).[140]

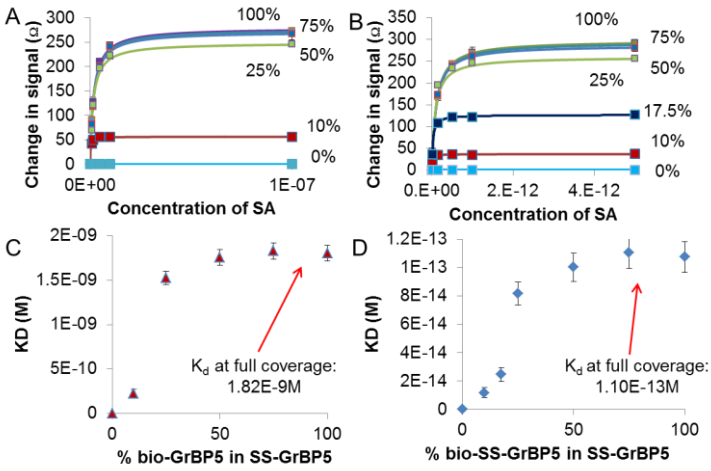

Figure 26. A, B) Change in sensor signal with respect to concentration at different ratios of bio-GrBP5 and bio-SS-GrBP5 to SS-BrBP5 respectively, with corresponding Langmuir fits.

The sensor devices used in this study were regenerated and reused by washing in boiling acetone. We observed some sensor degradation over the course of about 12 experiments, with the $\sigma 3$ noise levels increasing from near 2kΩ to about 10kΩ. However, it seems that the sensitivity of the device is not significantly affected between trials, meaning that it can be used to produce comparable data several times. This is a significant feature for practical application of graphene based sensors, and represents another advantage of peptide functionalization over covalent approaches. The details of the regeneration procedure are given in the Methods chapter (chapter 5).

Multi-analyte Sensor Platform Design

In order to allow for interchangeable probes we fused the SS-GrBP5 peptide with an antibody binding peptide sequence ABBP2 (FAGRLVSSIRV).[141] The ABBP2 peptide binds specifically to the Fc (conserved) section of the antibodies, meaning that a variety of ant-bodies can be used to functionalize the sensor, so that any analyte can be detected for which an antibody exist. The construct displays robust binding under the AFM, and is miscible in SS-GrBP5, making it acceptable for simultaneous graphene surface functionalization. We chose anti-maltose binding protein and maltose binding protein as pair as the model system, because of its strong interaction and because of our previous experience in using that system.

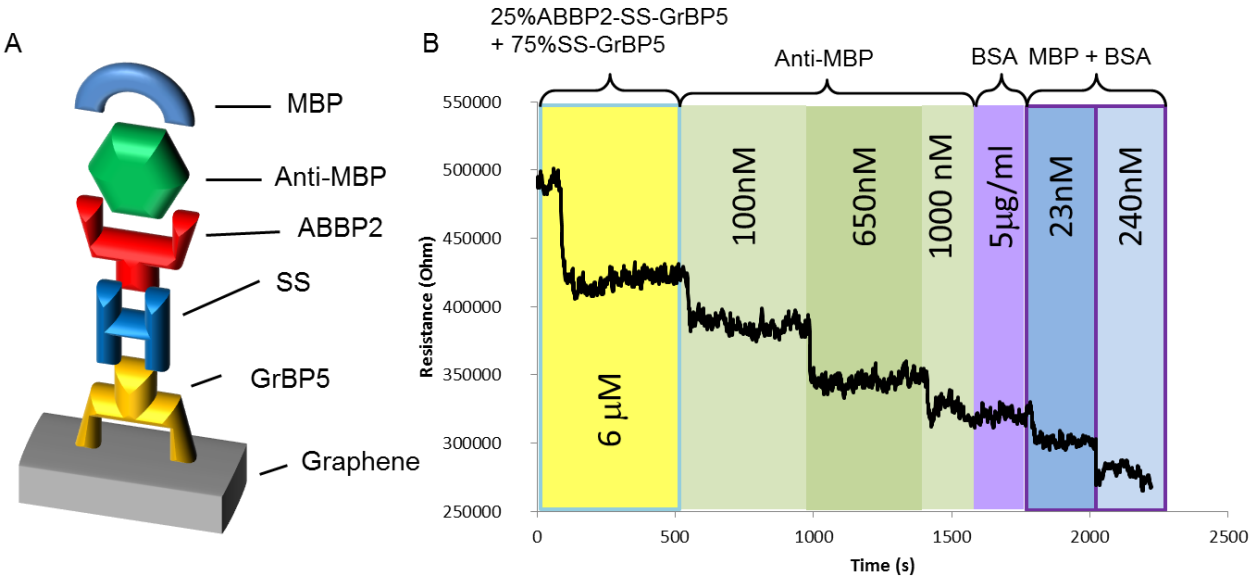

Figure 27. A) Schematic of the probe structure B) sensogram, where 25% ABBP2-SS-GrBP5 and 75%SS-GrBP5 peptide mixture is introduced first, followed by anti-MBP, then BSA, which shows no binding, and finally, streptavidin, which is MBP selectively.

The interface layer structure we envisioned is schematically represented in **Figure 27a.** To make it, we first incubated the sensor with the mixed peptide solution

(25%ABBP2-SS-GrBP5 + 75%SS-GrBP5). We then added a sequentially increasing quantity of anti-MBP until saturation was reached, as indicated by the stabilization of the signal. Thereupon, we added BSA, observing no change in signal, followed by increasing concentrations of MBP in BSA. Based on the shift in resistance during the anti-MBP introduction, Kd for the ABBP2-SS-GrBP5 interaction with anti-MBP is about 0.5μM (Figure 27b). No detectable shift after BSA introduction, indicates that the anti-fouling properties of the SS-GrBP5 monolayer were preserved. Although more data points are needed to reliably measure the Kd of the anti-MBP interaction with MBP, it is detectable, and is in the nanomolar range. In subsequent experiments we modify this system to detect cancer markers against a background of serum.

2.6 Selective Detection of Cancer Markers

In these experiments we develop a modular (multianalyte) graphene bio-sensor system for selective detection of cancer markers against a background of abundant serum proteins. In particular we employ a 4 probe graphene field effect transistor sensor, functionalized with a mix of peptides which allow for further functionalization with antibodies, and mitigate non-specific adsorption of serum proteins **(Figure 28).** As discussed in Chapter 1 we selected carcinoembryonic antigen (CEA) and carbohydrate antigen (CA19-9), which are both indicative of pancreatic cancer.[33] It

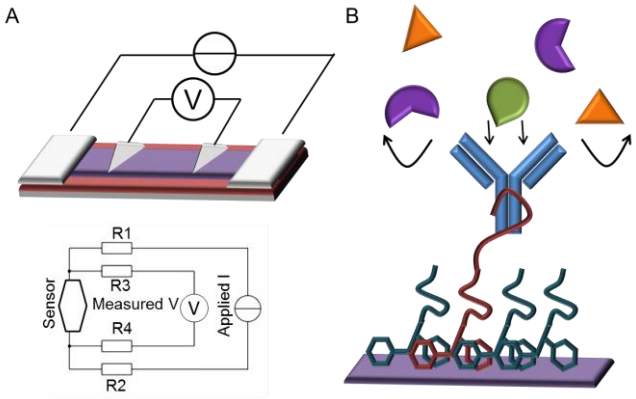

Figure 28: A) Schematic illustration of the four-probe graphene field effect transistor sensor; B) Proposed functionalization scheme, showing mixed self-assembled peptide monolayer, which prevents nonspecific adsorption and displays anti-bodies, which are chosen to bind to specific cancer markers.

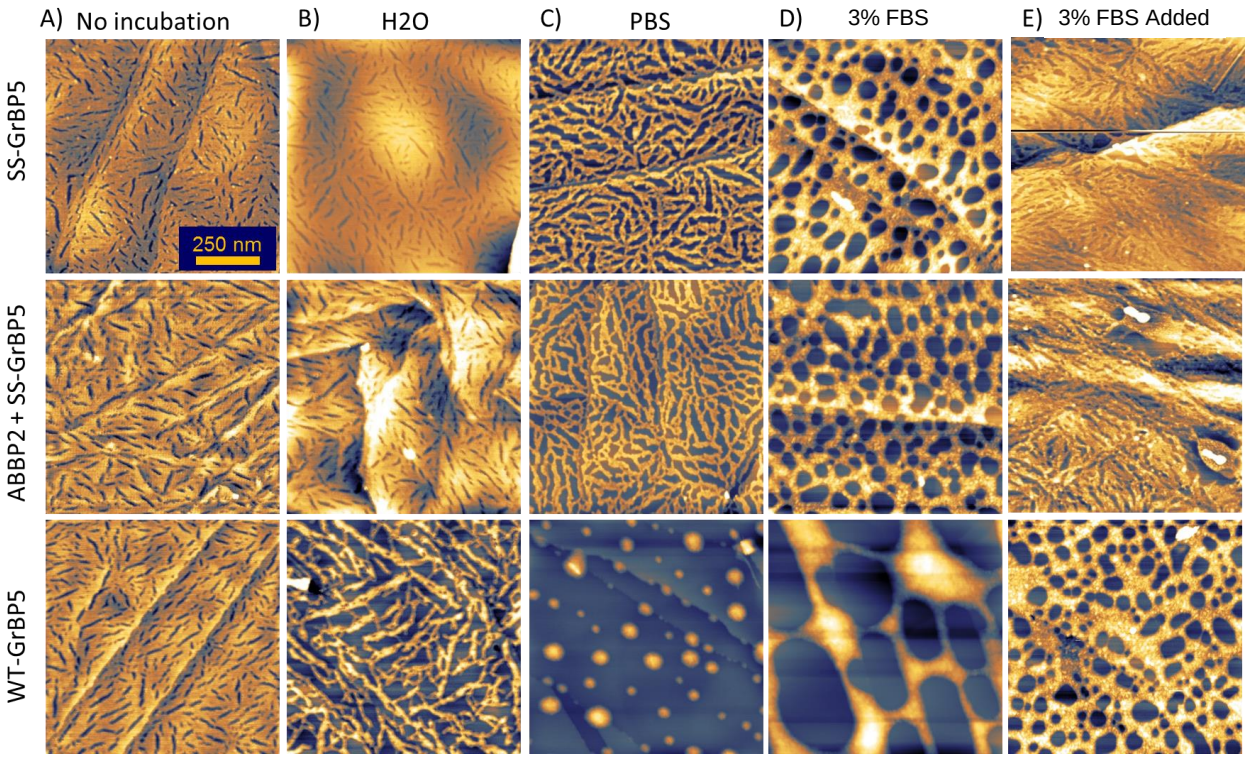

Figure 29: A) Peptide monolayers as assembled after 1hr, 6μM concentration. Samples incubated for 30 minutes in B) Deionized water, C) PBS, D) 3% FBS after removing the peptide solution. E) Peptides incubated with FBS while the peptide is still present in solution.

should be possible to easily modify this proof-of-principle system to detect any biomolecule for which an antibody exists, in a variety of complex solutions, and to apply it to any high sensitivity graphene sensor configuration demonstrated in the literature.

Optimization of Mixed Peptide Monolayer Stability in Sensing Environment

In order to test the stability of our bi-functional, antibody-binding/anti-fouling peptide monolayer under either buffer or FBS conditions we prepared a series of AFM samples. The first set of samples was prepared by pre-assembling the peptide (SS-GrBP5, 70% SS-GrBP5 + 30% ABBP2-SS-GrBP5, and WT-GrBP5) in de-ionized water (6μM, 1hr) followed by wicking, and introducing to de-ionized water, PBS buffer, or 3% FBS. The last set of samples was prepared without wicking, by adding a higher concentration of PBS buffer, and FBS into the peptide solution drop after incubation, so

that the final concentrations were the same. Based on the coverage, ordering and roughness, the AFM images in **Figure 29** are interpreted to indicate that: SS-GrBP5 modified peptides are more stable in deionized water than the wild type; all peptides are less stable in PBS, and 3% FBS; leaving a high concentration of peptides in solution slows down the adsorption of 3% FBS.

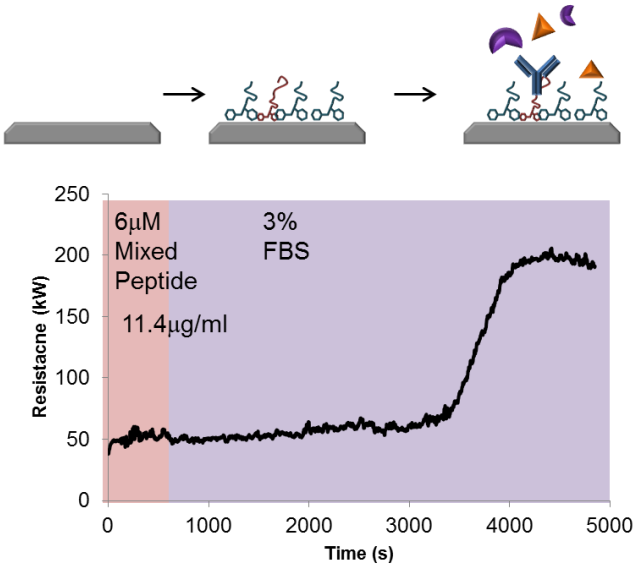

Figure 30: Schematic illustration and sensogram of FBS adsorbing over the long term to the mixed peptide monolayer.

Based on this data we hypothesized that when additional peptides are present in solution, as they are during our sensor experiments, the peptide monolayer is replenished faster than it is replaced by the FBS or other non-specific binding species, therefore, prolonging the anti-fouling function. To test this hypothesis we conducted a sensor experiment in which 70% SS-GrBP5 + 30% ABBP2-SS-GrBP5 was first bound to the surface, and then 3% FBS was added to the sensor. The results are shown in **Figure 30**. The sensogram shows no appreciable immediate binding of FBS to the mixed monolayer surface. There is some minor drift associated with slow 3% FBS adsorption over the first 50 minutes of the experiment, at which time (about 3400s) the adsorption becomes rapid, most likely because the critical amount of SS-GrBP5 is no longer present on the surface. These results are consistent with our observations in a previous experiment (Figure 26), where we found that if less than 2/3 of the surface is covered with SS-GrBP5, the anti-fouling effect is lost. The linear appearance of the transition region is consistent with a transport

limitation artifact (as on SPR), when in the absence of flow conditions, an analyte depletion zone is formed close to the surface, and therefore, the shape of sensogram reflects the diffusion of the analyte in solution, rather than binding to the surface. From this experiment we concluded that the stability of our anti-fouling modification is reliable for about 35-40 minutes, and have kept the rest of our experiments well below that length after adding 3% FBS.

Bi-functional peptide monolayer

It is necessary to impart two functions to the surface of the sensing material to make it selective: specific binding capability, and prevention of non-specific binding. Using genetically engineered peptides it is possible to impart these functions simultaneously through a mixed monolayer co-assembly.[135] We have chosen antibodies as probes to capture the cancer markers from solution because they are highly specific, widely available and have a conserved region, for which peptidic binders exist. We selected a peptide known to bind to the Protein A binding site of antibodies from many different of animal sources.[141] We chose this peptide over some of the other antibody binding peptides available because it contains few aromatics, which bind to graphitic materials readily,[133] and because it does not interfere with binding or assembly when fused with SS-GrBP5 (**Figure 31 A**).

Previously, we demonstrated that the SS-GrBP5 peptide reduces non-specific adsorption of bovine serum albumin (BSA) and 3% FBS, as long as it covers at least 66% of the sensor surface. By mixing the bi-functional ABBP2-SS-GrBP5 with SS-GrBP5 at 30% to 70% coverage respectively we expected to achieve a surface that has both antibody binding and anti-fouling capabilities. Based on the sensogram in figure 31B, the mixed appears to allow immobilization of antibodies, showing a shift in signal when the antibody is added. Moreover, the sensogram indicates that no non-specific antibody binding occurs in the absence of ABBP2-SS-GrBP5. The mixed monolayer also mitigates non-specific adsorption of 3% fetal bovine serum (FBS) at time-scales of the experiment (about 30min). Both types of antibodies used can be immobilized on the surface with roughly the same efficiency, and similar results were obtained for the anti-CEA antibody.

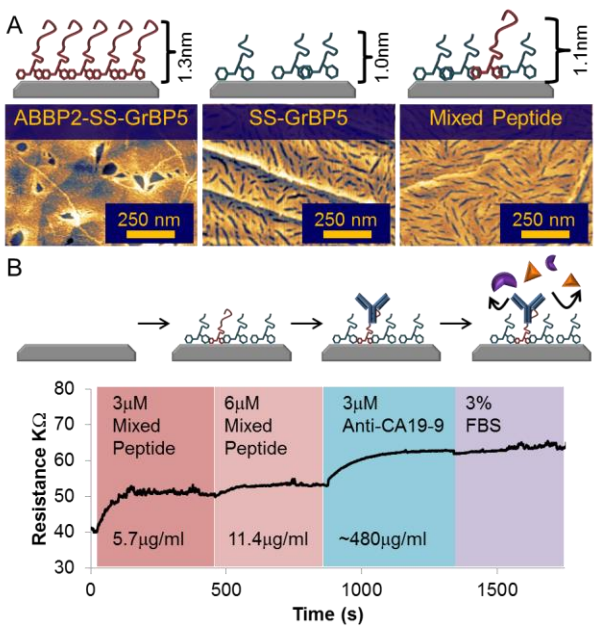

Figure 31: A) Schematic illustrations of the peptide self-assembled and co-assembled monolayers, and the corresponding AFM images; B) Schematic illustration of the self-assembled bi-functional peptide monolayer, functionalized with anti-bodies, and the corresponding sensogram, showing increases in resistance with the addition of modification s to the surface.

Detection of Cancer Markers

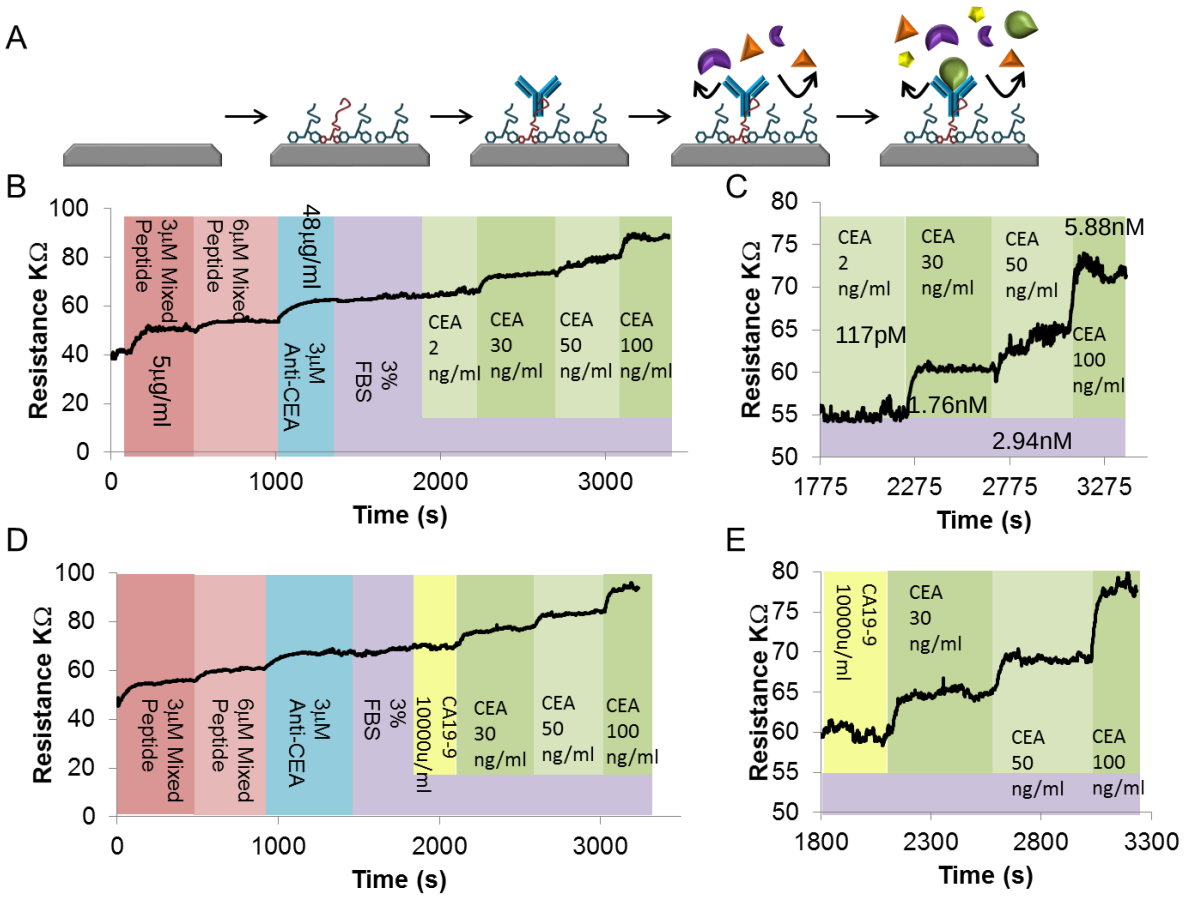

Figure 32: A) Schematic illustrations of the peptides forming co-assembled monolayers, followed by anti-CEA immobilization and selective detection of CEA; B) Limit of detection sensogram (unmodified) showing the signal from the formation of the surface functionalization layer, followed by increasing concentrations on CEA, against a background of 3%FBS; C) Enlarged portion of the CEA detection sensogram, corrected for FBS adsorption; D) Cross specificity sensogram (unmodified) showing that the sensor is specific and sensitive to CEA over the CA19-9 marker control; E) Enlarged portion of the cross specificity sensogram, corrected for FBS adsorption;

Increasing concentrations of CEA were added to the anti-CEA functionalized sensor. We were able to detect the 30ng/ml concentrations of CEA in 3% FBS (**Figure 32** A, B, C), however, by extrapolating the average 3σ sensitivity limit based on equilibrium noise from this and 7 other sensograms (2.7kΩ), the ultimate sensitivity limit is found to be 15ng/ml. 3σ detection limit is calculated by finding the standard deviation in the nominally unchanging signal of the device, and multiplying by 3. This value is considered a good measure of the smallest meaningful shift in the signal from a sensor. Due to experimental limitations, we were not able to achieve full surface coverage by the

analyte and determine the Kd of anti-body target interactions because sufficiently high concentrations of target could not be achieved. Additionally, we tested the device with the improper marker-antibody combination, showing that the anti-bodies remain specific even at high concentrations of the non-matching cancer marker because, apparently, anti-CEA does not bind strongly to CA 19-9 (Figure 32 D, E).

Similar results were obtained with CA19-9 cancer marker, with 3σ limit of detection of at 400u/ml (**Figure 33** A, B, C). This result is significantly higher than the nominal levels of this marker at about 40u/ml. More sensitive sensor configurations would have to be employed in the future to extend the range of this device, in order to satisfy the clinical requirements for diagnosis. The device shows specificity to CA19-9 as well, showing no adsorption at maximum tested concentration (Figure 33 D, E). Again, the drift after the introduction of BSA is consistent with our control experiment in figure 30.

It is important to note that the demonstrated sensor does not meet the clinically relevant requirements for sensitivity. The detection limit for CEA (15ng/ml) is about 10 times less sensitive than necessary to meet the diagnostic needs, since the nominal level of this marker in the blood is about 2.5ng/ml. In the case of CA19-9, the ideal detection limit is under 10u/ml, while our current system detects a minimum of about 400u/ml. While it represents a significant advance toward label free, rapid cancer diagnosis, this device will need to be greatly improved in sensitivity before it can become clinically relevant for cancer marker detection.

In order to improve the sensitivity of cancer marker sensor system in the future, it is necessary to understand what exactly causes the shift in resistance of graphene. To

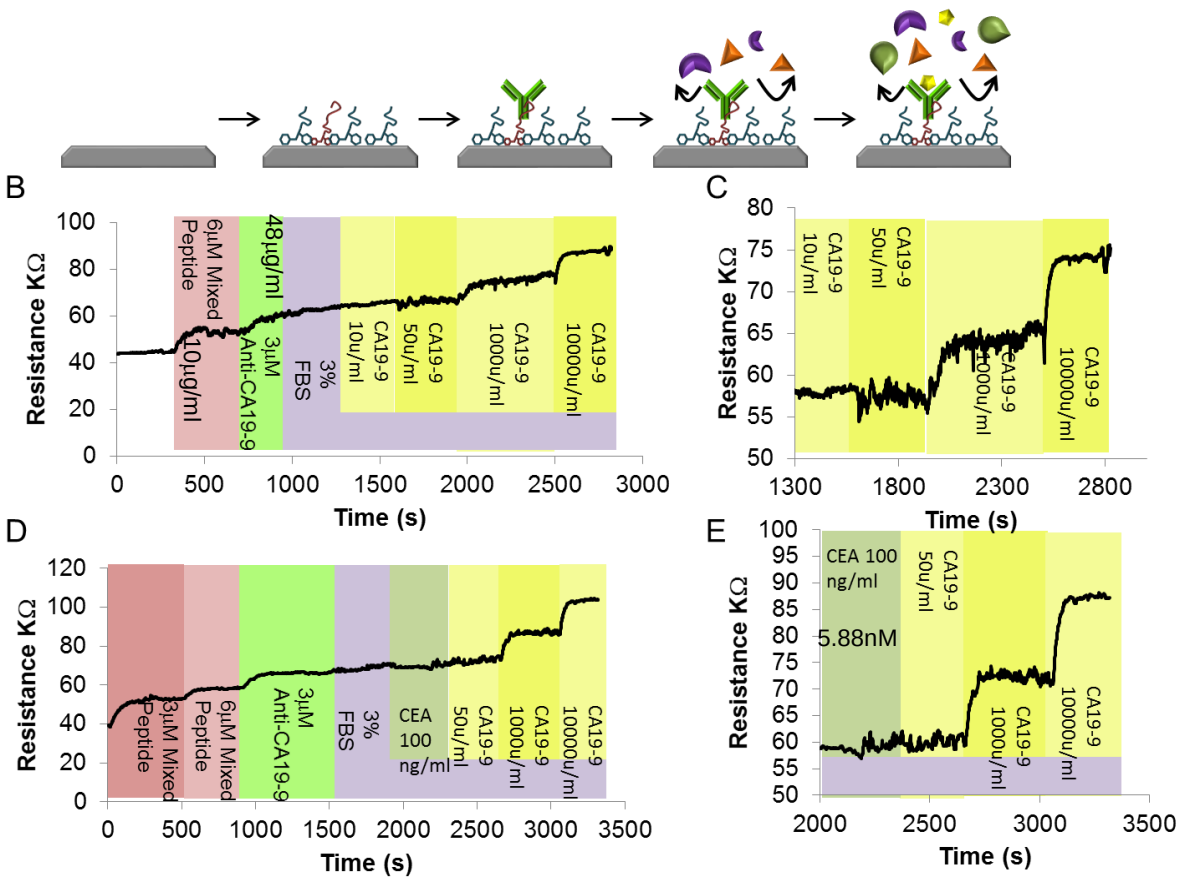

Figure 33: A) Schematic illustrations of the peptides forming co-assembled monolayers, followed by anti-CA19-9 immobilization and selective detection of CA19-9; B) Limit of detection sensogram (unmodified) showing the signal from the formation of the surface functionalization layer, followed by increasing concentrations on CA19-9, against a background of 3%FBS; C) Enlarged portion of the CA19-9 detection sensogram, corrected for FBS adsorption; D) Cross specificity sensogram (unmodified) showing that the sensor is specific and sensitive to CA19-9 over the CEA marker control; E) Enlarged portion of the cross specificity sensogram, corrected for FBS adsorption;

this end, others in our group have recently carried out a theoretical study to understand the nature of the affinity between the solid binding peptides and graphene (S. Dag, et al, in preparation). They found that when a peptide binds to the surface, it takes on a specific conformation, affecting the graphene in two major ways. Firstly, adsorption of peptides to graphene results in charge transfer, called Hall doping, to the graphene, changing the Dirac point and therefore, resistance of the sensor. Secondly, the dipole moment of the oriented peptides will have a collective effect on the graphene. Any component of the

moment which is perpendicular to the graphene will result in a change of surface potential (gating).[142] Taking advantage of this fact, it may be possible in future studies to predict the effect of a given analyte on the sensor signal and precisely control it by controlling its dipole orientation. GrBP5 peptide family members self-assemble in a predictable conformation on the surface, meaning that the orientation of the dipole can be controlled by controlling its sequence. This is discussed further in the future work chapter (Chapter 4).

3. Conclusions

Controlling surface properties through modification and self-assembly of peptides, which bind to specific solid materials, provides a novel approach for engineering biomolecule/solid interfaces. Mixed self-assembled peptide films prepared in water have led us to the development of bio-sensors with optimized bio-chemical properties and biocompatibility. Further understanding of the mechanisms of intermolecular interactions among different peptides in the ordered phase will allow tailoring the probe molecule to form novel, complex nanostructures with spatially controlled molecular conformations and functionality. Therefore, the ease with which displayed amino acid domains are introduced into short peptides could provide an opportunity to develop biomolecular constructs with proteins, peptide domains, and chemical groups to further control functionality of graphitic surfaces. This inherently biocompatible and non-covalent molecular immobilization approach is suitable for a variety of potential applications of graphitic materials in nanobiotechnology, such as tailoring, controlling and interrogating ligand-receptor interactions (by controlling and perhaps switching the orientation of the displayed moieties), in general, with potential implementations in screening for drug candidates in neurodegenerative diseases and anti-viral agents for small viruses.

We demonstrated a system for simultaneous passivation and functionalization of the graphene sensor using the GrBP5 modular graphite-binding peptide family, which is shown to be capable of selective detection of streptavidin in the presence of excess serum albumin **(Figure 34)**. We also demonstrated detection of two different cancer markers in 3% FBS, using a modular, anti-body based system. The same system can be extended to other, more efficient sensor architectures, and other single layer materials systems,

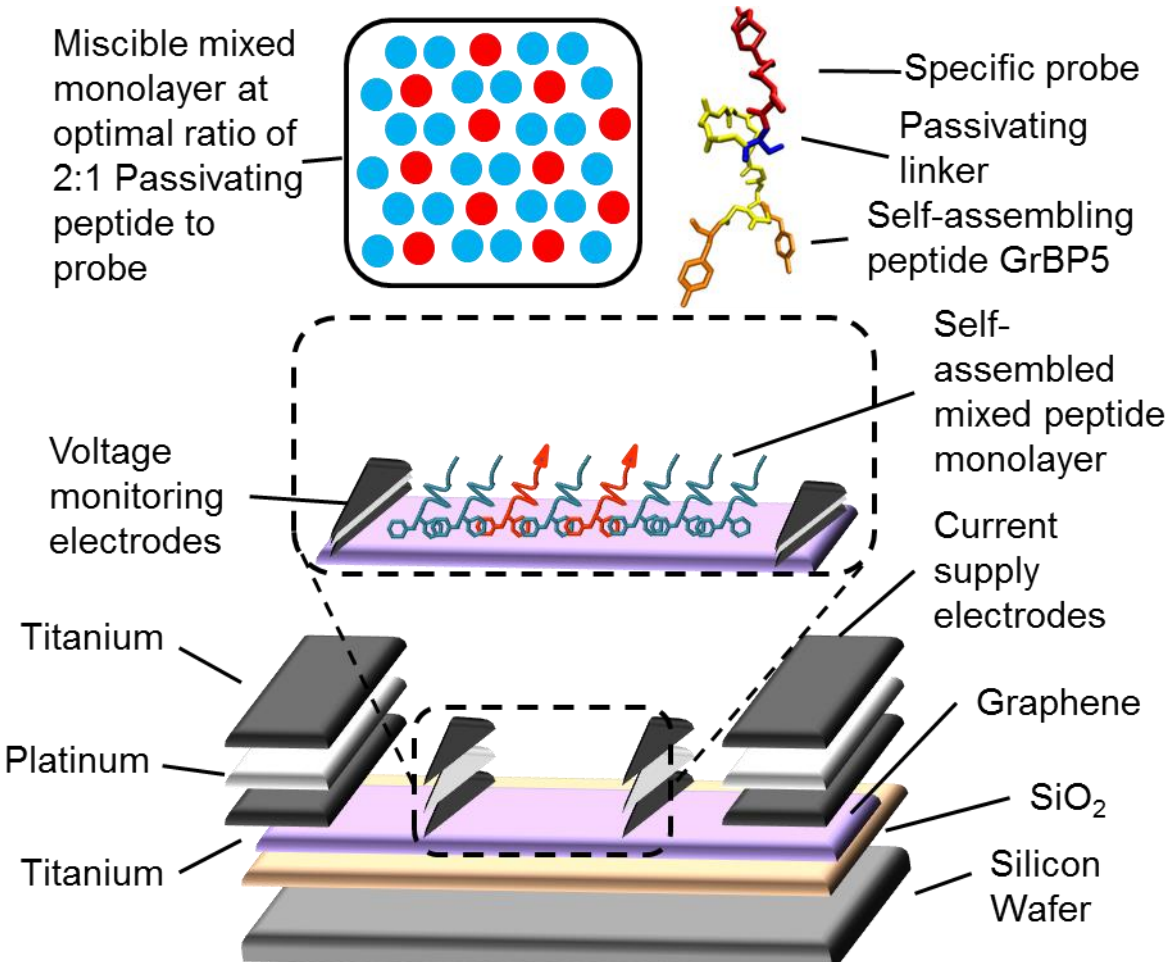

Figure 34. Schematic of the optimized self-assembled peptide functionalized graphene bio-sensor.

such as the semi-conducting MoS2 or WS2 (which could provide other means of detection, for example, optical fluorescence), either through rational mutation of the GrBP5-WT peptide, or through discovery of new peptides specific to those materials. The novel biosensors based on peptide-two-dimensional material conjugation establishes a new method for biomolecular detection, not only through electrical signals but also, potentially, through optical and magnetic signals, depending on the characteristics of the sensing material (for example, magnetically and plasmonically active materials, or light optical ring resonators) and the interaction of the target biomolecule with the peptide-displayed probe. Our ability to control the groups at the outer interface of the peptide

monolayers, as well as the possibility of creating mixed monolayers, allow for the construction of multi-functional sensors capable of selective detection of multiple probes in a complex environment. Self-assembled peptides offer unique opportunities for biosensor functionalization, including biocompatibility, non-covalent binding, ease of fusion with biological probes, and high degree of control over assembly. Since a variety of short peptidic probes have been identified for many disease biomarkers through phage and cell-surface display, the next step for this technology would be to complete a relevant diagnosis and monitoring system. However, the system is not limited to clinical applications. Specific ligand receptor interactions are of critical importance to all areas of molecular biology. It is possible to create a selective biosensor to study the kinetics of many ligand-receptor pairs, as long as the response of the biosensor remains linear, displaying one of the constituents on the graphene surface in a predictable fashion. Using our anti-body immobilization approach, the system can be easily modified to detect any molecule for with an antibody exists, making this system comparable with the conventional molecular adsorption techniques such as SPR and QCM.

More broadly, this study adds another tool to the peptide-based bio-nanotechnology toolkit, taking advantage of Nature’s way of putting together materials at the nano-scale.

4. Future Work

Having demonstrated the proof-of-principle modular system for selective detection of blood borne cancer markers, CEA and CA 19-9, which are implicated in pancreatic cancer, we have taken a significant step toward a clinically relevant, versatile diagnostic

tool. However, we have also initiated several avenues of research that could be pursued to continue this work toward the goal of an optimized bionanosensor:

1) Sensitivity: There are numerous graphene and carbon nano-tube sensors in literature, which have achieved incredibly low sensitivities, 2-3 orders of magnitude lower than our sensor (See motivation section). One of the ways to improve sensitivity would be to apply our peptide system to more sensitive sensor architecture (for example by creating an additional channel below the graphene, to allow binding on both sides of the material). Our surface functionalization system should perform well on any graphene based device, and could be optimized for other graphitic materials. Alternatively, the probe signal could be amplified through controlled orientation of its dipole moment over graphene. To do so we would need to know the geometry of the dipole moments of each molecular component. We can then engineer the system through peptide mutation to optimize its orientation.
2) Selectivity: Selectivity of the sensor functionalization depends on the stability of our modifications, which, though sufficient for the initial tests, could be improved. By substituting the binding domain of the GrBP5 peptide family, we could increase the binding strength in buffer, which would prevent peptide desorption and allow for a construction of a flow system.
3) Fabrication: The approach to sensor fabrication taken in this study is advantageous, because it results in graphene with little contamination and defects, while requiring no special instrumentation. However, in order to make a commercially viable device, it would be necessary to use a method which is amenable to mass production. CVD graphene offers a large scale alternative to

exfoliation (which is accomplished by random deposition of graphene on a surface using the scotch tape method) . Unfortunately graphene produced by CVD is prone to defects. Nevertheless, as the manufacturing methods improve, it would be advantageous to demonstrate our surface modification system on a sensor which could be mass produced.

4) Fundamentals: Much could be learned from further studies of our system about graphene properties, and the peptide-graphene interactions. Some of these studies have already been undertaken in our group to learn more about the effect of the peptide-graphene interactions, as well as the interaction of peptides with different number of layers of graphene (unpublished).

5. Methods

5.1 Methods for: Peptide Design for Surface Functionalization

Fmoc peptide synthesis: The peptide sequences used in this research, including QBP, AuBP, and the multi-functional peptides, QBP–AuBP and AuBP–QBP, were synthesized via automated Fmoc peptide synthesis using CSBio 336s peptide synthesizer (CSBio Inc., USA). The obtained crude peptides were then purified by C-18 reversed-phase high-performance liquid chromatography (HPLC system, Waters, USA). The mass of purified peptides were confirmed by mass spectroscopy using matrix-assisted laser desorption/ionization mass spectrometer linked with time-of-flight detector (MALDI-TOF) MS (Bruker AutoFlex II, Bruker Daltonics, USA).

Micro-contact printing: The PDMS stamps were fabricated by molding a mixture of polydimethyl siloxane and curing agent (10:1, Sylgard 184, Dow Corning, USA) on the surface of a patterned silanized master for 2 days at ambient condition. The stamps were then washed several times with ethanol, heptane, and again with ethanol, and dried with inert gas before being used. Patterned side of PDMS stamp was incubated with 100 µL of 100 µM or 200 µM peptide solutions for 5 min. The peptide solution was removed from the stamp surface by careful pipetting. The stamps were then dried with inert nitrogen gas. The silica surfaces were cleaned by ethanol and sonication, and then applied to the surface of the stamp and pressed using force for 10 s and left on stamp for 1 min. The surfaces were then washed with DI water for 2 min and dried with nitrogen.

Peptide-mediated immobilization of gold nanoparticles onto silica surface: Peptide-patterned silica surfaces were incubated with 100 µL of 50 nm pre-made gold nanoparticles (Ted Pella, USA) for 15 min. Then silica surfaces were washed with DI water for 2 min and dried with nitrogen.

Peptide-mediated formation of gold nanoparticle film onto silica surface: Peptide-patterned silica surfaces were incubated with 200 µL of 10 mM aqueous solution of $HAuCl_4$ for 48 h in moisture chamber to eliminate evaporation. The silica surfaces were then washed with DI water for 2 min and dried with nitrogen. In our combined approach nanoparticle-patterned silica surface were incubated with 200 µL of 10 mM aqueous solution of HAuCl4 for 48 h as described above.

Dark field optical microscopy: Silica surfaces with patterned gold nanoparticle arrays produced by peptide-mediated assembly of pre-made gold nanoparticle as well as by peptide-mediated gold nanoparticle formation were characterized using dark field optical microscopy on Nikon Eclipse TE-2000U Optical Microscope (Nikon, Japan). The dark field images, which are obtained from at least five different locations on each sample, were recorded through Metamorph imaging software (Universal Imaging, USA). Analyses were repeated in three independent experiments.

Molecular dynamics: To model the two different permutations of hetero-functional peptide, we built linear forms using the HyperChem's molecular modeling software (Hyperchem 7.5, USA). The energy minimization of these peptides was carried out under implicit solvent conditions using the conformational analysis program. By randomly changing predefined dihedral angles we created numerous initial configurations in order to increase the sampling space of the potential energy surface. Using the conformational search module, we found 1000 different local minima on the potential energy surface and chose the lowest one as the global minimum or the lowest-energy conformation. Then, the lowest energy conformations were solvated with TIP3P water explicitly; and finally the overall system was energy minimized using the Polak-Ribiere conjugate gradient method until convergence of the gradient (0.01 kJ/mol) was reached using the CHARMM 27 force field. The final configurations were generated using the VMD (Visual Molecular Dynamics) software.

Surface characterization: Produced gold nanoparticle arrays on silica surfaces were characterized using various surface characterization techniques, including atomic force

microscopy (AFM), scanning electron microscopy (SEM) and X-ray photoelectron spectroscopy (XPS) as follows.

Atomic force microscopy: AFM images were obtained in tapping mode on a Dimension 3100 SPM (Veeco, USA), in air, using silicon tips. The scans were obtained at a maximum of 30 μm with the maximum possible scan range of 90 μm. At least three different locations were observed on each sample.

Scanning electron microscopy: The samples of peptide-formed gold nanoparticle film were coated with platinum using an SPI sputter coater (SPI supplies, USA) and observed using a JSM 7000F SEM (JEOL Ltd., Japan) at 10 kV beam voltage.

X-ray photoelectron spectroscopy: The non-patterned PDMS stamps were used as described above to create maximum possible coverage of gold nanoparticle film on-silica surfaces so as to increase the photoelectron yield. Experiments were carried out in an UHV system ($P \leqslant 3.0 \times 10{-}9$ Torr) equipped with a monochoromatized Al Kα X-ray source and an X-ray photoelectron detector (SSL 300 from Surface Science Inc.). High resolution spectra were collected for 14 h from a 100 μm radius spot. The data was analyzed by peak shape fitting method.

5.2 Methods for: Peptide Mitigation of Non-specific Interactions

Peptide Synthesis: The peptides were produced by solid-state synthesis using a CSBio 336s automated peptide synthesizer (CSBio, USA) on Wang resin via Fmoc chemistry and HBTU activation. The crude peptides were purified by reverse phase high performance liquid chromatography to >98% purity (Gemini 10 μm C18 110A column). The purified peptides were verified by mass spectroscopy (MS) using a MALDI-TOF mass

spectrometer (Bruker Daltonics Inc., USA) The amino acid sequences and the physico-chemical properties of the peptides used in the study are shown in Table 6.

Table 6

Peptide	Amino acid sequence	pI	Gravy	M.W.	Net charge
GBP1	**M**HG**K**TQ**A**TSGT**I**Q	8.25	−0.743	1446.6	+1
3GBP1	**M**HG**K**TQ**A**TSGT**I**QS × 3	10.30	−0.743	4304.7	+3
PtBP1	CSQS**V**TSTKSC (cyclic)	8.47	−0.867	923.9	+1
AuBP1	**WAGA**K**R**L**V**L**R**RE	11.71	−0.567	1454.7	+3
AuBP2	**WAL**RRS**I**RRQSY	12.00	−1.267	1591.8	+4
3AuBP1	**WAGA**K**R**L**V**L**R**RE × 3	12.10	−0.567	4328.1	+9
3AuBP2	**WAL**RRS**I**RRQSY × 3	12.30	−1.267	4739.4	+12
QBP1	**PPPWLPYMPPW**S	5.95	−0.650	1467.7	0
QBP1-RGD	**PPPWLPYMPPWSGGGRGDS**	6.26	−0.958	2054.3	0
TiBP1	R**P**RE**N**R**G**RER**GL**	11.82	−2.633	1495.6	+3
TiBP1-RGD	R**P**RENR**G**RER**GLGGGRG**DS	11.70	−2.211	2082.2	+3
RGD	**GRG**DS	5.84	−1.920	490.4	0

The non-polar residues are displayed in bold. pI indicates the theoretical isoelectric points and GRAVY indicates the calculated grand average hydropathicities of the peptides.

The non-polar residues are displayed in bold. pI indicates the theoretical isoelectric points and GRAVY indicates the calculated grand average hydropathicities of the peptides.

PEG functionalization: Aldehyde-terminated methoxypolyethylene glycol 5000 (PEG-CHO) [42] was prepared through the condensation reaction of methoxypolyethylene glycol 5000 and 4-carboxylbenzaldehyde. The reaction was carried out in a 1:1 mixture of N,N-dimethylformamide (DMF) and methylene chloride, in the presence of 4-(dimethylamino)pyridium 4-toluenesulfonate (DPTS) and 1,3-dicyclohexylcarbodiimide (DCC). The reaction product was purified using a silica gel column with an ethyl acetate to methanol elution gradient. For selective on-resin functionalization of the AuBP1, PEG-CHO was reacted with the peptide still on the resin and with the ε-NH2 groups protected by a tert-butoxycarbonyl (Boc) group. In this way, conjugation occurred only through the α-NH2 at the N-terminus. The conjugation reaction was carried out for 4 h in ethanol under

a nitrogen atmosphere while stirring. The resin was then filter washed with 10 ml of ethanol. The Cdouble bond; length as m-dashN double bond at the peptide–PEG junction was reduced with 2.5 mM sodium borohydride in sodium acetate buffer (pH 5.5) at room temperature under nitrogen overnight. The Boc group on the ε NH2 was later removed from the peptide during its cleavage from the resin.

Substrate preparation: Standard 22 × 22 mm microscope coverslips (Fischer, USA) were used as the glass surface. The glass slips were cleaned by ultrasonication in 1:1 isopropanol:acetone mixture and were kept in ethanol prior to use. Gold, platinum and titanium surfaces were prepared by sputter coating the coverslips using a Gatan Precision Etching Coating System (Gatan Inc., USA). Both sides of the substrates were coated with 2 nm of chromium followed by 23 nm of gold or platinum, as measured using the built-in quartz crystal microbalance. Titanium substrates were prepared by directly coating a 25 nm titanium layer on glass. The substrates were used immediately after sputtering.

Surface modification: The GEPIs were attached to the surfaces by submerging the substrates in their respective peptide solutions. The gold substrates were submerged in 2 ml of 20 μM solutions of the original or triple tandem repeats of GBP1, AuBP1 and AuBP2 for 1 h at room temperature. The platinum substrates were submerged in 2 ml of a 150 μM solution of PtBP1 for 1 h at room temperature. The glass and titanium substrates were submerged in 2 ml of 20 μM QBP1–RGD and 20 μM TiBP1–RGD solutions, respectively, for 1 h at room temperature. Similarly, substrates coated with 20 μM QBP1, 20 μM TiBP1 and 20 μM fibronectin were prepared as controls. All surfaces were washed three times by dilution with water and dried with nitrogen after functionalization.

The gold and platinum substrates were then further modified with PEG by submerging in 2 ml of 100 μM PEG-CHO solution in ethanol overnight. The samples were then washed by dilution using ethanol and deionized water, followed by rinsing with deionized water and drying with nitrogen. The thiol control surfaces were prepared using a thiol oligo(ethylene glycol) (thiol-OEG) conjugate (HSC11(EG)3OH) (Sigma–Aldrich, USA). Gold substrates were submerged in 2 ml of a 1 mM solution of thiol-OEG in ethanol overnight and washed by dilution with ethanol and deionized water, followed by rinsing with deionized water and drying with nitrogen.

The surfaces were characterized by atomic force microscopy (AFM) to check the uniformity of the coverage and polymer agglomeration using a multimode Nanoscope IIIa in tapping mode (Veeco, USA). The presence of the peptide and the polymer on the surface was verified via X-ray photo-electron spectroscopy (XPS), using S-Probe (Surface Science Instruments, USA), at the Surface Analysis Recharge Center (University of Washington, USA).

Contact angle measurements: Static water contact angles were measured on each of the gold and platinum samples to verify the assembly of PEG on the peptides and the consistency of assembly between different experiments. The modified surfaces were allowed to equilibrate in air for 30 min after preparation prior to measurements. All measurements were made with a Rame-Hart Optical Goniometer 100-00 (Rame-Hart Instrument Co., USA) using >16 MΩ deionized water.

Cell adhesion and spreading analysis: NIH 3T3 mouse embryonic fibroblasts were used in the cell adhesion assays. The cells were maintained in Dulbecco’s modified Eagle’s

medium (D-MEM) with 10% fetal bovine serum (FBS) and 2 mM glutamine, 100 U/ml penicillin and 100 mg ml–1 streptomycin (Invitrogen, USA). Experiments with 3GBP1–PEG, QBP–RGD and TiBP–RGD were carried out in both the absence of serum proteins and the presence of 1% FBS.

The gold and the platinum surfaces were inoculated with 3 × 105 cells and the glass and the titanium surfaces with 5 × 103 cells in 500 µl of medium for 2 h at 37 °C and 5% CO2. The gold surfaces were also kept for 24 h after cell inoculation to further test the stability of the PEG layer. The samples were then rinsed three times with serum-free medium and the cells were either prepared for phalloidin staining or scanning electron microscopy (SEM), as described in the following sections. The number of cells on the surfaces was determined by counting the cells within four random areas using SEM and, in particular, fluorescence microscopy images using ImageJ image processing and analysis software (NIH, USA). The extent of cell spreading was quantified by measuring the cell contact areas from the detailed SEM images using ImageJ (NIH, USA).

Phalloidin staining: Following the 2 h incubation, the cells were fixed in 500 µl of 2% glutaraldehyde (Ted Pella, USA) solution in phosphate-buffered saline (PBS) for 10 min at room temperature and dehydrated with a series of ethanol solutions of increasing concentration (10%, 30%, 60%, 90% and 100% ethanol, 10 min in each). The slides were then rinsed twice with PBS and permeabilized in 500 µl of 0.1% Triton X-100 in PBS for 5 min and rinsed twice with PBS. The permabilized samples were blocked with 1% bovine serum albumin (Sigma–Aldrich, USA) in PBS for 30 min at room temperature to minimize non-specific staining. Previously prepared methanolic stock solution of Alexa Fluor488–Phalloidin (Invitrogen Co., USA) was diluted 40 times in PBS to obtain an approximately

165 nM working solution. 200 µl of the final working solution was added on top of each sample and kept at room temperature protected from light for 20 min. The samples where then rinsed twice with PBS and observed using a TE 300L microscope (Nikon, Japan).

SEM sample preparation: The cells were fixed in 500 µl of 2% glutaraldehyde (Ted Pella, USA) solution in PBS for 10 min at room temperature and dehydrated with a series of increasing concentration ethanol solutions (10%, 30%, 60%, 90% and 100% ethanol, 10 min in each). After ethanol dehydration the samples were coated with platinum using an SPI sputter coater (SPI Supplies, USA) and observed using a JSM 7000F scanning electron microscope (JEOL, Japan).

5.3 Methods for: Modular Bio-sensor Design

Preparation of biosensor surfaces: Gold-coated QCM and SPR slides of the specifications described below were used after cleaning by sequential sonication in acetone, ethanol, and water (three times per solvent, 5 min each) followed by UV ozone cleaning for 20 min. The GFP-tagged receptors were immobilized on clean chip surfaces via anti-GFP antibody linkage. First, the surfaces were drop-incubated with 1:50 dilution of anti-GFP solution (ab290, Abcam) in phosphate buffer (pH 7.4) in a humidity-controlled environment overnight at 4°C and rinsed 10 times by dilution rinse with phosphate buffer. The surfaces were then blocked in a 2% bovine serum albumin (BSA) solution for 2 h and washed by dilution as before. The resulting samples were incubated with a membrane fraction of either control (GFP only) or receptor solution for either 4 h (QCM) or 2 h (SPR), followed by the dilution rinse and an additional 1 h of BSA blocking to yield receptor-immobilized biosensor chips. All chips were used on the day they were produced.

QCM: QCM measurements were performed using QCM-Z500 (KSV Instruments) and commercially available AT-cut polished QCM crystals with a fundamental resonant frequency of 4.95 MHz (International Crystal Manufacturing Co.). The sensor surface was precoated by evaporation with a 100 Å titanium adhesion layer, followed by 1000 Å of gold. The QCM crystal dimensions used were 1.397 cm (0.550 in) blank diameter and 0.5 cm and 1.176 cm (0.440 in) wraparound electrode diameters. The receptor-modified QCM crystal (described above) was placed in the holder and sealed with two O-rings. In order to establish a stable baseline, a sufficient amount of phosphate buffer solution was injected to fill the QCM chamber, and the frequency shifts were monitored overnight. Then, sequential serial concentrations of recombinant MEPF1 or MEPF2 peptides in phosphate buffer solution were introduced to the QCM chamber, and the frequency change was recorded continuously until no further change was observed, indicating equilibrium. The QCM resonant frequency shifts recorded at the seventh harmonic were used to analyze ligand–receptor interactions, since the observed resonant QCM frequency decreases proportionally to the mass of adsorbed molecules.

All experiments were performed at 4°C in stop-flow mode in three independent experiments.

SPR: SPR measurements were made on a four-channel instrument (Kretschmann configuration: Radio Engineering Institute, Czech Republic) equipped with a polychromatic light source (Ocean Optics LS1). The slides were prepared via thermal evaporation by coating a BK-7 glass slide with 20 Å of chromium as the adhesion layer and 480 Å of gold. The instrument can detect changes at a level of 0.0001 refractive index unit and is temperature controlled (10°C–55°C). Buffer and recombinant MEPF solutions

were degassed to avoid bubble formation in the flow cell. First, phosphate buffer solution was flowed over the surface until a stable baseline signal was established (<0.05 nm change over 5 min). Then, recombinant MEPF solutions in phosphate buffer at concentrations indicated were flowed over the surface, and the adsorption was monitored. The temperature within the flow cell of the SPR was kept at a constant 25°C via a heating element and a cooling fan controlled by a temperature controller. All of the solutions used were introduced to the flow cell at a rate of 140 μL/sec. The Langmuir isotherm model was used to calculate the kinetics of the adsorption process using the experimental data obtained from SPR.

5.4 Methods for: Controlling the Surface Chemistry of Graphite by Engineered Self-Assembled Peptides

Peptide Synthesis: Peptides were prepared on an automated solid-phase peptide synthesizer (CS336X, CSBio Inc., Menlo Park, CA) employing standard batch-wise Fmoc chemistry procedures as reported previously. The synthesis was verified by MALDI-TOF mass spectrometry.

Surface Modification: Samples for contact angle measurements were prepared on HOPG pieces no smaller than 5mm by 5mm. The surfaces were prepared by removing a layer of graphite via scotch tape, which leaves a pristine surface as determined by AFM. An 80μl drop of the appropriate 1μM peptide solution in water was placed on the surface for times ranging from 10min to 5hrs. The drop was wicked with tissue and the sample dried in a nitrogen stream. The samples were allowed to equilibrate in air for 30min prior to contact angle measurements.

Contact Angle Measurements: Static contact angles were measured using an FTA1000B Goniometer (First Ten Angstroms, Inc., Portsmouth, VA) with an automatic camera system by placing 2µl of the same solution as was used to produce the sample in two different locations on each surface. The measurement was made immediately. The liquid surface tension was determined by pendant drop shape method, and was found not to vary significantly for different solutions. In all, two measurements were taken on two different samples for each data point. The samples were then dried with nitrogen and the coverage was measured by AFM.

AFM measurements: Atomic force imaging was carried out on a Digital Instruments (Veeco, Santa Barbara, CA) Multimode Nanoscope IIIa scanning probe microscope equipped with high frequency NanoSensors PPP-NCHR (NanoandMore USA, Ladys Island, SC, USA) non-contact probes, with a 42 N/m spring constant. Coverage was determined by image analysis of at least two 0.5µm x 4µm areas in at least three parts of each sample.

5.5 Methods For: Selective Detection of Proteins in Solution via Graphene Sensors Enabled by Self-Assembled Mixed Peptide Monolayer

Peptide preparation: The peptides were produced by solid-state synthesis using a CSBio 336s automated peptide synthesizer (CSBio, USA) on Wang resin via Fmoc chemistry and HBTU activation. The crude peptides were purified by reverse phase high performance liquid chromatography to >98% purity (Gemini 10 µm C18 110A column). The purified peptides' identities were verified by mass spectroscopy (MS) using a MALDI-TOF mass spectrometer (Bruker Daltonics Inc., USA). Streptavidin, anti-MBP, MBP and

bovine serum albumin were purchased from Sigma-Aldrich, USA, and used as received. All of the solutions were prepared with de-ionized water.

Surface Modification: Samples for contact angle measurements were prepared on HOPG pieces no smaller than 5mm by 5mm. The surfaces were prepared by removing a layer of graphite via scotch tape, which leaves a pristine surface as determined by AFM. An 80mlμl drop of the appropriate 1μM peptide solution in water was placed on the surface for times ranging from 10min to 5hrs. The drop was wicked with tissue and the sample dried in a nitrogen stream.

Contact Angle Measurements: The samples were allowed to equilibrate in air for 30min prior to contact angle measurements. Static contact angles were measured using an FTA1000B Goniometer (First Ten Angstroms, Inc., Portsmouth, VA) with an automatic camera system by placing 2μl of the same solution as was used to produce the sample in two different locations on each surface. The measurement was made immediately. The liquid surface tension was determined by pendant drop shape method, and was found not to vary significantly for different solutions. In all, at least two measurements were taken on two different samples for each data point. The samples were then dried with nitrogen and the coverage was measured by AFM.

AFM measurements: Atomic force imaging was carried out on a Digital Instruments (Veeco, Santa Barbara, CA) Multimode Nanoscope IIIa scanning probe microscope equipped with high frequency NanoSensors PPP-NCHR (NanoandMore USA, Ladys Island, SC, USA) non-contact probes, with a 42 N/m spring constant. Coverage was

determined by image analysis of at least two 0.5μm x 4μm areas in at least three parts of each sample.

Sensor construction: Graphene was prepared by exfoliation method, [54] on SiO_2 wafers, which were pre-treated with acidic piranha solution (75% sulfuric acid, 25% hydrogen peroxide). Specifically, HOPG powder was deposited on scotch tape and cleaved using another piece of tape at least 30 times. The resulting strip was then pressed against a sample of SiO_2 wafer, resulting in a transfer of graphene, and graphite flakes. Graphene was discovered using an optical microscope, and determined to be single layer through color comparison. Orientation markers were made via indium micro-soldering,[136] and a PMMA coating was applied to the wafer by spin-coating 5% PMMA solution for 1 min at 1000 RPM. The electrode patterns (Figure 21b) were made via electron beam lithography on JOEL 7000 SEM (JOEL Ltd., Japan). The pattern was developed in IPA and then extended by hand to lengthen the electrodes. The electrodes were made by sputtering 2nm of titanium as adhesion layer, followed by 46nm of platinum, and 2nm of titanium, as insulating layer using Gatan Precision Etching Coating System Model 682 (Gatan Inc., USA). The PMMA was removed in boiling acetone, and the device annealed in a tube furnace under a 60% argon / 40% hydrogen atmosphere at 450C^o for 1 hour. The terminals of indium solder were added at the ends of the electrodes. The contacts were current-annealed under nitrogen atmosphere by cycling currents of up to 1mA at up to 60 volts through the device using Agilent U2722A USB Modular Source Measure Unit (Agilent. USA), until the resistance of the device remained constant between cycles. The devices were re-cleaned between experiments by boiling in acetone for 1 hour, followed by current-annealing.

Sensor Measurement: The device was connected to the Agilent U2722A USB Modular Source Measure Unit (Agilent, USA) in a four probe configuration, with current kept constant at 0.1μA between R1 and R2 terminals, and voltage measured between R3 and R4 terminals (Figure 23C). A 20μl drop of water was placed on the sensor and the resistance was allowed to equilibrate. The device was maintained in a hydration chamber at 100% humidity to prevent evaporation. Analyte was added to the static drop on the sensor in the appropriate concentrations, so that the total volume of the drop never exceeded 35μl. Data was collected from two distinct devices and each experiment was reproduced at least twice.

6. List of Recurring Abbreviations

Abbreviation	Meaning
AFM	Atomic Force Microscopy
AP	Amorphous Phase
BSA	Bovine Serum Albumin
CA	Contact Angle
CA19-9	Cancer Antigen 19-9
CEA	Carcinoembryonic Antigen
CNT	Carbon Nanotube
CVD	Chemical Vapor Deposition
DF	Dark Field Optical Microscopy
DI	De-ionized
EDS	Energy Dispersive Spectroscopy
EDXS	Energy Disersive X-ray Spectroscopy
FBS	Fetal Bovine Serum
FET	Field Effect Transistor
GEPI	Genetically Engineered Peptide for Inorganics (solid-binding peptide)
gFET	Graphene Field Effect Transistor
GFP	Green Fluorescent Protein
GRAVY	Grand Average of Hydropathicity
HOPG	Highly Oriented Pyrolytic Graphite
HPLC	High Performance Liquid Chromatography
MALDI-TOF	Matrix-assisted Laser Desorption Time-of-flight
MBP	Maltose Binding Protein
MS	Mass Spectroscopy
OEG	Oligoethylene Glycol
OP	Ordered Phase
PBS	Phosphate Buffered Saline
PDMS	Polydimethylsiloxane
PEG	Polyethylene Glycol
PSA	Prostate Specific Antigen
QCM	Quartz Crystal Microbalance
SA	Streptavidin
SAM	Self-assembled Monolayer
SEM	Scanning Electron Microscopy
SPM	Scanning Probe Microscopy
SPR	Surface Plasmon Resonance Spectroscopy
SRS	Surface Resistivity Spectroscopy
VMD	Visual Molecular Dynamics
XPS	X-ray Photoelectron Spectroscopy

7. Highlights of Candidate's Personal Contributions

The following is a summary of highlights from the work accomplished during my graduate studies, which represent my personal contribution to the fields of molecular biomimetics, including diverse areas such as surface functionalization, bio-sensing, and functional peptide design. They are presented in chronological order and relate to the topics of biocompatibility, nano-particle formation and functionalization, ligand-receptor interactions, functionalization and property control of graphitic materials, selective sensing with gFETs, and sensing of cancer markers, using antibodies, in 3% FBS.

a. Biofuntionalization of implant materials via peptides: The purpose of this study was to demonstrate the utility of solid binding peptides as molecular linkers in the biofunctionalization of solid substrate to impart cytocompatibility or anti-fouling properties, on titanium, glass, and noble metals such as gold and platinum, respectively. In the latter case, I used Schiff-base chemistry to immobilize PEG onto the peptide-functionalized solid surfaces in sufficient concentrations to prevent cell adhesion. This experiment was a novel demonstration of using solid-binding peptides to modify surface properties of substrates by functional molecule immobilization.

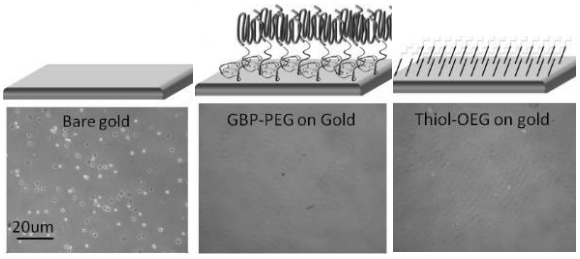

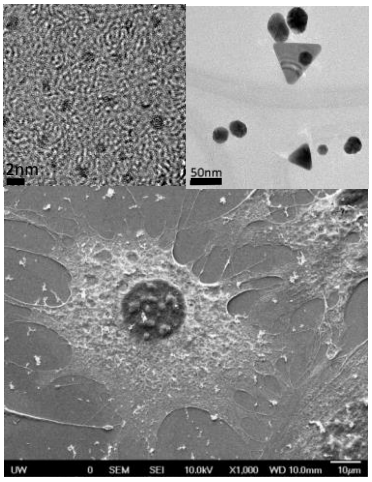

b. Single step controlled fabrication of functional gold nano-particles: After we discovered that our gold-binding peptides are capable of reducing gold from a $HAuCl_4$ solution (Au^{3+}) into Au^{+1} ions and subsequently into particles (Au^0), I

set out to use a multi-functional gold-binding peptide – RGD construct to simultaneously form particles of controlled size, and functionalize them in a single step. By controlling the temperature and concentrations of the reaction components, I demonstrated synthesis of particles with controlled diameters between 2 and 50 nm, which preferentially bind to cells. This study is a first demonstration of multi-functional designed, solid forming peptides, capable of reducing, capping, and functionalizing in a single step.

c. SPR and QCM selective bio-sensor design for ligand-receptor binding characterization: The goal of this study was to measure and compare interactions between several ligands and receptors involved in stomatal patterning, as part of our group's collaboration with Prof. Keiko Torii in Molecular Biol. Dept. I designed, produced and used SPR- and QCM-based biosensors, which employed GFP antibodies, to capture and display the GFP-tagged receptors, resulting in a novel, versatile sensor, which could be used to selectively detect the interactions between any ligand-receptor pair in unpurified samples.

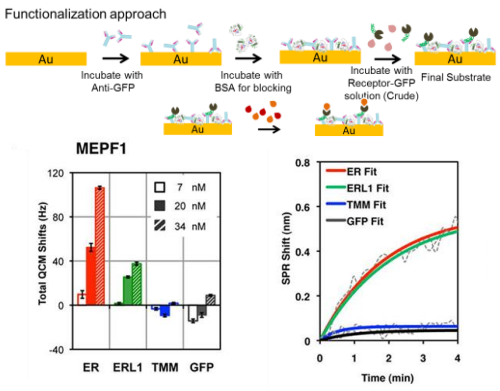

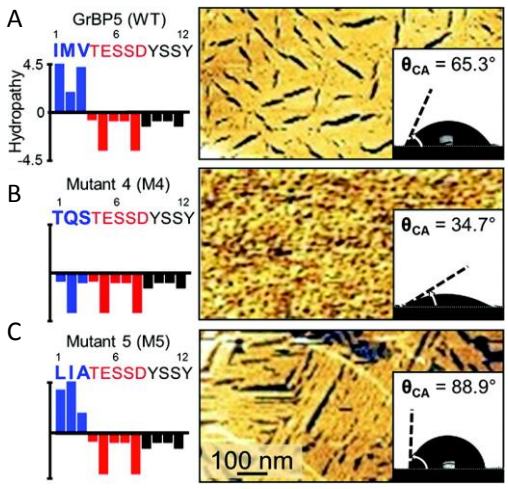

d. Interrogation of the assembly domain of GrBP5: As part of the analysis of the GrBP5 graphite-binding, self-assembling peptide sequence, it was necessary to interrogate the amphiphilic tail, believed to be responsible for the ordering of the peptides on the surface. Through a series of mutations on the

hydrophobic amino acids I was able to determine that the amphiphilic nature of the assembly domain was indeed critical to ordering. More importantly, I discovered that the amino acids closest to the N-terminus are the ones best displayed to the solution, a finding which is instrumental to design of surfaces using GrBP5.

e. Controlling the surface properties of graphite through peptide functionalization: The discovery of the display principles of GrBP5, one of the most effective graphite-binding

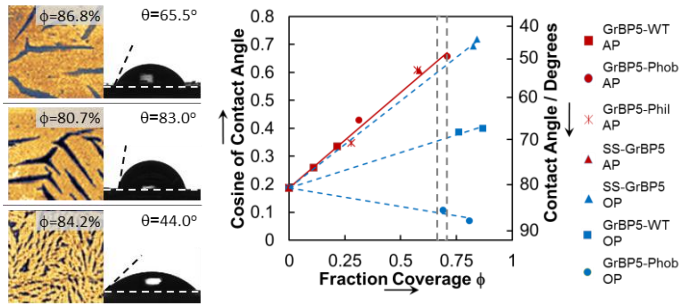

dodecapeptides originally selected by phage display in the research group, enabled me to control the surface properties of graphite through addition an mutation of specific amino acids on the N-terminus of the GrBP5 peptide. In this case, I was able to vary the contact angle of (normally hydrophobic) graphite between 44 and 92 degrees. This experiment served as a powerful demonstration of the possibility of rationally designing surface properties through peptide mutation, which helped to develop the novel concepts of modifying the physical (in addition to chemical) properties of solid substrates, in particular single layer atomic materials, starting with graphene and MoS2, representing a significant step towards genetically engineered devices.

f. Controlling surface properties of graphite through mixed peptide monolayers: As a simpler alternative to controlling surface properties through mutation, I proposed and demonstrated continuous control in contact angle between 44 and 92 degrees *via* mixed

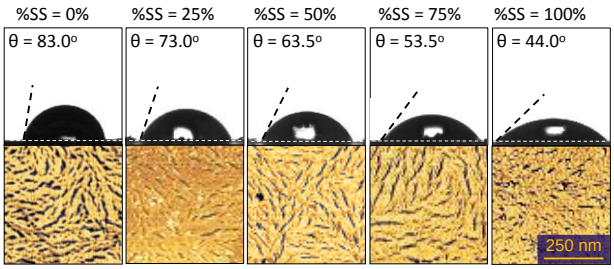

peptide monolayers. Additionally, I found that peptides are miscible within the monolayer, which, in combination with to molecular phase separation and controlled conformational change on surfaces in self-assembled peptide systems opens up numerous new approaches to multi-functional graphitic surfaces.

g. Selective sensing of proteins by gFET using mixed peptide monolayers: Selective sensing of proteins in complex biological solution conditions is a major problem in molecular biology and medicine. By taking advantage of the extreme sensitivity of graphene based sensors, along with the mixed peptide monolayer approach to functionalization of graphitic materials, I proposed a potential solution to this problem. By employing a biotinilated peptide alongside an anti-fouling peptide of my own design, I was able to selectively detect streptavidin against a background of bovine serum albumin. This study represents a major step towards the development of a novel graphene-based, peptide-enabled molecular biosensor.

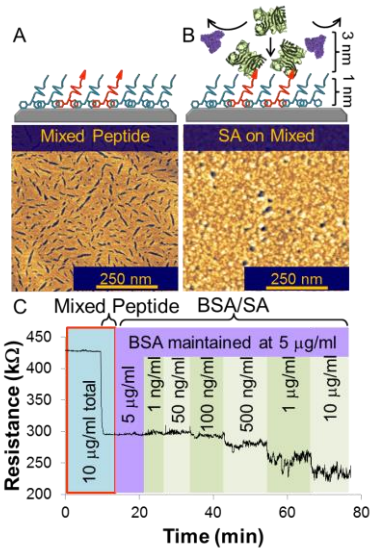

h. Stability of Cancer sensor under 3% FBS conditions: The stability of the peptide mixed monolayer in the testing conditions is critical for its performance of the sensor with respect to selectivity. I tested the stability of my sensor functionalization scheme in 3% FBS, finding that it remains stable after 30 minutes of exposure. This performance is

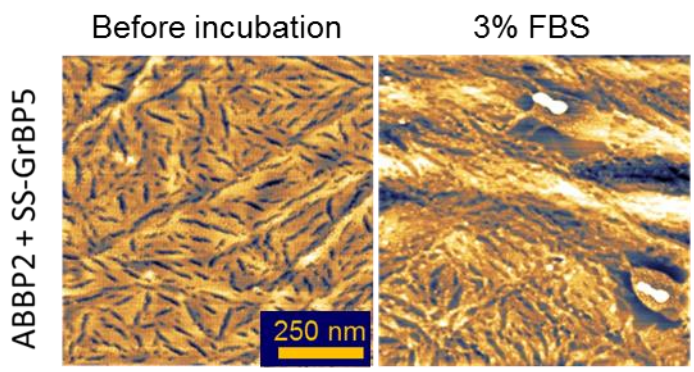

sufficient for detection of cancer markers, with experiments running about 10 minutes in length. It also compares favorably with the stability of other graphene modifications in literature, highlighting the ability of the solid-binding peptides to modify the surface in a non-perturbative, robust fashion.

i. Selective sensing of cancer markers by gFET using antibodies displayed via mixed peptide monolayers: In order to detect cancer markers, I envisioned a modular system, which relies on a bi-functional peptide construct capable of simultaneous binding to graphene and, through binding to the conserved portion of an antibody, exposing it to the solution. The advantage of this system lies in the possibility of displaying any given antibody making the sensor useful for detecting any potential analyte, for which an anti-body exists. Using this system, assembled *via* the best methodologies from my previous experiments, I was able to detect two different cancer markers in the tens of ng/ml range. This unique system takes full advantage of the particular capabilities of the peptidic approach to result in a device with numerous potential applications.

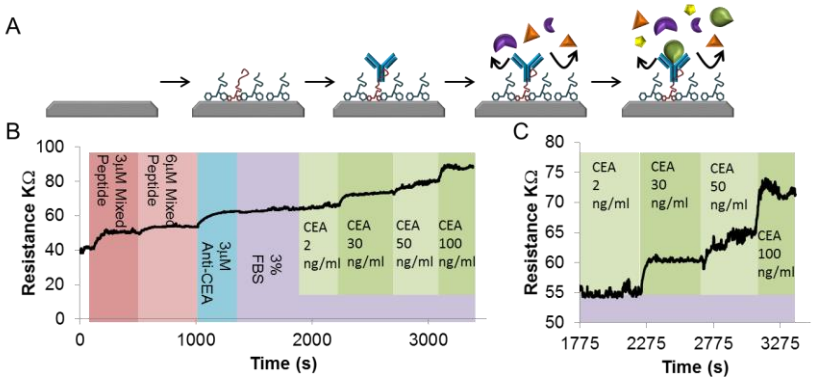

8. Acknowledgments

This research was supported by NSF-BioMaterials (DMR-0706655) and MRSEC programs (DMR-0520567) at GEMSEC, Genetically Engineered Materials Science and Engineering Center, University of Washington. It was additionally supported by the NCI Training Grant T32CA138312. The work was carried out GEMSEC-SECF, a member of the Materials Facilities Network of MRSEC. I would like to especially thank my advisor, Prof. M. Sarikaya, my co-advisers Prof. C. Tamerler and Dr. W. Grady, other members of my Doctoral Supervisory Committee Prof. T Horbett and Prof. D. Ratner, as well as my mentors, Dr. H. Fong, Dr. M. Gungormus, Dr. Y. Hayamizu, Dr. M. Hnilova, Dr. C. R. So, Dr. B. Wilson, my colleagues, C. Gresswell, T.R. Page, D. Starkebaum, all of my collaborators, and all the members of the GEMSEC team.

9. Candidate's Publications

1. C. Tamerler, **D. Khatayevich**, M. Gungormus, T. Kacar, E. E. Oren, M. Hnilova, and M. Sarikaya "Molecular biomimetics: GEPI-based biological routes to technology", Biopolymers Peptide Science, 94, 78-94 (2010)
2. **D. Khatayevich**, M. Gungormus, C. So, S. Getinel, H. Ma, A. K.-Y. Jen, C. Tamerler, and M. Sarikaya, "Biofunctionalization of Materials for Implants Using Engineered Peptides", Acta Biomaterialia. 6 (12), 4634-4641 (2010)
3. M. Hnilova, **D. Khatayevich**, A. Carlson, E. E. Oren, C. Gresswell, S. Zheng, F. Ohuchi, M. Sarikaya, and C. Tamerler, "Single-Step Fabrication of Patterned Gold Film Array by an Engineered Multi-Functional Peptide," J. Colloid Interface Sci., 365(1) 97-102 (2012)

4. J. S. Lee, T. Kuroha, M. Hnilova, **D. Khatayevich**, M. M. Kanaoka, J. M. McAbee, M. Sarikaya, C. Tamerler, and K. U. Torii, "Direct Interaction of Ligand-Receptor Pairs Specifying Stomatal Patterning," Gene Dev. 26, 126-136 (Journal Cover, January 2012)
5. C. R. So, Y. Hayamizu, H. Yazici, C. Gresswell, **D. Khatayevich**, C. Tamerler, and M. Sarikaya, “Controlling Self Assembly of Engineered Peptides on Graphite by Rational Mutation,”ACS Nano, 6(2) 1648-1656 (Journal Cover, April 2012)
6. **D. Khatayevich**, C. R. So, Y. Hayamizu, C. Gresswell, and M. Sarikaya, “Controlling the Surface Chemistry of Graphite by Engineered Self-Assembled Peptides,” Langmuir, 28(23) 8589-8593 (Journal Cover, June 2012)
7. **D. Khatayevich**, T. Page, Y. Hayamizu, W. Grady, and M. Sarikaya, “Selective Detection of Proteins via Graphene Sensors Enabled by Self-Assembled Mixed Peptide Monolayers,” Revisions submitted to Small, (August, 2013)
8. **D. Khatayevich**, W. Grady, and M. Sarikaya, “Multifunctional Peptide Enabled Graphene Nano-Sensor Platform for Cancer Marker Screening,” To be submitted (September, 2013)

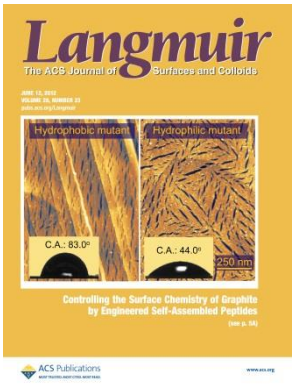

9. References

[1] Sarikaya M, Tamerler C, Jen AKY, Schulten K, Baneyx F. Molecular biomimetics: nanotechnology through biology. Nature Materials. 2003;2:577-85.

[2] Lu ZJ, Murray KS, Vancleave V, Lavallie ER, Stahl ML, McCoy JM. Expression of Thioredoxin Random Peptide Libraries on the Escherichia-Coli Cell-Surface as Functional Fusions to Flagelin - a System Designed for Exploring Protein-Protein Interactions. Bio-Technology. 1995;13:366-72.

[3] Smith GP, Petrenko VA. Phage display. Chemical Reviews. 1997;97:391-410.

[4] Tamerler C, Oren EE, Duman M, Venkatasubramanian E, Sarikaya M. Adsorption kinetics of an engineered gold binding peptide by surface plasmon resonance spectroscopy and a quartz crystal microbalance. Langmuir. 2006;22:7712-8.

[5] Oren EE, Tamerler C, Sahin D, Hnilova M, Seker UOS, Sarikaya M, et al. A novel knowledge-based approach to design inorganic-binding peptides. Bioinformatics. 2007;23:2816-22.

[6] Hnilova M, Oren EE, Seker UOS, Wilson BR, Collino S, Evans JS, et al. Effect of Molecular Conformations on the Adsorption Behavior of Gold-Binding Peptides. Langmuir. 2008;24:12440-5.

[7] Huang Y, Chiang CY, Lee SK, Gao Y, Hu EL, De Yoreo J, et al. Programmable assembly of nanoarchitectures using genetically engineered viruses. Nano Letters. 2005;5:1429-34.

[8] Naik RR, Stringer SJ, Agarwal G, Jones SE, Stone MO. Biomimetic synthesis and patterning of silver nanoparticles. Nature Materials. 2002;1:169-72.

[9] Nam KT, Lee YJ, Krauland EM, Kottmann ST, Belcher AM. Peptide-mediated reduction of silver ions on engineered biological scaffolds. Acs Nano. 2008;2:1480-6.

[10] Seker UOS, Wilson B, Dincer S, Kim IW, Oren EE, Evans JS, et al. Adsorption behavior of linear and cyclic genetically engineered platinum binding peptides. Langmuir. 2007;23:7895-900.

[11] Thai CK, Dai HX, Sastry MSR, Sarikaya M, Schwartz DT, Baneyx F. Identification and characterization of Cu2O- and ZnO-binding polypeptides by Escherichia coli cell surface display: Toward an understanding of metal oxide binding. Biotechnology and Bioengineering. 2004;87:129-37.

[12] Sano KI, Shiba K. A hexapeptide motif that electrostatically binds to the surface of titanium. Journal of the American Chemical Society. 2003;125:14234-5.

[13] Gungormus M, Fong H, Kim IW, Evans JS, Tamerler C, Sarikaya M. Regulation of in vitro calcium phosphate mineralization by combinatorially selected hydroxyapatite-binding peptides. Biomacromolecules. 2008;9:966-73.

[14] Gaskin DJH, Starck K, Vulfson EN. Identification of inorganic crystal-specific sequences using phage display combinatorial library of short peptides: A feasibility study. Biotechnology Letters. 2000;22:1211-6.

[15] Whaley SR, English DS, Hu EL, Barbara PF, Belcher AM. Selection of peptides with semiconductor binding specificity for directed nanocrystal assembly. Nature. 2000;405:665-8.

[16] Lee SW, Mao CB, Flynn CE, Belcher AM. Ordering of quantum dots using genetically engineered viruses. Science. 2002;296:892-5.

[17] Khatayevich D, Gungormus M, Yazici H, So C, Cetinel S, Ma H, et al. Biofunctionalization of materials for implants using engineered peptides. Acta Biomaterialia. 2010;6:4634-41.

[18] Yuca E, Karatas AY, Seker UOS, Gungormus M, Dinler-Doganay G, Sarikaya M, et al. In vitro labeling of hydroxyapatite minerals by an engineered protein. Biotechnology and Bioengineering. 2011;108:1021-30.

[19] Kacar T, Zin MT, So C, Wilson B, Ma H, Gul-Karaguler N, et al. Directed Self-Immobilization of Alkaline Phosphatase on Micro-Patterned Substrates Via Genetically Fused Metal-Binding Peptide. Biotechnology and Bioengineering. 2009;103:696-705.

[20] Hnilova M, So CR, Oren EE, Wilson BR, Kacar T, Tamerler C, et al. Peptide-directed co-assembly of nanoprobes on multimaterial patterned solid surfaces. Soft Matter. 2012;8:4327-34.

[21] Zhao MA, Deng K, Jiang P, Xie SS, Fichou D, Jiang C. Binary-Component Self-Assembled Monolayer Comprising Tetrathiafulvalene and n-Tetradecane Molecules with Periodic Ordered Phase Separation Structures on a Highly Oriented Pyrolytic Graphite Surface. Journal of Physical Chemistry C. 2010;114:1646-50.

[22] Tao F, Goswami J, Bernasek SL. Self-assembly and odd-even effects of cis-unsaturated carboxylic acids on highly oriented pyrolytic graphite. Journal of Physical Chemistry B. 2006;110:4199-206.

[23] Lee B, Chen Y, Duerr F, Mastrogiovanni D, Garfunkel E, Andrei EY, et al. Modification of Electronic Properties of Graphene with Self-Assembled Monolayers. Nano Letters. 2010;10:2427-32.

[24] Smith RA, Cokkinides V, Brawley OW. Cancer Screening in the United States, 2009: A Review of Current American Cancer Society Guidelines and Issues in Cancer Screening. Ca-a Cancer Journal for Clinicians. 2009;59:27-41.

[25] Hammarstrom S. The carcinoembryonic antigen (CEA) family: structures, suggested functions and expression in normal and malignant tissues. Seminars in Cancer Biology. 1999;9:67-81.

[26] Hollingsworth MA, Swanson BJ. Mucins in cancer: Protection and control of the cell surface. Nature Reviews Cancer. 2004;4:45-60.

[27] Balk SP, Ko YJ, Bubley GJ. Biology of prostate-specific antigen. Journal of Clinical Oncology. 2003;21:383-91.

[28] Thompson IM, Pauler DK, Goodman PJ, Tangen CM, Lucia MS, Parnes HL, et al. Prevalence of prostate cancer among men with a prostate-specific antigen level <= 4.0 ng per milliliter. New England Journal of Medicine. 2004;350:2239-46.

[29] Siegel R, Naishadham D, Jemal A. Cancer statistics, 2013. Ca-a Cancer Journal for Clinicians. 2013;63:11-30.

[30] Sohn TA, Yeo CJ, Cameron JL, Koniaris L, Kaushal S, Abrams RA, et al. Resected adenocarcinoma of the pancreas - 616 patients: Results, outcomes, and prognostic indicators. Journal of Gastrointestinal Surgery. 2000;4:567-79.

[31] Stathis A, Moore MJ. Advanced pancreatic carcinoma: current treatment and future challenges. Nature Reviews Clinical Oncology. 2010;7:163-72.

[32] Gold P, Freedman SO. Demonstration of tumor-specific antigens in human colonic carcinomata by immunological tolerance and absorption techniques. Journal of Experimental Medicine. 1965;121:439-&.

[33] Bunger S, Laubert T, Roblick UJ, Habermann JK. Serum biomarkers for improved diagnostic of pancreatic cancer: a current overview. Journal of Cancer Research and Clinical Oncology. 2011;137:375-89.

[34] Steinberg W. THE CLINICAL UTILITY OF THE CA 19-9 TUMOR-ASSOCIATED ANTIGEN. American Journal of Gastroenterology. 1990;85:350-5.

[35] Ona FV, Zamcheck N, Dhar P, Moore T, Kupchik HZ. Carcinoembryonic antigen (cea) in diagnosis of pancreatic cancer. Cancer. 1973;31:324-7.

[36] Herreros-Villanueva M, Gironella M, Castells A, Bujanda L. Molecular markers in pancreatic cancer diagnosis. Clinica Chimica Acta. 2013;418:22-9.

[37] Yalow RS, Berson SA. Immunoassay of endogenous plasma insulin in man. Journal of Clinical Investigation. 1960;39:1157-75.

[38] Ludwig JA, Weinstein JN. Biomarkers in cancer staging, prognosis and treatment selection. Nature Reviews Cancer. 2005;5:845-56.

[39] Vaisocherova H, Yang W, Zhang Z, Cao ZQ, Cheng G, Piliarik M, et al. Ultralow fouling and functionalizable surface chemistry based on a zwitterionic polymer enabling sensitive and specific protein detection in undiluted blood plasma. Analytical Chemistry. 2008;80:7894-901.

[40] Chou SF, Hsu WL, Hwang JM, Chen CY. Development of an immunosensor for human ferritin, a nonspecific tumor marker, based on surface plasmon resonance. Biosensors & Bioelectronics. 2004;19:999-1005.

[41] Di Natale C, Macagnano A, Martinelli E, Paolesse R, D'Arcangelo G, Roscioni C, et al. Lung cancer identification by the analysis of breath by means of an array of non-selective gas sensors. Biosensors & Bioelectronics. 2003;18:1209-18.

[42] Yu X, Munge B, Patel V, Jensen G, Bhirde A, Gong JD, et al. Carbon nanotube amplification strategies for highly sensitive immunodetection of cancer biomarkers. Journal of the American Chemical Society. 2006;128:11199-205.

[43] Liu X, Dai Q, Austin L, Coutts J, Knowles G, Zou JH, et al. A one-step homogeneous immunoassay for cancer biomarker detection using gold nanoparticle probes coupled with dynamic light scattering. Journal of the American Chemical Society. 2008;130:2780-+.

[44] Mani V, Chikkaveeraiah BV, Patel V, Gutkind JS, Rusling JF. Ultrasensitive Immunosensor for Cancer Biomarker Proteins Using Gold Nanoparticle Film Electrodes and Multienzyme-Particle Amplification. Acs Nano. 2009;3:585-94.

[45] Liu GD, Lin YY, Wang J, Wu H, Wai CM, Lin YH. Disposable electrochemical immunosensor diagnosis device based on nanoparticle probe and immunochromatographic strip. Analytical Chemistry. 2007;79:7644-53.

[46] Curreli M, Zhang R, Ishikawa FN, Chang HK, Cote RJ, Zhou C, et al. Real-Time, Label-Free Detection of Biological Entities Using Nanowire-Based FETs. Ieee Transactions on Nanotechnology. 2008;7:651-67.

[47] Alam MM, Wang J, Guo YY, Lee SP, Tseng HR. Electrolyte-gated transistors based on conducting polymer nanowire junction arrays. Journal of Physical Chemistry B. 2005;109:12777-84.

[48] Ohno Y, Maehashi K, Matsumoto K. Label-Free Biosensors Based on Aptamer-Modified Graphene Field-Effect Transistors. Journal of the American Chemical Society. 2010;132:18012-3.

[49] Stine R, Robinson JT, Sheehan PE, Tamanaha CR. Real-Time DNA Detection Using Reduced Graphene Oxide Field Effect Transistors. Advanced Materials. 2010;22:5297-300.

[50] Someya T, Small J, Kim P, Nuckolls C, Yardley JT. Alcohol vapor sensors based on single-walled carbon nanotube field effect transistors. Nano Letters. 2003;3:877-81.

[51] Page TR, Hayamizu Y, So CR, Sarikaya M. Electrical detection of biomolecular adsorption on sprayed graphene sheets. Biosensors & Bioelectronics. 2012;33:304-8.

[52] Zhang B, Li Q, Cui TH. Ultra-sensitive suspended graphene nanocomposite cancer sensors with strong suppression of electrical noise. Biosensors & Bioelectronics. 2012;31:105-9.

[53] Castro Neto AH, Guinea F, Peres NMR, Novoselov KS, Geim AK. The electronic properties of graphene. Reviews of Modern Physics. 2009;81:109-62.

[54] Novoselov KS, Geim AK, Morozov SV, Jiang D, Zhang Y, Dubonos SV, et al. Electric field effect in atomically thin carbon films. Science. 2004;306:666-9.

[55] Balandin AA, Ghosh S, Bao WZ, Calizo I, Teweldebrhan D, Miao F, et al. Superior thermal conductivity of single-layer graphene. Nano Letters. 2008;8:902-7.

[56] Lu J, Do I, Drzal LT, Worden RM, Lee I. Nanometal-decorated exfoliated graphite nanoplatelet based glucose biosensors with high sensitivity and fast response. Acs Nano. 2008;2:1825-32.

[57] Ratinac KR, Yang WR, Gooding JJ, Thordarson P, Braet F. Graphene and Related Materials in Electrochemical Sensing. Electroanalysis. 2011;23:803-26.

[58] Zhang MN, Gong KP, Zhang HW, Mao LQ. Layer-by-layer assembled carbon nanotubes for selective determination of dopamine in the presence of ascorbic acid. Biosensors & Bioelectronics. 2005;20:1270-6.

[59] Wu KB, Fei JJ, Hu SS. Simultaneous determination of dopamine and serotonin on a glassy carbon electrode coated with a film of carbon nanotubes. Analytical Biochemistry. 2003;318:100-6.

[60] Alwarappan S, Erdem A, Liu C, Li CZ. Probing the Electrochemical Properties of Graphene Nanosheets for Biosensing Applications. Journal of Physical Chemistry C. 2009;113:8853-7.

[61] Shang NG, Papakonstantinou P, McMullan M, Chu M, Stamboulis A, Potenza A, et al. Catalyst-Free Efficient Growth, Orientation and Biosensing Properties of Multilayer Graphene Nanoflake Films with Sharp Edge Planes. Advanced Functional Materials. 2008;18:3506-14.

[62] Besteman K, Lee JO, Wiertz FGM, Heering HA, Dekker C. Enzyme-coated carbon nanotubes as single-molecule biosensors. Nano Letters. 2003;3:727-30.

[63] Anker JN, Hall WP, Lyandres O, Shah NC, Zhao J, Van Duyne RP. Biosensing with plasmonic nanosensors. Nature Materials. 2008;7:442-53.

[64] Leong K, Chen YC, Masiello DJ, Zin MT, Hnilova M, Ma H, et al. Cooperative Near-Field Surface Plasmon Enhanced Quantum Dot Nanoarrays. Advanced Functional Materials. 2010;20:2675-82.

[65] Willner I, Baron R, Willner B. Integrated nanoparticle-biomolecule systems for biosensing and bioelectronics. Biosensors & Bioelectronics. 2007;22:1841-52.

[66] Haynes CL, Van Duyne RP. Nanosphere lithography: A versatile nanofabrication tool for studies of size-dependent nanoparticle optics. Journal of Physical Chemistry B. 2001;105:5599-611.

[67] Hammond PT. Form and function in multilayer assembly: New applications at the nanoscale. Advanced Materials. 2004;16:1271-93.

[68] Wang Y, Tang ZY, Podsiadlo P, Elkasabi Y, Lahann J, Kotov NA. Mirror-like photoconductive layer-by-layer thin films of Te nanowires: The fusion of semiconductor, metal, and insulator properties. Advanced Materials. 2006;18:518-+.

[69] Schreiber F. Structure and growth of self-assembling monolayers. Progress in Surface Science. 2000;65:151-256.

[70] Porter MD, Bright TB, Allara DL, Chidsey CED. Spontaneously organized molecular assemblies .4. Structural characterization of normal-alkyl thiol monolayers on gold by optical ellipsometry, infrared-spectroscopy, and electrochemistry. Journal of the American Chemical Society. 1987;109:3559-68.

[71] Xia YN, Whitesides GM. Soft lithography. Annual Review of Materials Science. 1998;28:153-84.

[72] Qin D, Xia YN, Whitesides GM. Soft lithography for micro- and nanoscale patterning. Nature Protocols. 2010;5:491-502.

[73] Nath N, Chilkoti A. Label-free biosensing by surface plasmon resonance of nanoparticles on glass: Optimization of nanoparticle size. Analytical Chemistry. 2004;76:5370-8.

[74] Seo HS, Kim SE, Park JS, Lee JH, Yang KY, Lee H, et al. A Three-Dimensional Nanostructured Array of Protein Nanoparticles. Advanced Functional Materials. 2010;20:4055-61.

[75] Kacar T, Ray J, Gungormus M, Oren EE, Tamerler C, Sarikaya M. Quartz Binding Peptides as Molecular Linkers towards Fabricating Multifunctional Micropatterned Substrates. Advanced Materials. 2009;21:295-9.

[76] Matmor M, Ashkenasy N. Peptide directed growth of gold films. Journal of Materials Chemistry.21:968-74.

[77] Tamerler C, Khatayevich D, Gungormus M, Kacar T, Oren EE, Hnilova M, et al. Molecular Biomimetics: GEPI-Based Biological Routes to Technology. Biopolymers. 2010;94:78-94.

[78] Tamerler C, Khatayevich D, Gungormus M, Kacar T, Oren EE, Hnilova M, et al. Molecular Biomimetics: GEPI-Based Biological Routes to Technology. Biopolymers.94:78-94.

[79] Turkevich J, Stevenson PC, Hillier J. A study of the nucleation and growth processes in the synthesis of colloidal gold. Discussions of the Faraday Society. 1951:55-&.

[80] Slocik JM, Naik RR. Biologically programmed synthesis of bimetallic nanostructures. Advanced Materials. 2006;18:1988-+.

[81] Slocik JM, Stone MO, Naik RR. Synthesis of gold nanoparticles using multifunctional peptides. Small. 2005;1:1048-52.

[82] Slocik JM, Naik RR, Stone MO, Wright DW. Viral templates for gold nanoparticle synthesis. Journal of Materials Chemistry. 2005;15:749-53.

[83] Levy R, Thanh NTK, Doty RC, Hussain I, Nichols RJ, Schiffrin DJ, et al. Rational and combinatorial design of peptide capping Ligands for gold nanoparticles. Journal of the American Chemical Society. 2004;126:10076-84.

[84] Wang Z, Levy R, Fernig DG, Brust M. The peptide route to multifunctional gold nanoparticles. Bioconjugate Chemistry. 2005;16:497-500.

[85] Ratner BD. Biomaterials science : an introduction to materials in medicine. Amsterdam; Boston: Elsevier Academic Press; 2004.

[86] Griffith LG, Naughton G. Tissue engineering - Current challenges and expanding opportunities. Science. 2002;295:1009-+.

[87] Anselme K. Osteoblast adhesion on biomaterials. Biomaterials. 2000;21:667-81.

[88] Hench LL. Bioceramics. Journal of the American Ceramic Society. 1998;81:1705-28.

[89] Tang LP, Eaton JW. Inflammantory Responses to Biomaterials. American Journal of Clinical Pathology. 1995;103:466-71.

[90] Brodbeck WG, Shive MS, Colton E, Nakayama Y, Matsuda T, Anderson JM. Influence of biomaterial surface chemistry on the apoptosis of adherent cells. Journal of Biomedical Materials Research. 2001;55:661-8.

[91] Hubbell JA. Biomaterials in Tissue Engineering. Bio-Technology. 1995;13:565-76.

[92] Schierholz JM, Beuth J. Implant infections: a haven for opportunistic bacteria. Journal of Hospital Infection. 2001;49:87-93.

[93] Williams DF. On the mechanisms of biocompatibility. Biomaterials. 2008;29:2941-53.

[94] Rezania A, Johnson R, Lefkow AR, Healy KE. Bioactivation of metal oxide surfaces. 1. Surface characterization and cell response. Langmuir. 1999;15:6931-9.

[95] Harder P, Grunze M, Dahint R, Whitesides GM, Laibinis PE. Molecular conformation in oligo(ethylene glycol)-terminated self-assembled monolayers on gold and silver surfaces determines their ability to resist protein adsorption. Journal of Physical Chemistry B. 1998;102:426-36.

[96] Dalsin JL, Hu BH, Lee BP, Messersmith PB. Mussel adhesive protein mimetic polymers for the preparation of nonfouling surfaces. Journal of the American Chemical Society. 2003;125:4253-8.

[97] Pierschbacher MD, Ruoslahti E. Cell Attachment Activity of Fibronectin Can Be Duplicated by Small Synthectic Fragments of the Molecule. Nature. 1984;309:30-3.

[98] Liu XH, Won YJ, Ma PX. Porogen-induced surface modification of nano-fibrous poly(L-lactic acid) scaffolds for tissue engineering. Biomaterials. 2006;27:3980-7.

[99] Chung TW, Lu YF, Wang SS, Lin YS, Chu SH. Growth of human endothelial cells on photochemically grafted Gly-Arg-Gly-Asp (GRGD) chitosans. Biomaterials. 2002;23:4803-9.

[100] Mrksich M, Whitesides GM. Using self-assembled monolayers to understand the interactions of man-made surfaces with proteins and cells. Annual Review of Biophysics and Biomolecular Structure. 1996;25:55-78.

[101] Munday R, Toxicity of thiols and disulphides: Involvement of free-radical species. Free Radical Biological Medicine. 1989;659-673

[102] Dalsin JL, Lin LJ, Tosatti S, Voros J, Textor M, Messersmith PB. Protein resistance of titanium oxide surfaces modified by biologically inspired mPEG-DOPA. Langmuir. 2005;21:640-6.

[103] Lee MH, Adams CS, Boettiger D, DeGrado WF, Shapiro IM, Composto RJ, et al. Adhesion of MC3T3-E1 cells to RGD peptides of different flanking residues: Detachment strength and correlation with long-term cellular function. Journal of Biomedical Materials Research Part A. 2007;81A:150-60.

[104] Salim M, Mishra G, Fowler GJS, O'Sullivan B, Wright PC, McArthur SL. Non-fouling microfluidic chip produced by radio frequency tetraglyme plasma deposition. Lab on a Chip. 2007;7:523-5.

[105] Acosta EJ, Nguyen T, Witthayapanyanon A, Harwell JH, Sabatini DA. Linker-based bio-compatible microemulsions. Environmental Science & Technology. 2005;39:1275-82.

[106] Murugesan S, Xie J, Linhardt RJ. Immobilization of heparin: Approaches and applications. Current Topics in Medicinal Chemistry. 2008;8:80-100.

[107] Thygesen MB, Jensen KJ. Peptides on nanoparticles: Linkers for chemoselective, biocompatible immobilization. John Wiley & Sons Inc; 2007. p. 616-.

[108] Walton C, Gergely S, Economides AP. Platinum Pacemaker Electrodes - Origins and Effects of the Electrode-Tissue Interface Impedance. Pace-Pacing and Clinical Electrophysiology. 1987;10:87-99.

[109] Stroganova EE, Mikhailenko NY, Moroz OA. Glass-based biomaterials: Present and future (a review). Glass and Ceramics. 2003;60:315-9.

[110] Chua PH, Neoh KG, Kang ET, Wang W. Surface functionalization of titanium with hyaluronic acid/chitosan polyelectrolyte multilayers and RGD for promoting osteoblast functions and inhibiting bacterial adhesion. Biomaterials. 2008;29:1412-21.

[111] Faucheux N, Schweiss R, Lutzow K, Werner C, Groth T. Self-assembled monolayers with different terminating groups as model substrates for cell adhesion studies. Biomaterials. 2004;25:2721-30.

[112] Chen D, Wang G, Li JH. Interfacial bioelectrochemistry: Fabrication, properties and applications of functional nanostructured biointerfaces. Journal of Physical Chemistry C. 2007;111:2351-67.

[113] Nel AE, Madler L, Velegol D, Xia T, Hoek EMV, Somasundaran P, et al. Understanding biophysicochemical interactions at the nano-bio interface. Nature Materials. 2009;8:543-57.

[114] Cha T, Guo A, Zhu XY. Enzymatic activity on a chip: The critical role of protein orientation. Proteomics. 2005;5:416-9.

[115] Tamerler C, Sarikaya M. Molecular biomimetics: nanotechnology and bionanotechnology using genetically engineered peptides. Philosophical Transactions of the Royal Society a-Mathematical Physical and Engineering Sciences. 2009;367:1705-26.

[116] Hu WB, Peng C, Luo WJ, Lv M, Li XM, Li D, et al. Graphene-Based Antibacterial Paper. Acs Nano. 2010;4:4317-23.

[117] Dai HJ. Carbon nanotubes: Synthesis, integration, and properties. Accounts of Chemical Research. 2002;35:1035-44.

[118] Gorton L. Biosensors and modern biospecific analytical techniques. Amsterdam; Boston: Elsevier; 2005.

[119] Du D, Zou ZX, Shin YS, Wang J, Wu H, Engelhard MH, et al. Sensitive Immunosensor for Cancer Biomarker Based on Dual Signal Amplification Strategy of Graphene Sheets and Multienzyme Functionalized Carbon Nanospheres. Analytical Chemistry. 2010;82:2989-95.

[120] Lin YH, Lu F, Tu Y, Ren ZF. Glucose biosensors based on carbon nanotube nanoelectrode ensembles. Nano Letters. 2004;4:191-5.

[121] Li D, Muller MB, Gilje S, Kaner RB, Wallace GG. Processable aqueous dispersions of graphene nanosheets. Nature Nanotechnology. 2008;3:101-5.

[122] Niyogi S, Bekyarova E, Itkis ME, McWilliams JL, Hamon MA, Haddon RC. Solution properties of graphite and graphene. Journal of the American Chemical Society. 2006;128:7720-1.

[123] Choi EY, Han TH, Hong JH, Kim JE, Lee SH, Kim HW, et al. Noncovalent functionalization of graphene with end-functional polymers. Journal of Materials Chemistry. 2010;20:1907-12.

[124] Ghosh A, Rao KV, Voggu R, George SJ. Non-covalent functionalization, solubilization of graphene and single-walled carbon nanotubes with aromatic donor and acceptor molecules. Chemical Physics Letters. 2010;488:198-201.

[125] Yu X, Wang ZQ, Jiang YG, Zhang X. Surface gradient material: From superhydrophobicity to superhydrophilicity. Langmuir. 2006;22:4483-6.

[126] Yang H, Fung SY, Sun W, Mikkelsen S, Pritzker M, Chen P. Ionic-complementary peptide-modified highly ordered pyrolytic graphite electrode for biosensor application. Biotechnology Progress. 2008;24:964-71.

[127] Cui Y, Kim SN, Jones SE, Wissler LL, Naik RR, McAlpine MC. Chemical Functionalization of Graphene Enabled by Phage Displayed Peptides. Nano Letters. 2010;10:4559-65.

[128] Wang QH, Hersam MC. Room-temperature molecular-resolution characterization of self-assembled organic monolayers on epitaxial graphene. Nature Chemistry. 2009;1:206-11.

[129] Kim SN, Kuang ZF, Slocik JM, Jones SE, Cui Y, Farmer BL, et al. Preferential Binding of Peptides to Graphene Edges and Planes. Journal of the American Chemical Society. 2011;133:14480-3.

[130] Kase D, Kulp JL, Yudasaka M, Evans JS, Iijima S, Shiba K. Affinity selection of peptide phage libraries against single-wall carbon nanohorns identifies a peptide aptamer with conformational variability. Langmuir. 2004;20:8939-41.

[131] Tomasio SM, Walsh TR. Modeling the Binding Affinity of Peptides for Graphitic Surfaces. Influences of Aromatic Content and Interfacial Shape. Journal of Physical Chemistry C. 2009;113:8778-85.

[132] Han TH, Lee WJ, Lee DH, Kim JE, Choi EY, Kim SO. Peptide/Graphene Hybrid Assembly into Core/Shell Nanowires. Advanced Materials. 2010;22:2060-+.

[133] So CR, Hayamizu Y, Yazici H, Gresswell C, Khatayevich D, Tamerler C, et al. Controlling Self-Assembly of Engineered Peptides on Graphite by Rational Mutation. Acs Nano. 2012;6:1648-56.

[134] Meyers SR, Khoo XJ, Huang X, Walsh EB, Grinstaff MW, Kenan DJ. The development of peptide-based interfacial biomaterials for generating biological functionality on the surface of bioinert materials. Biomaterials. 2009;30:277-86.

[135] Khatayevich D, So CR, Hayamizu Y, Gresswell C, Sarikaya M. Controlling the Surface Chemistry of Graphite by Engineered Self-Assembled Peptides. Langmuir. 2012;28:8589-93.

[136] Girit CO, Zettl A. Soldering to a single atomic layer. Applied Physics Letters. 2007;91.

[137] Cassie ABD, Baxter S. Wettability of porous surfaces. Transactions of the Faraday Society. 1944;40:0546-50.

[138] Ohno Y, Maehashi K, Yamashiro Y, Matsumoto K. Electrolyte-Gated Graphene Field-Effect Transistors for Detecting pH Protein Adsorption. Nano Letters. 2009;9:3318-22.

[139] Menzies KL, Jones L. The Impact of Contact Angle on the Biocompatibility of Biomaterials. Optometry and Vision Science. 2010;87:387-99.

[140] Holmberg A, Blomstergren A, Nord O, Lukacs M, Lundeberg J, Uhlen M. The biotin-streptavidin interaction can be reversibly broken using water at elevated temperatures. Electrophoresis. 2005;26:501-10.

[141] Krook M, Mosbach K, Ramstrom O. Novel peptides binding to the Fc-portion of immunoglobulins obtained from a combinatorial phage display peptide library. Journal of Immunological Methods. 1998;221:151-7.

[142] Newaz AKM, Puzyrev YS, Wang B, Pantelides ST, Bolotin KI. Probing charge scattering mechanisms in suspended graphene by varying its dielectric environment. Nature Communications. 2012;3:6.